THE DYNAMICS AND MORPHOLOGY OF SPRITES

A

THESIS

Presented to the Faculty

of the University of Alaska Fairbanks

in Partial Fulfillment of the Requirements

for the Degree of

DOCTOR OF PHILOSOPHY

By

Dana Moudry, B.S.

Fairbanks, Alaska

May 2003

UMI Number: 3092292

Copyright 2003 by

Moudry, Dana

All rights reserved.

UMI®

UMI Microform 3092292

Copyright 2003 by ProQuest Information and Learning Company.

All rights reserved. This microform edition is protected against

unauthorized copying under Title 17, United States Code.

ProQuest Information and Learning Company
300 North Zeeb Road
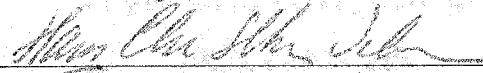P.O. Box 1346
Ann Arbor, MI 48106-1346
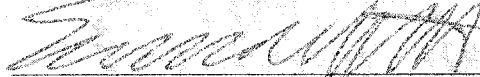
THE DYNAMICS AND MORPHOLOGY OF SPRITES
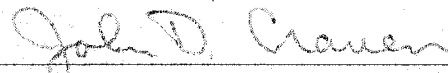
By

Dana Moudry

RECOMMENDED:

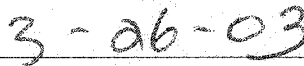Advisory Committee Chair

Chair, Department of Physics

APPROVED:

Dean, College of Science, Engineering and Mathematics

Dean of the Graduate School

3 - 06 - 03

Date

Abstract

In 1999 the University of Alaska Fairbanks fielded a 1000 fields-per-second intensified CCD camera to study sprites and associated upper atmospheric phenomena occurring above active thunderstorms as part of the NASA Sprites99 campaign. The exceptional clarity and definition obtained by this camera the night of August 18, 1999, provides the most detailed image record of these phenomena that has been obtained to date. The result of a frame-by-frame analysis of the data permits an orderly classification of upper atmospheric optical phenomena, and is the subject matter of this thesis.

The images show that both elves and halos, which are diffuse emissions preceding sprites, are largely spatially unstructured. Observations of sprites initiating outside of main parts of halos, and without a halo, suggest sprites are initiated primarily from locations of atmospheric composition and density inhomogeneities.

All sprites appear to start as tendrils descending from approximately 75 km altitude, and may form other dynamic or stationary features. Dynamic features include downward developing tendrils and upward developing branches. Stationary features include beads, columns, and diffuse "puffs," all of which have durations greater than 1 ms. Stationary sprite features are responsible for a significant fraction of the total optical emissions of sprites. Velocities of sprite tendrils were measured. After initial speeds of $10^6 - 10^7$ m/s, sprite tendrils may slow to 10^5 m/s. Similarly, on some occasions the dim optical emission left behind by the descending tendrils may expand horizontally, with speeds on the order of 10^5 m/s.

The volume excited by the sprite tendrils may rebrighten after 30-100 ms in the form of one of three different sprite after effects collectively termed "crawlers." A "smooth crawler" consists of several beads moving upward ($\sim 10^5$ m/s) without a large vertical extent, with "smooth" dynamics at 1 ms timescale. "Embers" are bead-like forms which send a downward-propagating luminous structure towards the cloudtop at speeds of 10^6 m/s, and have irregular dynamics at 1 ms timescales. In TV-rate observations, the downward-propagating structure of an ember is averaged out and appears as a vertically-extended ribbon above the clouds. The third kind of crawler, so-called "palm tree," appears similar to an ember at TV-rates, but with a wider crown at top.

Table of Contents

List of Figures

List of Tables

Acknowledgements

I thank my advisor Dr Dave Sentman for financial support, and Hans Nielsen for the use of his data and many useful discussions. Likewise I thank the rest of my committee: Gene Wescott, Roger Smith and Antonius Otto.

This work was supported by NASA Grants NAG5-5019 and NAG5-0131, Geophysical Institute internal research funds and by the University of Alaska Fairbanks Graduate School. Funding for the Sprite 1999 campaign was provided by NASA grant NAS5-5125 to the Geophysical Institute, University of Alaska Fairbanks. A thank-you also goes out to the University of Wyoming for permission to use the Wyoming Infrared Observatory at Jelm Mountain, WY during the various sprite campaigns. While not used in this thesis, other locations used included the University of Denver Mount Evans Observatory (CO) and the Bear Mountain fire lookout (SD).

Without the engineers, none of the fieldwork would have happened, so Dan Osborne and Jim Desrochers deserve special thanks, as well as those who did the fieldwork: Don Hampton before my time, Matt Heavner, Laura Peticolas, Veronika Besser, Fernanda Tavares, and of course the professors mentioned above.

I also thank the people who collaborated with me: Martin Füllekrug, Geoff McHarg, Jeff Morrill, Eric Bucsela, and those who had helpful comments on my presentations at conferences: Victor Pasko, the students at Stanford, Steve Cummer, and others.

Matt Heavner was my officemate and fellow graduate student for much of the time. He is an extremely nice geek who can do pretty much everything, including probably making his Linux box brew some beer. Laura Peticolas partnered with Veronika Besser and then I had no choice but to shave my head together with them, for a first experience for me in that realm. I am slightly disappointed in Curt Szuberla who kept promising to write a chapter or two of my thesis but never delivered. At least his LaTex style file which was used for this thesis was extremely useful for myself as well as a multitude of others. On the computer side, it is only thanks to both Matt and Dave Covey that "elf" and "gnome" stayed up.

Crane Court was an experience in itself in its heyday. Jen Simmons and Peter Delamere created excellent egghunts at Eastertime, and Peter was responsible for my partner Martin's introduction to football, "the chess of sports world". Bevin had an amazing mastery of

mixed drinks, and Ryan always provided some entertainment. And then there was Laura, who was generally in one of three states, possibly mixed: happy, poor or sad. In a separate group by herself, Doerte Mann is a water person - both frozen water (skiing) and wet water (kayaking), and she witnessed my internal struggle during the day trip with Rune when I pointed out a poor ptarmigan (or was it a grouse?) to him. I learned my lesson - Rune did not even share the meal :).

The fourth floor group here at the Geophysical Institute has let me eat lunch there on nearly everyday basis since I started hanging out with Martin. Keith Echelmeyer probably still thinks he was responsible for getting us together since apparently he kept a watch out for possible single women for Martin. I met Keith and Susan for the first time at Tolovana Hot Springs, and started hanging out with Martin soon thereafter. Tolovana provided many really funny moments. I still remember Dorte Dissing (ssssweetheart) giving the poor undergrad student who was willing to do anything but the dishes such a hard time that my stomach hurt from the laughter (he ended up doing the dishes). Many beautiful adventures to her and BJ.

Dorte together with Rune Storvold were a funny looking team in 2-on-2 volleyball - one super tall, one not, yet they kicked everyone's butt. Thanks to Pavel Sekanina and George Minassian for introducing me to the volleyball group that I played regularly with for the first couple years, and Pavel special thanks for the visit to his family's cellar in Moravia. Sorry to be required by you to be disappointed that you're happy.

Back to the glaciers lab, thanks to Adam Bucki for taking me along to the Fireweed Glacier by McCarthy with Leif and Dan (both glacier people) and the subsequent Labor Day party at the McCarthy Lodge. Adam and Martin had much patience a year earlier during our Alaska Range trip from Black Rapids over to McKinley Village. The only time I wished Adam wasn't there was on the Yanert River as we were skating out, with Adam, and consequently the lunch, so far ahead I could hardly see him, much less yell at him to stop so that we can eat. Lesson: don't give lunch food to someone who's nuts about skiing. It was a beautiful trip, not soon repeateable due to the surge of Yanert Glacier that same year and the earthquake which deposited enormous landslides on Black Rapids Glacier.

Eloise Brown and Kevin Petrone have a great sauna and we did some nice hikes and doggie walks with them, since Choly is really fond of his brother Lew in that family. I got

introduced to a few British traditions via Eloise - pancake Tuesday being one, and British Christmas Pudding. I did not know that christmas pudding can be boiled for twelve hours or more without apparent damage, as we found out at Circle Hot Springs the New Year's of 2001 when it was left to boil inadvertedly overnight. Carrie Talus introduced us to Eloise and Kevin, and has been a great friend since. Her marriage to Matt at Thanksgiving was certainly Alaskan, with Myste and Kita as the bridesdogs.

Hilary Fletcher and Chris Larsen deserve special thanks for letting me help them carry batteries when setting up or downloading GPS stations put up after the M7.9 earthquake of November 3, 2002. It made me realize what the difference is between geophysics and physics (answer: batteries, batteries, and more batteries).

And then there is of course my family. Thanks to my parents and brother for a great childhood and fun trips in adulthood, though these days we see each other only occasionally.

Other people include the Boulder contingent of Ex-Fairbanksans (Rob Fatland, Don Hampton and Anne Ruggles, Cecile Hannay, Vincent Dols, and Kolya, Jen and Peter and Sam Delamere) who have put me up during conference and forced me to remember that I am getting a year older each year. And thanks to people with whom I spent many an hour here in Fairbanks playing with frisbees.

Last but of course not least, there's Martin, who of course deserves more thanks that there's space for in this section. Not the least for all the times he's pushed me into the snow. Martin's first intro to my dad was a trip to Hawaii where we spend a grand total of half an hour on the beach. After that introduction, Argentina was no problem. Martin's postdoc in Tasmania gave me an excuse to visit it for the first time. Beautiful land, where one can go diving and hiking in the same day. Here in Alaska, Martin, Choly (Tschooli) and I enjoyed the trip in the Wrangell-St. Elias Range from Chisana (Shushana on old maps) to McCarthy. In the olden days apparently they took horses across this route that doesn't have a straw of grass over tens of miles. The use of horses in an area that produced large amounts of moonshine may explain the name of "Whiskey-Hill Glacier" that we passed. No matter how much I looked, I did not see any whiskey there anywhere. Biggest surprise was having to ford an opened Nizina River in March. That was cold. Thanks kid.

There are many others who are not mentioned by name, so let me finish by saying:

Thanks everyone!

Chapter 1

Introduction

It is now more than a decade since the first recorded images of upper atmospheric optical emissions above very active thunderstorms [*Franz* et al., 1990] brought to life a new field of aeronomy. Much has been learned in that decade, and much remains unknown. We have learned that there are many types of optical emissions at various time scales, corresponding to different discharge or breakdown types long known to discharge physicists. Due to the large number of optical emissions above active thunderstorms, which have been named sprites, elves, halos, embers/trolls, jets, etc, I will use the overall term Mesospheric Transient Luminous Events - "MeTLEs" - to describe these. This acronym expands on the acronym "TLE" used by previous researchers while specifying that the events occur in the upper atmosphere, specifically the mesosphere. Strictly speaking, some events occur outside of the mesosphere - either above, such as the elves, or below, such as jets or embers/trolls. Overall, however, the modified acronym better describes the overall group of phenomena by identifying that the events occur in the atmosphere near a specific atmospheric region. In the Introduction, I first describe the conditions and background of this investigation in order to lead into the four chapters presented as part of this thesis in Chapters 3-6. These chapters describe, respectively, the initiation of sprites, sprite varieties, the velocities of sprite tendrils, and events occurring after sprites.

1.1 Overview of Mesospheric Transient Luminous Events

Of MeTLEs (Mesospheric Transient Luminous Events), the best-known are (red) sprites [*Sentman* et al., 1995] and (blue) jets [*Wescott* et al., 1995]. Blue jets tend to appear above very active thunderstorms. They move upward from cloudtops as an upward-expanding cone of blue light, at speeds of 100 km/s. The upward propagation is readily visible in TV records. There also exists a phenomenon smaller than blue jet named a blue starter [*Wescott* et al., 1996a], which appears to start as a blue jet that terminates at a lower altitude. Blue jets and starters start in cloudtops and reach up to 40 km and 25 km, respectively. Compared with blue jets, sprites are brief in duration, and may have the appearance of a simple column centered near 70 km altitude with downward-splitting tendrils below it, or a more extensive region with downward-diverging tendril structures below and upward-diverging branch structure above topped by diffuse emissions near 85 km. The downward tendrils move with speeds on the order of below 10^6 to 10^8 m/s [*Stanley* et al., 1999; *McHarg* et al., 2002], and as a result sprites often appear on TV-rate videos from one frame to the next.

Of the lesser-known atmospheric MeTLEs, elves appear a fraction[1] of a ms before sprites as a very-fast expanding ring of diffuse emission above 90 km [*Barrington-Leigh* et al., 2001]. Photometers have been used to observe this expanding ring [*Barrington-Leigh and Inan*, 1999], which is not resolved on most imagers. Halos occur at nearly the same time as, or slightly before sprites, and are a disk of diffuse light near 75 km altitude and ~50 km in diameter [*Wescott* et al., 2001]. They are brighter than elves, and were initially misidentified as such [*Barrington-Leigh* et al., 2001].

Elves and halos generally precede sprites, though they can also appear in isolation. There is a separate class of MeTLEs that appear to occur only in the wakes of sprites. The three subsets of the phenomena, collectively known as "crawlers," appear with temporal delays of 30 - 100 ms following the parent sprites. One of these subsets of crawlers, termed smooth crawlers, are beads (small compact regions of luminosity) which brighten, within decayed sprite tendrils, and move upward at speeds of $10^4 - 10^5$ m/s, without any apparent connection to the underlying cloudtop[2]. A second subset of crawlers, called embers, can

---

[1] ~8/10 ms based on averaging of delays of 9 elves and halos/sprites observed with the high speed imager in this study

[2] Presented at Coupling, Energetics and Dynamics of Atmospheric Regions (CEDAR) conference in June 1999 in Boulder, Colorado. No proceedings or abstracts were published.

occur with the same time delay, but unlike smooth crawlers, they appear as a ribbon or channel connected to the underlying cloudtop[3]. They have also been called sprite-jets [*Stanley* et al., 1996] and trolls [*Lyons* et al., 1999]. Finally, a third subset of crawlers, termed "palm-trees', appear as a single stem connecting the cloudtops to a wider crown of emissions near 60 km [*Desroschers* et al., 1995], and may resemble embers. All of these optical emissions above active thunderstorms are summarized in Figure 1.1. In addition, other phenomena (dots, pixies) have been reported in the literature but have not yet been well documented [*Lyons* et al., 2001].
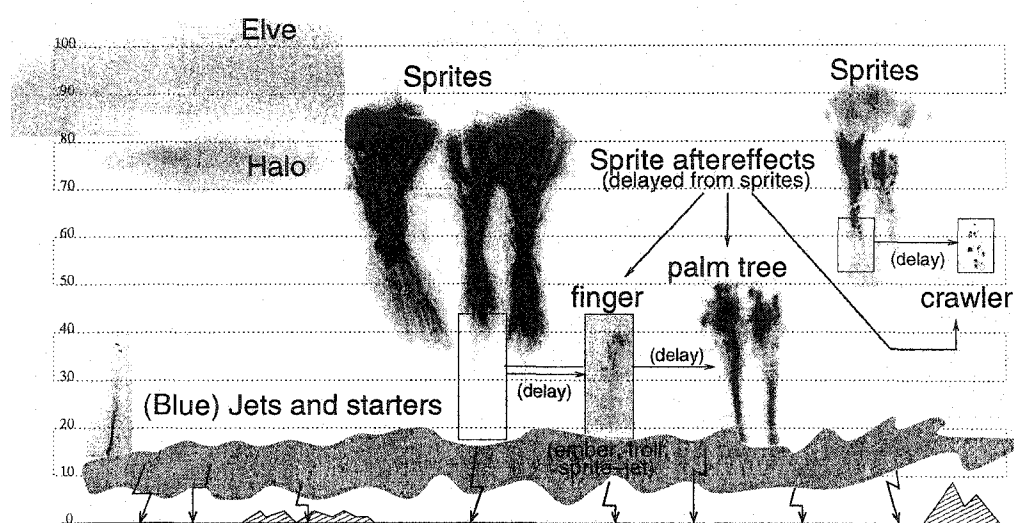
Figure 1.1. Examples of well-documented upper atmospheric emissions. On the left coming out of the cloud is a blue jet [*Wescott* et al., 1995]. All other phenomena are associated with a parent lightning flash (not shown). A very diffuse and dim emission near 90 km altitude is called an elve [*Barrington-Leigh* et al., 2001]. Also diffuse, but in lower altitude and brighter is a halo [*Wescott* et al., 2001]. Two groups of sprites are also shown [*Sentman* et al., 1995]. In the wake of sprites, in the region of sprite tendrils, occur three types of sprite aftereffects: (1) fingers [see footnote 2 for reference] or embers [*Stenbaek-Nielsen* et al., 2000] (2) palm trees [*Desroschers* et al., 1995], and (3) "smooth crawler" [see footnote 3 for reference].

---

[3]Also presented at CEDAR.

1.2   Statement of Thesis Investigation

1.2.1   Motivation for Investigation

Most sprite and halo observations have been made using CCD-based TV systems with 17 ms time resolution or photometers with 1 μs time resolution (1 - 16 pixel), giving either good temporal or spatial resolution, but not both. Images from the first high speed (0.3 - 1 ms time resolution) camera observations of sprites and halos were first published by *Stanley* et al. [1999] and *Barrington-Leigh* et al. [2001], respectively. Elves were not observed with cameras, with perhaps one exception [*Barrington-Leigh* et al., 2001]. Most elves have been observed with photometers [*Barrington-Leigh* et al., 2001].

For the 1999 Sprites NASA Balloon campaign, the University of Alaska Fairbanks deployed a 1 ms high speed imager into the field. Initial results from the campaign and from the high speed imager have already been described [*Bering III* et al., 2002; *Stenbaek-Nielsen* et al., 2000]. The higher time resolution compared to conventional television cameras (17 ms or 20 ms) allowed excellent images of the three phenomena temporally separate from each other to be obtained. Analysis of images of elves, halos, sprites, and sprite aftereffects constitutes the material in the four central chapters of this thesis.

1.2.2   Outline of Thesis

The four central chapters of this thesis have either been accepted for publication or are to be submitted. The first of the four chapters (Chapter 3) explores the initiation of sprites, and compares these observations to predictions by several theoretical models. The second chapter (Chapter 4) focuses on observations of different varieties of sprites. Chapter 5 explores the speed of sprite tendrils, and identifies previously unreported sideways propagation and multiple tendrils. Chapter 6 explores the phenomenology of the wakes of sprites, describing so-called "crawlers," in particular focusing on optical phenomena termed embers that move downward from stratospheric heights.

1.2.3   Summary of Thesis

Analysis of images of elves and halos indicates that the causal lightning-generated electromagnetic pulse and quasi-electro static fields are homogeneous and any small-scale (sub-

10 km) structure, if visible, is most likely due to a structured atmosphere. Observations of sprites initiated to the side of a halo, without a halo, and from beads left over from a previous sprite, respectively, all suggest sub-pixel (<0.5 km) background structures in atmospheric pressure or composition as being the dominant factors in determining the sprite "seed" location, or site of sprite initiation. This presentation, on elves, halos and sprite initiation, is presented in Chapter 3.

In Chapter 4, both TV rate (17 ms) images and 1 ms high speed images of sprites are presented, showing the development of a multitude of varieties of sprites. These sequences indicate that all sprites start with the downward development of tendrils. The characteristics of different optical emissions within sprites are described, separating optical emissions into dynamic and stationary forms. It is proposed that once a sprite is initiated, its shape and form is determined to a large extent by the temporal form and magnitude of the driving electric field emanating from the underlying thunderstorm.

In Chapter 5, the velocity and development of downward spatial structures known as tendrils are described. Examples are presented of multiple sets of temporally distinct tendrils that develop from the same sprite event and tendrils that have a horizontal component of expansion.

Lastly, streaks of luminosity have been reported to propagate upwards from the lower regions in sprite tendrils of some large sprites during the decay phase of an event. These are collectively called crawlers, and they are presented in Chapter 6.

1.2.4 Contribution of Investigation

To date, upper atmospheric optical phenomena have been loosely termed elves, halos and sprites, with occasional indications of other phenomena. Sprites have further been subclassified into columniform-sprites, carrot-sprites and jellyfish sprites. In this thesis, 1 ms time resolution images of the initiation, type of development and rate of development of these and other sprites are presented. Results indicate there are also many smaller sprite types than have been previously catalogued, and that there is little difference between the small sprite types and an intermediate stage of the large sprites. In turn, this indicates that growth of sprites depends mainly on electric field. In contrast, the initiation of sprites, as discussed in Chapter 3, is proposed to be mainly dependent on compositional variation

of the background atmosphere at mesospheric heights. In other words, it is proposed here that while sprites are initiated at sites determined by compositional inhomogeneities in the atmosphere, it is the electric field that determines the sprite form. These two determinations are new components in our understanding of initiation and development of sprites. As the sprite develops, multiple tendrils sometimes propagate downward from the upper portions of the sprite body. This results in additional complicated development within and above the sprite body, which has not yet been considered in sprite models. Also, in some cases, sprite tendrils propagating through the stratosphere slow down to 10^5 m/s, and/or propagate horizontally. Mechanisms leading to this behavior have not been considered to date. The decay behavior of sprite tendrils is the subject of Chapter 6, where the formation of sprite aftereffects collectively termed crawlers is considered, especially the unexpected behavior of sprite embers. Our observations of sprites, sprite aftereffects, and their dynamics at 1 ms time resolution constitutes additional new knowledge about upper atmospheric phenomena.

1.3   Region, Processes Investigated

In order to describe the optical emissions observed in the various campaigns and the models to explain the observations, in this section the region characteristics are described together with a basic information on processes, in particular collisional processes involving breakdown.

1.3.1   Composition and Temperature

Mesospheric Transient Luminous Events (MeTLEs) occur in or near the mesosphere. The mesosphere acts as a transition region between mainly molecular atmosphere below and increasingly hotter atomic and ionized atmosphere above. These properties are shown in the three panels of Figure 1.2.

At left are shown densities of molecular nitrogen and oxygen, and atomic oxygen. Both molecular species decrease approximately exponentially with height, seen with the nearly straight line on the log-scaled graph. Atomic oxygen is nearly nonexistent below 80 km altitude but dominates molecular oxygen above 120 km altitude. The data plotted were
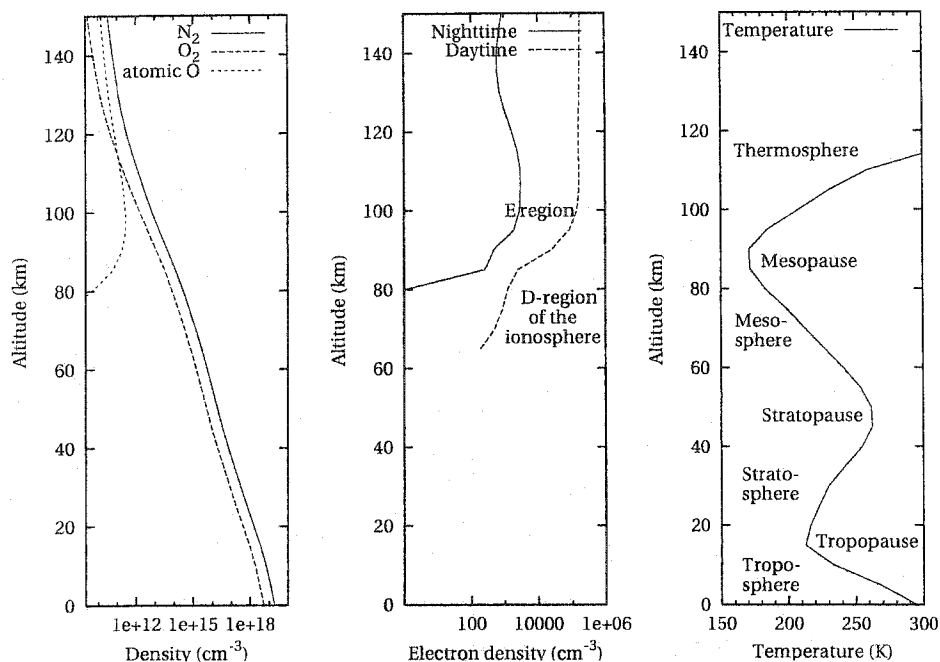
Figure 1.2. Profiles of densities and temperatures in altitudes up to 150 km. Data is for August 18, 1999 at 6 UT and 40N latitude and 100W longitude. Left: Densities of molecular nitrogen and oxygen, and atomic oxygen (MSIS-90 model). Center: electron densities at 6 UT (nighttime) and 18 UT (daytime) (IRI-95 model). Right: temperature (MSIS-90).

obtained from the MSIS-90 atmospheric model[4] for 6 UT (Universal Time) on August 18, 1999, at geographical coordinates 40° North and 100° West. The center panel shows data for electron density profiles for the same date and place, for both daytime (18 UT) and nighttime (6 UT), as determined by the IRI-95 ionospheric model[5]. The right panel shows the temperature profile from the MSIS model.

Lower atmospheric region names are based on either temperature or electron density. Dealing with the temperature-based nomenclature first, the lowest region of the atmosphere is the troposphere, from the ground up to approximately 15 km. In the troposphere the temperature decreases with height, highest temperature being close to the surface of the earth where most of the solar radiation is absorbed. Above 15 km, the decreasing temperature trend reverses, and the temperature of the atmosphere starts to increase, due to a

[4] Available at http://nssdc.gsfc.nasa.gov/space/model/models/msis.html.

[5] Available at http://nssdc.gsfc.nasa.gov/space/model/models/iri.html.

presence of ozone in this region. The ozone absorbs solar ultraviolet radiation, and that energy cascades through the system to other molecules, increasing temperature throughout and creating the stratosphere. The ozone layer protects life on earth from damaging ultraviolet radiation, yet owes its existence to animal life which first created the oxygen-rich atmosphere. The ozone is created from molecular oxygen via absorption of ultraviolet radiation. This radiation splits the oxygen molecule into two oxygen atoms, which can then react with another oxygen molecule to create ozone. In turn, ozone itself can be destroyed by sunlight. The balance between the source and loss reactions constrict ozone to a layer centered on approximately 30 km altitude.

The atmospheric temperature reaches a local maximum near 45 km altitude and, due to decreasing relative ozone concentrations, decreases above that altitude. This region of decreasing temperature with increasing altitude is the mesosphere. Its dominant composition is similar to the troposphere, though more rarefied. Minor species play important roles in the chemistry of the region due to their wide variety. The upper "end" of the mesosphere, termed the mesopause, also marks the approximate boundary above which a significant fraction of the atmosphere is ionized. Most positive ions in the mesosphere (below $\sim$90 km altitude) appear to be hydrated water molecule chains $H^+(H_2O)_n$, replaced by NO^+ and O_2^+ above 90 km [*Wayne*, 1991, p.293], and simpler ions in higher altitudes. Negative ion population characteristics are not well known, but many different chemical species appear to be involved [*Wayne*, 1991, p.298]. Terminal negative ions of the chemical processes in the mesosphere appear to be CO_3^-, HCO_3^-, and Cl^- [*Wayne*, 1991, p.293].

The mesopause is, during summer months, the coldest place in the terrestrial system, with temperatures below 200 K. This is the result of atmospheric winds and convection. It is in this very low temperature region that another, probably unrelated, phenomenon of recent interest resides, *viz.* polar noctilucent clouds, and polar mesospheric summer echoes. Future research may show whether both may be dependent on clusters of large molecules [*Baumgarten* et al., 2002; *Kirkwood* et al., 2002, see introductions of]. Slightly higher is a region in which thin metallic layers form, such as sodium (Na) near 92 km altitude [*Clemesha* et al., 1997] or iron (Fe) layers at 87-97 km altitude [*Raizada and Tepley*, 2002], also currently of great interest.

Atmospheric regions may also be defined in terms of their electron densities, as shown

in the center panel of Figure 1.2. During the daytime, electrons are created by sunlight and solar particles below 100 km altitude, the so-called ionospheric D-region. At night, the solar input disappears, and electrons either recombine with positive ions or form negative ions. The D-region thus nearly disappears, leaving electrons at higher altitudes, the E- and F-regions. Comparing Figure 1.2, we note that daytime D-region, determined from electron density profile, roughly overlaps with upper mesosphere, determined from the temperature profile.

The density of nitrogen molecules n_{N_2} can be approximated as an exponential function from the MSIS model output by an exponential function, in particular, for heights h below 80 km altitudes this function is

$$n_{N_2}(h) = n_{N_2}(80)e^{-\frac{h-80}{7.0}},$$

where density of nitrogen at 80 km is $n_{N_2}(80) = 3.1 \times 10^{14}/\text{cm}^3$, and overall particle density is $n_{N_2}/0.78$. Above 80 km altitude, the scale height decreases from 7.0 km to 5.3 km.

Similarly, the electron density n_e at night may be approximated for the upper mesosphere using the IRI model output. For the upper mesosphere at height $80 < h < 85$ kilometers,

$$n_e(h) = n_e(80)e^{\frac{h-80}{0.72}},$$

where the electron density at 80 km altitude is $n_e(80) = 1/\text{cm}^3$, and electron density at 85 km is $10^3/\text{cm}^3$. Above 85 km altitude the height scale doubles from ~ 0.72 km to ~ 1.4 km up to approximately 100 km altitude. The densities of both neutrals and electrons are important for electric field propagation and penetration, and electric breakdown, discussed in a later section.

1.3.2 Energy Inputs

Energy input into the stratosphere and the mesosphere is from both above and below. During daytime, the most important source of energy is the sun. Other sources, such as cosmic rays or auroral-type precipitation from above, or gravity wave and tidal forcing from below, become the dominant sources of energy at night. Gravity waves can be formed by mountains, by thunderstorms, or other sources. Modulation of nightglow (Na or oxygen) reveals the periodic signature of these waves, as well as cases of wave breaking and

the resulting turbulence [*Yamada* et al., 2001]. Thunderstorms drive both gravity waves and the global electrical circuit, which includes a downward fairweather electric field in areas without storms balancing the upward electric field of lightning regions. With the observations of sprites and other MeTLEs, the energy input into the mesosphere due to thunderstorms was shown to be more important than previously thought [*Heavner* et al., 2000]. In terms of molecular diffusion processes, eddy diffusion is the dominant mechanism below approximately 100 km altitude, compared to molecular diffusion.

1.3.3 Townsend Breakdown and Streamer Breakdown

In order to discuss the thunderstorm energy input into the mesosphere, we first take a detour into discharge physics and describe the processes occurring in a discharge. These will apply both to lightning and also to sprites, as well as perhaps other MeTLEs.

"Breakdown" in a medium is defined to occur when electrons multiply faster under an applied electric field than they disappear from attachment or recombination, resulting in a medium which becomes capable of carrying current at a substantially increased level. The multiplication of electrons is governed by their sources and sinks, a complete treatment of which can be found in *Raizer* [1997, Chapter 4]. Here, only one source and two sinks of electrons are considered: ionization, attachment and recombination. The rate of ionization can be expressed as $\nu_i n_e$, where n_e is the electron density, and ν_i is the ionization frequency, a frequency with which electrons collide with molecules, ionizing them. This rate of ionization assumes that only a single electron is knocked out of any molecule at a time. This rate is altitude-dependent, both on electron density and molecular density. Potentially important, but so far not treated in models of sprites, is the so-called step-wise ionization [*Raizer*, 1997, p.57], where molecules are first brought via a collision into an excited, but not ionized state, and subsequently ionized from the excited state. Due to this initial "step," less energy is required for the subsequent ionization. For example, in one type of plasma known as the "positive column" [*Raizer*, 1997, p.202], associative recombination and ionization $N_2 + N_2 \rightarrow N_4^+ + e$ of nitrogen in upper vibrational levels ≥ 16 takes place in relatively weak electric fields [*Raizer*, 1997, p.203]. Future models will show whether this process may be important in upper atmospheric glows.

For electrons moving within the gas, there are multiple sinks. Electrons can attach to

molecules forming negative ions at a rate equal to $\nu_a n_e$ where ν_a is the attachment frequency. Electrons can also recombine with positive ions such as those left over from ionization, at a rate equal to $\nu_r n_e$ where ν_r is the recombination frequency. Other loss terms may include diffusional losses, which are important in laboratory discharges [*Raizer*, 1997, p.143, 203]. Attachment is thought to be the dominant sink term for near-breakdown regimes [*Bazelyan and Raizer*, 1997], giving the following relation for breakdown to occur:

$$\frac{dn_e}{dt} = (\nu_i - \nu_a)n_e > 0.$$

This relation indicates the necessary condition for creation of an electron avalanche, where under a sufficiently large electric field, one seed electron ionizes a molecule, freeing another electron, and both of these electrons ionize other molecules, etc., creating an avalanche. It needs to be noted that the creation of an avalanche, at not very high electric fields or pressures, depends on both the electric field magnitude E and the molecular density n, specifically on the E/n ratio. This dependence allows one to consider breakdown conditions for high altitudes by comparing them to similar E/n conditions in laboratory.

The E/n dependence can be arrived at as follows: both the inization frequency ν_i and attachment frequency ν_a depend on electron drift in the applied field E. The drift veolcity of electrons in an applied electric field is given by

$$\vec{v}_{drift} = \mu_e \vec{E},$$

where μ_e is the mobility of electrons, relating the velocity to the electric field. The mobility is in turn defined as

$$\mu_e = -e/m_e \nu_m,$$

with ν_m being the collision frequency of electrons with neutral molecules. This collision frequency (ν_m) depends on molecular density n, *i.e.* $\nu_m \propto n$. Retracing the steps, the mobility is then inversely proportional to density, $\mu_e \propto 1/n$, and the drift velocity is dependent on the E/n ratio:

$$\vec{v}_{drift} \propto \frac{E}{n}.$$

Since both attachment and ionization frequencies depend on the electron speed in the applied electric field, both ν_i and ν_a can be plotted on a graph as a function of E/n, as

Ionization & Attachment vs. E/N
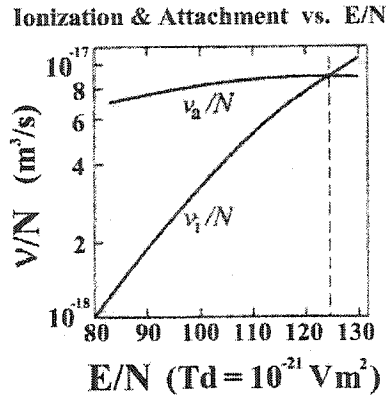
Figure 1.3. Attachment frequency ν_a and ionization frequency ν_i as a function of E/n. Figure is from *Stanley* [2000], Figure 2.1, referencing *Bazelyan and Raizer* [1997].

shown in Figure 1.3. When ionization exceeds attachment, to the right of the dashed curve in the figure at a value of 123 Td, breakdown occurs.

The electron cloud forming the avalanche initially expands by a diffusion process [*Raizer*, 1997, p.328], but as the population of the electron cloud reaches approximately 10^6 electrons [*Raizer*, 1997, p.333], electrostatic repulsion takes over and the expansion rate of the electron cloud is increased [*Raizer*, 1997, p.333], beginning the transition from an avalanche to a so-called streamer. The separation of the ions and electrons within the cloud creates a larger field in front of the avalanche, and smaller field between the two charge centers. When the electron cloud reaches the size of approximately one ionization length, the expansion of the cloud nearly ceases [*Raizer*, 1997, p.334], and the streamer continues its propagation with nearly constant cross-sectional radius if conditions do not change.

The streamer propagates at speeds greater than the electron drift speed due to photoemission in the streamer head ionizing molecules in front of the streamer [*Raizer*, 1997, p.335] and creating free electrons. Depending on the direction of the electric field, small avalanches form either towards or away from the streamer head from the electrons created by ionization. The ends of these small avalanches closer to the streamer head neutralize the streamer head, while the farther ends create the new streamer head. The streamer body thus consists of a weakly ionized neutral plasma, unlike an avalanche, in which the charges are separated. Since the field is enhanced in front of the streamer head, while the

photons are emitted homogeneously in all directions, there is a slightly preferred direction of propagation. The randomness of the emitted photons within the preferred direction may account for some of the zig-zagging nature of streamers [*Raizer*, 1997, p.336]. At present it is assumed that it is oxygen molecules which are ionized by photons emitted from highly excited nitrogen molecules [*Raizer*, 1997, p.337], since oxygen requires less energy for ionization than nitrogen.

A schematic of the seed electron to avalanche to streamer transition is shown in Figure 1.4, for a given laboratory geometry between two plates. In this geometry, a streamer crossing the gap often results in a return wave through the weakly ionized plasma left behind by the streamer, creating a spark, which further expands the channel due to Joule heating. With some simplifications (discussed in next paragraph), Figure 1.4 could represent a lightning discharge: the cathode plate representing a thundercloud from which lightning originates, the anode plate representing the ground. When the streamer connects to the ground, the ionizing wave travels back up the channel, with increasing current resulting in channel expansion, would be equivalent to a return stroke of lightning.

1.3.4 Lightning: Leader Breakdown

Lightning, the tropospheric discharge causing many of the MeTLEs, is a complex phenomenon. In the simplest model, a thundercloud consists of two charge regions, generally a negative charge region in the lower part of the cloud and a positive charge region in the upper part. Either of the two regions can be discharged to ground. Lightning neutralizing the positive charge to ground is called positive cloud-to-ground (+CG) lightning or discharge, lightning neutralizing negative charge to ground is -CG. Intracloud lightning, where parts of the positive and negative charge in the cloud neutralize each other, can also occur.

In lightning, the breakdown process is extended one step further beyond the streamer, due to the large distances involved. Similarly, as many small electron avalanches feed a streamer head, in lightning it is many streamers that feed a so-called leader. The main difference between a streamer and a leader is that a streamer has a finite conductivity and its head does not have the same electric potential as the location where it started from. In contrast, a leader is highly conductive and transfers the potential of its starting point to its head much more effectively [*Raizer*, 1997, p.364]. As the leader advances, the same electric
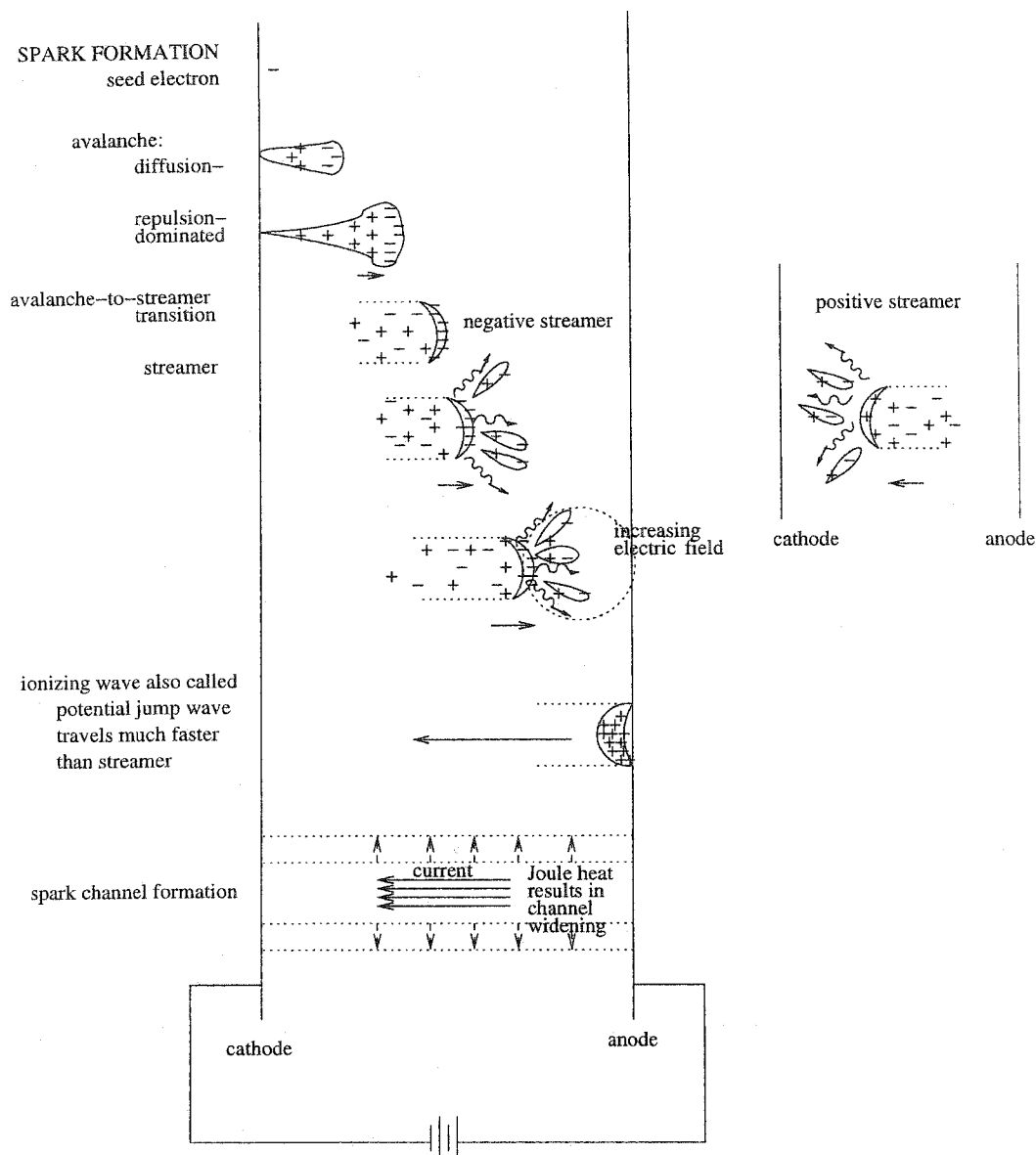
Figure 1.4. Spark channel formation in laboratory conditions starts with seed electrons forming avalanches. The avalanche moves with electron drift speed. In the wake are left positive ions. The avalanche head initially widens due to diffusion, but at some point becomes large enough that the faster electron repulsion takes over as the main mechanism for widening. At a certain size, the avalanche transforms into a streamer, no longer with a widening head. The streamer moves at a speed greater than that of the avalanche. In the body of a streamer the plasma is electrically neutral. As the streamer nears the electrode, the intense electric field creates high ionization, and a returning potential jump is set up, moving again much faster than the streamer, leaving behind a dense plasma.

potential which was originally applied across the entire gap is now applied only between the leader head and the anode, resulting in an increased electric field. Just as streamers can be either positive or negative, reflecting the charge in the head, so also can leaders.

The mechanism of electron density growth to create higher conductivities within a leader has been suggested to be due to Joule heating liberating electrons that had attached to oxygen molecules, forming O_2^- [*Raizer*, 1997, p.365]. The Joule heating comes from the combined efforts of the currents in the multiple streamers converging at the head of the leader. The elevated temperature in a leader head results in decreased attachment compared to a streamer [*Raizer*, 1997, p.368]. In order for Figure 1.4 to reflect a lightning discharge, a leader formation should be included between streamer propagation and the return ionizing wave.

A lightning flash often has more than one stroke, each composed of a leader followed by a return stroke. The above description of leaders works for leaders initiating second or later return strokes of lightning, but not for the first. While the formation of the first "stepped leader" of a lightning discharge is not understood, Figure 1.5, taken from *Raizer*[1997, Figure 12.21], shows a suggestion for its formation. On the right of Figure 1.5b is shown a snapshot at some point in time, while Figure 1.5a shows a scan of the same features as a function of time. Raizer suggests that in front of the leader tip (denoted by (1) in the figure), a plasma blob (4) appears. This leader is attached to an "electrode" or charge region, keeping its electric potential constant. Between the leader and blob, streamers bridge the moving gap as both the leader and blob propagate under the applied electric field, downward in this picture. In front of the blob, steamers of opposite polarity forge the way ahead. At some point, leaders initiate from both ends of the blob, one leader moving towards the attached leader, the other towards the blob which is again ahead. When the attached leader joins with the leader coming from the former blob, a surge in current produces optical emisions and the leader channel can be observed momentarily as a step of the stepped leader (6). This procedure, of two leaders coming off the blob at some point in time and growing to join the attached leader, resulting in optical emissions, repeats in time until the stepped leader hits the ground. The times of attachment of the leaders are the so-called steps of a stepped-leader.

When a stepped leader hits the ground, a return wave, equivalent to that described at
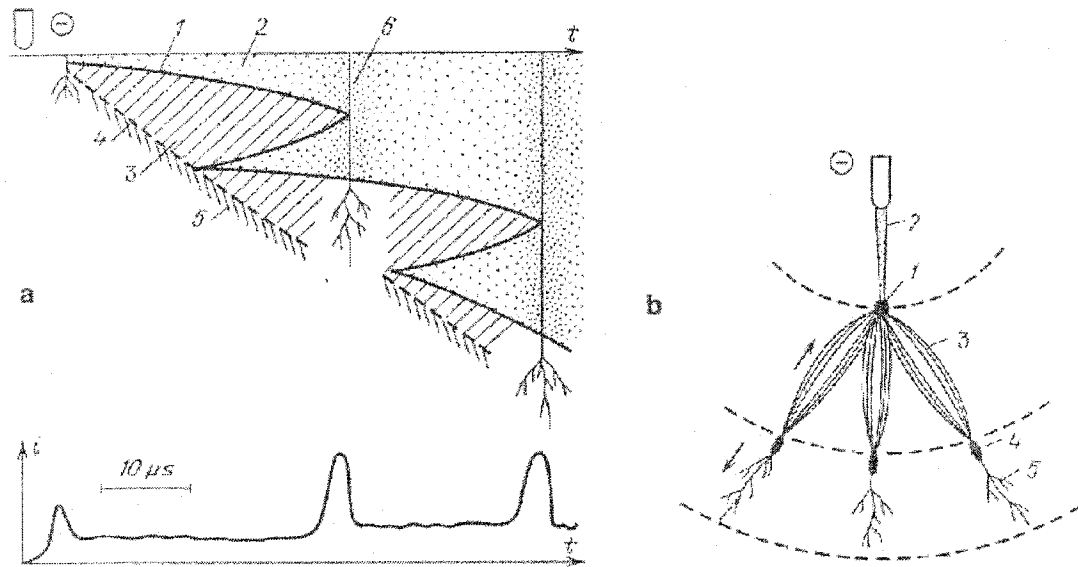
Figure 1.5. Step-leader process of lightning. Figure is from is from [*Raizer*, 1997, Fig. 12.21]. Figure (a) shows the time evolution of a negative step leader evolution, (b) shows the process at some point in time. The numbers refer to the same elements. (1) is head of the leader channel, (2) leader channel, (3) cathode-directed streamers starting from a plasma blob (hypothetical leader propagating in both directions), (4) plasma "blob," (5) anode-directed streamers, (6) a step of the leader (in (a) only).

the end of Section 1.3.3 moves back up the channel, expanding it via Joule heating and resulting in a return stroke. Current that may flow for a longer period of time following a return stroke is known as continuing current. During the continuing current, the lightning channel may be luminous. A brightening of the lightning channel during continuing current with an associated rapid electric field variation is known as an "M-component" [*Uman*, 1987, p.173]. M-components are associated with steplike electric field changes when measured on ground near the lightning, similar to "K-changes," which occur in periods of no continuing current. Following a return stroke, additional leaders from newly tapped charge regions can propagate down from the cloud resulting in additional return strokes, re-brightening the lightning channel. These "dart" leaders move in the simpler way outlined in the first half of Section 1.3.4 as opposed to the more complicated way outlined in Figure 1.5.

1.3.5 Lightning Parameters

Sprites appear to have a strong correlation to positive cloud-to-ground lightning [*Boccippio* et al., 1995], though there exist sprite events that have been associated with -CGs [*Barrington-Leigh* et al., 1999a]. This section will thus focus on +CGs. *Uman* [1987] references multiple sources that find that +CG's as a fraction of total CGs range from 0 to 30% [p.188]. Most +CGs consist of a single stroke [p.190], half or more have continuing currents [p.196], and in one study of a severe storm, the percentage of positive flashes increased with the age of the storm [p.190]. Electric fields due to continuing currents were on average 50-120 ms in duration, ranging between 5 and 240 ms [p.196]. Flash duration ranged from 100 to 1200 msec [p.196]. The rise time of vertical electric fields from 10 to 90% of peak occurs in 4-8 μs [p.197].

Comparing return stroke currents for negative and positive CGs, 50% of +CG return stroke currents exceeded 35 kA, and 5% exceeded 250 kA; respectively compared with 30 kA and 80 kA for -CGs [*Uman*, 1987, p.124]. In terms of charge transferred, there is even a larger difference: 50% of +CGs transferred more than 80 C, and 5% transferred more than 350 C, compared with 7.5 C and 40 C for -CGs [p.124]. These statistics show that while +CGs tend to be rarer than -CGs, they tend to have larger currents and transfer more charge.

1.3.6 Effects of Lightning on Upper Atmosphere

The thunderstorms create both longer duration, smaller amplitude electric fields due to the charges within the storm, and shorter duration, larger amplitude fields due to individual lightning strokes within the storm. A good analytical treatment of fields due to a lightning stroke was given by *Fernsler and Rowland* [1996]. In short, if we take the charge moment of the lightning to be $M =$ (charge $\times$ altitude of charge), the electric field a distance r away will have a quasistatic component proportional to $\frac{M}{r^3}$, an inductive component proportional to $\frac{M'}{r^2}$, and a radiative component proportional to $\frac{M''}{r}$, also called the electromagnetic pulse. M' and M'' denote first and second derivative with respect to time, respectively. The three different components of the electric field maximize at different times and at different frequencies and depend on the specific current profile of the lightning discharge. The time-

dependent field acts collectively on any free electrons, accelerating them, as can be described by a classic plasma theory approach. The electrons also interact with molecules, exciting or ionizing them, or both, and if the electric field exceeds the critical field for breakdown, may form into a discharge. Subsequent interaction between all the species may be treated by a standard atmospheric chemistry approach. The excited molecules may undergo spontaneous emission, resulting in optical emissions, which may be observed by suitable sensors if the photons are not scattered or absorbed on the way through the intervening atmosphere.

In order to treat the electromagnetic fields from a thunderstorm in more detail, Maxwell's electrodynamic equations are introduced. These describe the electric and magnetic fields in terms of their sources (charges, currents, etc) and in cgs units are

$$\nabla \cdot \vec{E} = 4\pi\rho \qquad \nabla \cdot \vec{B} = 0$$

$$\nabla \times \vec{E} = -\frac{1}{c}\frac{\partial \vec{B}}{\partial t} \qquad \nabla \times \vec{B} = \frac{1}{c}\frac{\partial \vec{E}}{\partial t} + \frac{4\pi}{c}\vec{J}$$

where $\vec{E}$ and $\vec{B}$ are the electric and magnetic fields, respectively, ρ is the charge, $\vec{J}$ is the electric current, c is the speed of light, and t is time [*Jackson*, 1975].

Let us consider a brief treatment of the quasistatic and radiative fields here, following the example of *Fernsler and Rowland* [1996]. Consider the return stroke current J that moves at a speed βc along z-axis, from which distance ρ is measured in cylindrical coordinates. The current may be specified as:

$$J(\rho, z, t) = \beta c Q_z(\rho, z, t) = J_o\delta(\rho)H(z)H(t - z/\beta c),$$

where Q_z is the distributed charge, δ is the Dirac delta function constraining the current to the z-axis, and H are Heaviside step functions. Additional charge Q needs be placed at discharge origin for conservation, and is given by $Q(\rho, z, t) = -J_o t H(t)\delta(\rho)\delta(z)$. The vector potential is generically determined from: $\vec{A} = \frac{\mu_o}{4\pi}\int \frac{\vec{J}}{r}d\tau$ so the z-component becomes: $A_z(\rho, z, t) = \frac{1}{c}\int_0^{z_d} dz' \frac{J_o}{\sqrt{\rho^2 + (z - z')^2}}$ where z_d is the retarded lightning discharge length[6]. From these, the vector and scalar potential may be calculated:

$$A_z(\rho, z, t) = \frac{1}{c}\int_{-\infty}^{+\infty} dz' \frac{J(z', t - \sqrt{\rho^2 + (z - z')^2}/c)}{\sqrt{\rho^2 + (z - z')^2}} = \frac{J_o}{c}\int_0^{z_d} \frac{1}{\sqrt{\rho^2 + (z - z')^2}}$$

---

[6]the length that the lightning appears to be to an observer stationed at the sprite location at a particular time t

$$\phi(\rho, z, t) = \frac{A_z(\rho, z, t)}{\beta} - \frac{(t - r/c)J_o}{r} H(t - r/c),$$

where $r = (\rho^2 + z^2)^{1/2}$ is distance from the origin of both the coordinates and of lightning. These equations can be reduced by the far-field approximation assuming $r \gg z_d$. The total radiation field is then

$$E_\theta = \frac{\beta I_o}{zc} \frac{sin2\theta}{1 - \beta^2 cos^2\theta},$$

where θ is the angle from vertical to the sprite direction. The radiation field has two maxima, one direct from the source, and one from the image currents. Here, reflections off the ionosphere have been ignored.

Quasielectrostatic fields from continuing currents may be estimated by using the scalar potential, without retardation effects:

$$\phi(\rho, z, t) = J_o t \left(\frac{1}{\sqrt{\rho^2 + (z - z_d)^2}} - \frac{1}{\sqrt{\rho^2 + z^2}} \right)$$

yielding

$$E_\rho(r, \theta, t) = \frac{2J_o t z_d}{r^3} \cos(\theta) = \frac{2M}{r^3} \cos(\theta)$$

$$E_\theta(r, \theta, t) = \frac{J_o t z_d}{r^3} \sin(\theta) = \frac{M}{r^3} \sin(\theta),$$

where $J_o t = Q$ is the total charge transferred, and $Q z_d = M$ is the charge moment. Including the conducting ground for vertical discharges results in doubling of z_d, which doubles the electric field. Ionospheric reflection can also be included.

1.3.7 Plasma Treatment

The electric field acts on all electrons, both those present initially and any liberated by ionization. Plasma treatment allows for calculation of various quantities of interest without having to follow every individual electron. The distribution function $f_s(\vec{x}, \vec{v}, t)$ defines the number of electrons at a particular time t within a volume $x \ldots (x + \delta x), y \ldots (y + \delta y), z \ldots (z + \delta z)$, whose velocity is within the range $\vec{v}$ to $\vec{v} + \Delta \vec{v}$. From the electron distribution function f_s, the current and charge as a function of space and time may be obtained by integrating over the velocity space:

$$\rho(\vec{x}, t) = e \int d\vec{v} \, f_s(\vec{x}, \vec{v}, t)$$

$$\vec{J}(\vec{x}, t) = e \int d\vec{v} \, \vec{v} \, f_s(\vec{x}, \vec{v}, t).$$

Taking the total time derivative of the electron distribution function $\frac{D}{Dt}$ yields how the electron distribution is changing in time due to external forcing, and this value must equal the differential change per unit time due to interval sources and sinks, or the Boltzmann equation:

$$\frac{D}{Dt}f_s(\vec{x},\vec{v},t) =$$

$$\frac{\partial f_s(\vec{x},\vec{v},t)}{\partial t} + [\frac{d\vec{x}}{dt}\cdot\nabla_x]f_s(\vec{x},\vec{v},t) + [\frac{d\vec{v}}{dt}\cdot\nabla_v]f_s(\vec{x},\vec{v},t) =$$

$$\frac{\partial f_s(\vec{x},\vec{v},t)}{\partial t} + [\vec{v}\cdot\nabla_v]f_s(\vec{x},\vec{v},t) + \frac{e}{m_e}[(\vec{E}+\frac{\vec{v}}{c}\times\vec{B})\cdot\nabla_v]f_s(\vec{x},\vec{v},t) = sources - sinks,$$

where we used velocity $\vec{v} = \frac{d\vec{x}}{dt}$, acceleration $\vec{a} = \frac{d\vec{v}}{dt}$, and Newton's law $\vec{F} = m\vec{a}$ to substitute the force $\vec{F} = \frac{e}{m_e}(\vec{E}+\frac{\vec{v}}{c}\times\vec{B})$ felt by a charged particle in electric and magnetic fields into the above equation. The electric and magnetic fields in these equations satisfy Maxwell's equations described in Section 1.3.6.

On the right side of the Boltzmann equation is the term $(sources - sinks)$. When this term is null, the equation becomes the Vlasov equation. In the case of MeTLEs however, this term is non-null, and describes the collisions of electrons with molecules, exciting them. The excited molecules then undergo either spontaneous decay and emit a photon which we may observe as the MeTLE, or collide with other molecules and transfer some or all of the energy to the colliding particle.

Whether the collisional $(sources - sinks)$ term in the Boltzmann equation is important depends on the specific collisional regime under consideration. Space and plasma physics study systems in different regimes of electron density and electron temperature. Figure 1.6 shows these regimes in terms of the above-mentioned variables, without any reference to the $(sources - sinks)$ term. Overlaid on this plot is also the region occupied by MeTLEs, sprites in particular, which occur in the D-region of the atmosphere where the background electron number density is in the 1-1000/cm^3 range. Within sprites, the electron densities are higher than the background, and the electron temperature is in the eV range [*Green* et al., 1996; *Morrill* et al., 2002]. The main distinguishing feature between the various regimes in the vicinity of sprites, and sprites, is then the $(sources - sinks)$ term in the Boltzmann equation. Sprites occur in a highly collisional regime.

Sprites have not been observed with strong ionization signature [*Heavner*, 2000], in-
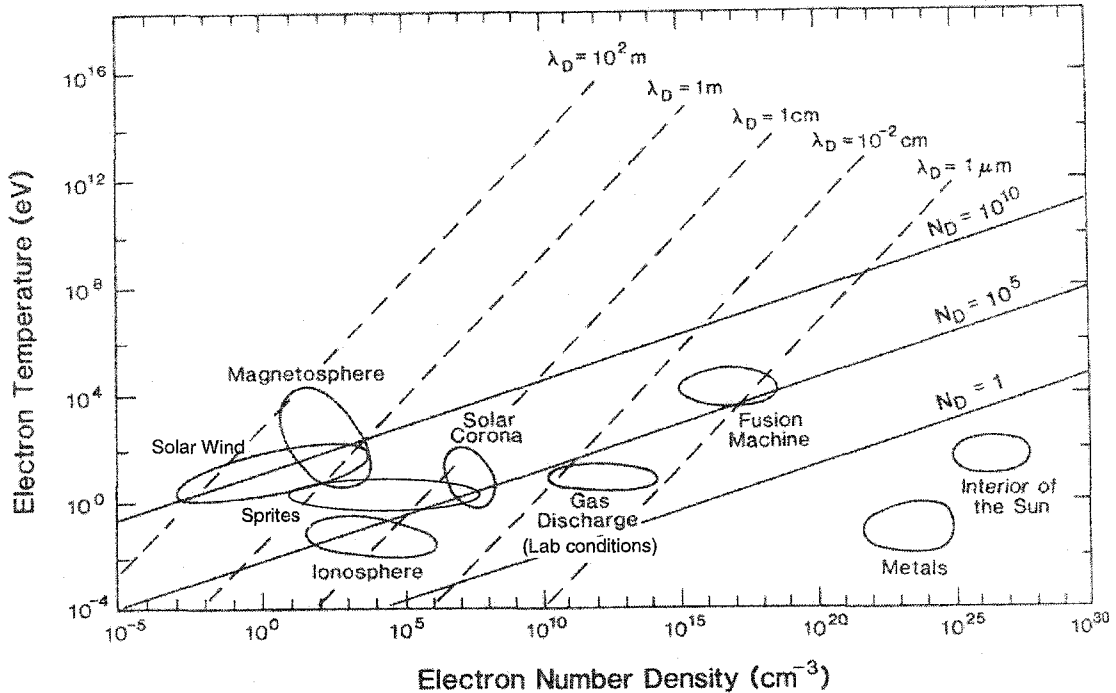
Figure 1.6. Regimes of plasma physics in terms of electron number density and electron temperature. Figure is from *Kivelson* [1995], their Fig. 2.4, overlaid with typical electron density and temperature regime found in sprites. λ_D refers to Debye length, and N_D to number of particles in a Debye sphere.

dicating that the electron temperature is on average below 10 eV, and that most of the electrons participating in the sprite dynamics are either free electrons or detached electrons split from negative ions, but not from ionization of neutral molecules. As such, the region of sprites in Figure 1.6 is quite constrained. Other MeTLEs may occur in regions without any free electrons but with non-zero negative ion density. Thus, the other MeTLEs are likely to occur in the same general plasma regime as sprites on the electron density vs electron temperature graph. Gas discharge physics is currently undergoing strong advances in terms of numerical simulation [e.g. *Kulikovsky*, 2000]. However, gas discharges in lightning and laboratory set-ups occur under different electron density conditions. Sprites, currently understood to be discharges, may thus prove important for validating the models and theories of discharge physics in conditions different from typical laboratory conditions.

1.3.8 Particle and Photon Processes

Electrons (e) accelerated by the electric fields, photons ($h\nu$), and atoms and molecules (A, B, AB, ...) can undergo the processes outlined in Table 1.1 when colliding with molecules. A star (*), double star or dagger (†) indicate molecules or atoms in excited electronic states. Plus ($^+$) or minus ($^-$) superscripts indicate positive and negative ions, respectively. Processes believed to play a role in sprites are in bold.

Possible perturbations could potentially occur in the densities of NO, N_2O and other important greenhouse gases due to sprites. Such perturbations have been suggested [*Green et al.*, 1996; *Stenbaek-Nielsen* et al., 2000] but so far no calculations have been published.

1.3.9 Excitation and Optical Emissions

The collisions between electrons and molecules can be approximated using the scattering cross section, if enough collisions occur to allow a statistical approach. The scattering cross section depends both on angle and energy of the incoming electron, assuming the molecule is stationary relative to the electron. The scattering cross section may also be averaged over all scattering angles to give the total scattering cross section, dependent on energy only. This cross section σ for various molecules, as a function of energy, is often found in books on auroral physics [*Rees*, 1989; *Vallance Jones*, 1974]. The rate ν_{exc} at which the molecules of nitrogen are excited into an electronic state is then given by

$$\nu_{exc} = \int_E \sigma(E)\phi_e(E)n_{N_2}dE,$$

where n_{N_2} is the number density of molecules in the ground state and ϕ_e is the flux of electrons, given by velocity and density of electrons. A similar expression, with appropriate cross-section and density, is valid for oxygen and other species.

However, this approach only gives the rate of particle excitation by electrons, and not the total number of particles in the upper state. A more rigorous approach includes the rate of decay of excited particles due to spontaneous emission, creation of excited particles due to a cascade from a higher-level state, and energy pooling.

The excited states of a diatomic molecule, such as N_2 or O_2, are designated by a label which includes a single letter designation together with the quantum numbers of the state. For example, the most common molecular nitrogen states discussed in sprites are the neutral

Table 1.1. List of electron, photon and chemical processes, in terms of excitation, ionization, decay, and chemical reactions. Those believed to play a role in sprites are in **bold**.

Excitation by electron impact, photon or collision

$A + e$	$\rightarrow$	$A^* + e$	**Electron impact excitation**
$A + h\nu$	$\rightarrow$	A^*	Photoexcitation
$A^* + B^*$	$\rightarrow$	$A^{**} + B$	**Energy pooling**
AB^*	$\rightarrow$	$AB^\dagger$	Intramolecular energy transfer
$A^* + B$	$\rightarrow$	$A^\dagger + B$	**Intersystem collisional transfer**
$AB^* + CD$	$\rightarrow$	$AB + CD^*$	Intermolecular energy transfer
$AB + CD$	$\rightarrow$	$AC^* + BD$	Chemical reaction

Ionization (detachment), attachment

$A + e$	$\rightarrow$	$A^+(^*) + e + e$ (or A^-)	**Electron impact ionization**
$A^* + e$	$\rightarrow$	$A^+(^*) + e + e$	Step-wise ionization
$A + h\nu$	$\rightarrow$	$A^+ + e$ (via AB^*)	**Photoionization**
A^*	$\rightarrow$	$A^+ + e$	**Ionization**
$A + e$	$\rightarrow$	A^-	**(Electron) attachment**
$A^+ + e$	$\rightarrow$	A	Recombination
$A^+ + B^-$	$\rightarrow$	AB	Associative recombination
$AB + e$	$\rightarrow$	$A + B^-$	Dissociative attachment
$A + B^-$	$\rightarrow$	$A^- + B$	Charge transfer

Decay, often via photon emission

$AB + CD$	$\rightarrow$	$AC^* + BD$	
	$\rightarrow$	$AC + h\nu + BD$	Chemiluminescence
A^*	$\rightarrow$	$A + h\nu$	**Spontaneous emission, luminescence**
$A^* + h\nu$	$\rightarrow$	$A + h\nu + h\nu$	Stimulated emission
$A + h\nu$	$\rightarrow$	$A^* \rightarrow A + h\nu$	Fluorescence
A^{**}	$\rightarrow$	$A^* + h\nu$	**Cascade**
$A^* + B$	$\rightarrow$	$A + B$	**Quenching** (collisional de-excitation)

Reactions

$AB + e$	$\rightarrow$	$A + B + e$ (via AB^*)	Electron impact dissociation
$AB + h\nu$	$\rightarrow$	$A + B$ (via AB^*)	Photolysis
$AB + C$	$\rightarrow$	$A + BC$	Chemical reaction
AB^*	$\rightarrow$	$A + B(^*)$	Dissociation

states $C^3\Pi_u$, $B^3\Pi_g$, and $A^3\Sigma_u^+$, also called the C-state, B-state, or A-state, respectively. All are triplet states, with a degeneracy of 3, meaning the spin quantum number S is equal to 1, such that $2S + 1 = 3$. The capital greek letter denotes the total angular momentum L about the intermolecular axis, with $\Sigma = 0$, $\Pi = 1$, and, not shown, $\Delta = 2$. This is similar to atomic angular momentum designations s, p, d, f, ... The subscript denotes the parity of the quantum state under inversion through center, either g = gerade (even) parity or u = ungerade (odd) parity. Lastly, a superscript for Σ states denotes even (+) or odd (-) parity under reflection in plane containing the bond axis [*Svanberg*, 1991].

The molecule in an excited state may spontaneously relax into a lower state by emitting a photon. Electric dipole transitions possess the highest occurrence probability and thus have a short lifetime. These have the following change in the quantum numbers between the upper and lower levels: $\Delta S = 0$; $\Delta L = 0, \pm 1$; inversion: switched (g $\rightarrow$ u, or u $\rightarrow$ g); and, for Σ states, reflection: same (+ $\rightarrow$ +, or - $\rightarrow$ -). The first two rules are more important, and transitions violating one of them will be less likely to occur than those violating one of the other two, the upper states of these transitions will have longer lifetimes. A longer radiative lifetime results in a greater possibility of a collision occurring before the molecule can spontaneously emit light. A molecule in an excited state undergoing a collision has elevated internal energy compared to its ground state, and in the collision may undergo a chemical reaction.

The probability of spontaneous transition by photon emission is given by the Einstein coefficient A_{nm}. Multiplying the population density of the upper state of a molecule with the Einstein coefficient for that transition from that upper state yields the number of photons emitted per unit volume per unit time, under the assumption of no collisions. Any collision of the excited molecule with some other molecule will decrease the number of molecules available for spontaneous emission. For example, the rate of change of density of nitrogen in the B sate is given by:

$$\frac{\partial [N_2(B)]}{\partial t} = -A_{21}[N_2(B)] + A_{32}[N_2(C)] + \nu_{exc} - k_1[N_2(B)][O_2] - k_2[N_2(B)][N_2] + sources - sinks,$$

where $[N_2(B)]$ is the density of the species $N_2(B)$, A_{21} is the Einstein coefficient for spontaneous decay for B state into A state, A_{31} is that for C to B state, ν_{exc} is the rate of excitation of nitrogen into the B state by electron impact, k_1 and k_2 denote the rate constants of the

quenching of nitrogen in the B state by O_2 and N_2, respectively, and any other *sources* and *sinks* can be specified.

1.3.10 Atmospheric Transmission

Any photon emitted by a source in the upper atmosphere propagates through the atmosphere in order to reach the observer. Rayleigh scattering of photons interacting with neutrals is proportional to $1/\lambda^4$ for a given scattering particle interacting with a photon of wavelength λ. This results in blue light (wavelengths near 400 nm) being much more strongly scattered than red light (wavelengths near 650 nm). In addition to Rayleigh scattering, additional processes may prevent a photon of a particular wavelength from reaching the observer, such as by absorption by atmospheric constituents. Water vapor in the atmosphere strongly absorbs in the 500-650 nm region, as well as particular bands of molecular oxygen.

A modeled transmittence of the atmosphere, computed for a source at 65 km altitude and 500 km range, is shown in Figure 1.7. Four different observer altitudes were used: 20 km, 10 km, 5 km and 0 km, shown in the top-to-bottom curves, respectively. The model used was a radiative transfer model named MOSART: Moderate Spectral Atmospheric Radiance and Transmittance Code[7].

1.4 Background and History

Having described the region in which MeTLEs occur and some of the characteristics and processes occurring there, we next describe the "historical" search for optical emissions above thunderstorms up to present.

1.4.1 Wilson Speculations

Anecdotal reports of upward lightning and flashes above thunderstorms have been reported as early as the late 19th century [*Franz* et al., 1990, and references therein]. In 1925, C.T.R. Wilson predicted that discharges may occur in the atmosphere above thunderstorms by speculating that

---

[7]Information available at http://www2.bc.edu/~sullivab/soft/mosart.html.
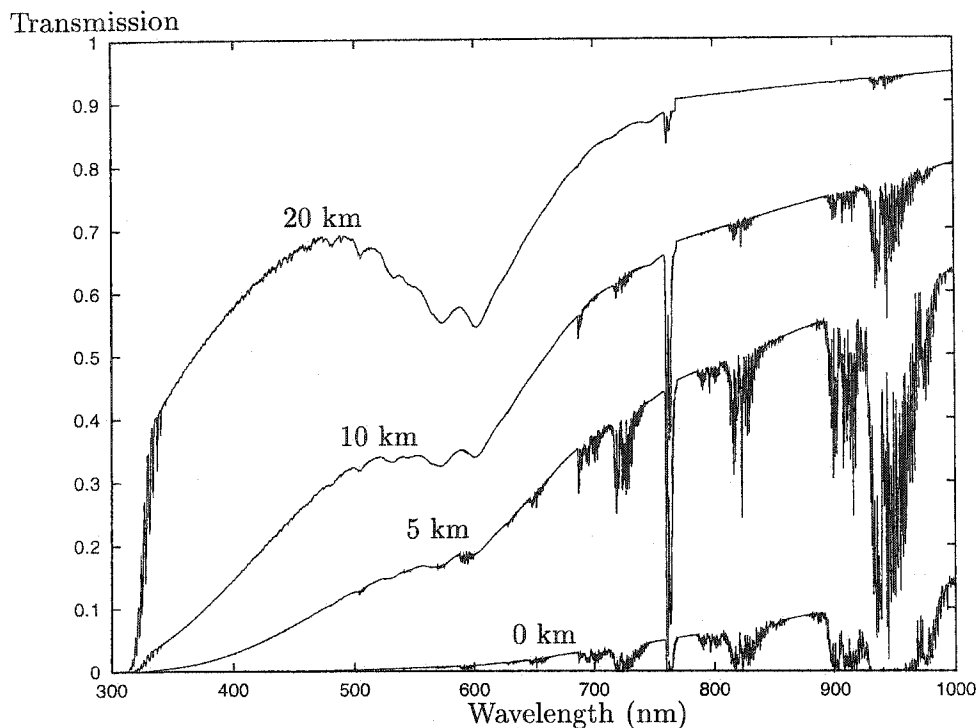
Figure 1.7. Atmospheric transmission at 500 km range for a source at 65 km altitude and an observer at 0 km, 5 km, 10 km and 20 km altitude. [Matt Heavner, private communication, 2002.]

> "... the electric field of a [thunder]cloud may cause ionization at great heights, the result being continuous or discontinuous discharge between the cloud and the upper atmosphere ..."

[*Wilson*, 1925]. Thirty years later, he restated his prediction that

> "... what is likely to be a more normal accompaniment of a discharge to earth, but one which is only likely to be visible under very special conditions, is a diffuse discharge [above the clouds] ..."

[*Wilson*, 1956]. In this second paper, C.T.R. Wilson also mentions he may have observed such a discharge above a thundercloud below the horizon.

1.4.2 Early Attempts at Observations of Optical Flashes Above Thunderstorms

Other researchers have also collected additional anecdotal reports of phenomena above thunderstorms. These include reports of upward lightning such as those published in *Vaughan and Vonnegut* [1982] and *Vaughan and Vonnegut* [1989]. Such reports led the researchers to put imagers into the NASA U-2 aircraft [*Christian* et al., 1983] and into the space shuttle, the latter as part of an experiment called a Night/Day Optical Survey of Lightning [*Vonnegut* et al., 1980]. The lack of spatial orientation of the images of optical flashes above thunderstorms recovered during that mission, several of which presented by *Vonnegut* et al. [1983], did not allow for spatial location of the observed phenomena. A later experiment called the Mesoscale Lightning Experiment, also from the space shuttle, used a limb-viewing camera to observe lightning. This experiment provided the images from an orbiting platform of optical emissions occurring above thunderstorm cloudtops, but the observations were not published until 1992 and 1995 [*Boeck* et al., 1992, 1995], and are described further below.

1.4.3 First Fortuitous Observations from Ground and Space

Independent of the space shuttle, the first video-recorded ground-based observations of optical emissions above thunderstorms came by chance from the University of Minnesota group headed by John Winckler. In 1989, they were testing at night a low-light level camera designed for a rocket, and pointed it near the horizon, towards a distant thunderstorm. As they were testing it, to their surprise they noticed a flash on the TV screen, which was also luckily recorded on a video tape recorder. Based on the shape of the optical emissions, the flashes would be classified as two "carrot" sprites in today's terminology. Winckler and colleagues postulated that if the flash occurred over the center of the thunderstorm, it would extend from cloudtops near 14 km altitude and vertically upward an additional 20 km [*Franz* et al., 1990] for an estimated terminal altitude of 34 km. As it turned out, they underestimated the vertical extent of the phenomena by nearly a factor of three.

A different type of event was observed on the tapes from the space shuttle from the mesoscale lightning experiment. The observations of one single event were published by

Boeck et al. [1992], showing a horizontally extensive transient luminosity at ~95 km altitude coincident with a lightning flash. Based on current terminology, *Boeck* et al. [1992] probably saw an elve. The dimensions ~10 km thick and ~500 km in diameter would agree with this interpretation, though this event appears rather long in duration, 2-4 fields (at 60 fields per second). One possible interpretation given by *Boeck* et al. [1992] was that this event could be the glow predicted the previous year by *Inan* et al. [1991].

The observations of the "elve" led the team to re-analyze all the video tapes from the space shuttle mission. They found examples of other optical emissions, and published the results in 1995 [*Boeck* et al., 1995]. By that time, other research teams had launched campaigns to capture on video these previously elusive flashes.

1.4.4 Sprite Campaigns 1993-1999

Many research institutions and companies started campaigns for MeTLE observations in the early 1990's. The initial investigations focused on sprites[8] and reported on the basics: shape, duration, occurrence rates, relation to parent lightning, nature of optical emissions etc. A list of sprite and other campaigns and field seasons is reported in Tables 1.2 to 1.10. Locations for ground-based observations are summarized in Table 1.11.

1993-1994

Sentman and Wescott [1993] reported the top of the upper atmospheric optical flashes above thunderstorms to lie between 60 and 100 km altitude, the duration to be less than 17 ms, and also reported the relative frequency in comparison with positive and negative cloud-to-ground flashes. *Lyons* [1994a] and *Lyons* [1994b] found that sprites are unusual but not rare and can be complex. The altitude was more accurately measured the following year, indicating the tops of sprites approach 100 km altitude [*Sentman* et al., 1995], and the first color images were obtained. A video showing the spectacular results of the Sprites'94 campaign [*Sentman and Wescott*, 1994] launched a number of groups into initiating sprite research. *Sentman* et al. [1995] also reported more definite results that sprites are D-region phenomena, also noting the general shape and the red color of sprites with bluish tendrils,

---

[8]The term sprites replaced the earlier term "Cloud to Stratosphere Discharge" since the latter implied a direction and a specific (incorrect) atmospheric region.

Table 1.2. Sprite campaigns 1989 - 1993. U of MN is the Univ. of Minnesota group [John Winckler], UAF is Univ. of Alaska Fairbanks [Dave Sentman and Gene Wescott, later joined by Hans Nielsen]. FMA is FMA Research, Inc [Walt Lyons and Tom Nelson].

1989				
Group	Platform	Location	Instruments	Campaign
U of MN	ground	O'Brien	TV imager	
Vaughan *et al.*	orbital	space shuttle	TV imager	Mesoscale Lightning Exp.
1992				
U of MN	ground	O'Brien	TV imager	
1993				
UAF	airborne	S. Am./ U.S. Midwest	TV imager	Sprites'93
U of MN	ground	O'Brien	TV imager	
FMA	ground	Yucca	TV imager	

and occurrence of sprites in regions of positive cloud-to-ground strokes. *Wescott* et al. [1995] reported a newly identified phenomenon, the blue jet, that starts from cloudtops and reach 40 to 50 km with velocities of 10^5 m/s, lasting $\sim$200 ms. *Winckler* [1995], describing sprites observed in 1993, reported that sprites come in a variety of shapes and sizes. *Boccippio* et al. [1995] identified the positive cloud-to-ground stroke as the causative lightning for most sprites, and *Lyons* [1996] showed sprites occur over mesoscale convective systems, in other words, large thunderstorms.

1995

Sprites had been shown to be red in 1994 [*Sentman* et al., 1995], and both the University of Alaska Fairbanks and UC Berkeley deployed spectrographs into field in the summer of 1995 in order to identify the species responsible for the optical emissions. The spectra of sprites obtained [*Mende* et al., 1995; *Hampton* et al., 1996] and subsequent analysis [*Green* et al., 1996] showed that the emissions from sprites are mainly spontaneous emissions from neutral nitrogen excited by electron impact. Their calculations showed the spectra to be

Table 1.3. Sprite campaigns 1994 - 1995. USU is Utah State Univ. group [Mike Taylor]. Berkeley is the Univ. of CA Berkeley group [Steve Mende].

1994				
Group	Platform	Location	Instruments	Campaign
UAF	airborne	US Mid-west	TV imager, color imager, ELF/VLF	Sprites'94
U of MN	ground	O'Brien	TV imager	
FMA	ground	Yucca	TV imager	1994 Colorado SPRITE campaign
1995				
UAF	airborne	S. Am.	TV imager, ELF	Peru'95
UAF	airborne	Centr. Am.	TV imager, spectral, ELF/VLF	Blue Sand
UAF	ground	Evans	TV imager, spectral	GASP'95
FMA	ground	Yucca	TV imager	Colorado SPRITES '95
USU	ground	Yucca	TV imager	
Berkeley	ground	Yucca	TV imager, spectral	

consistent with an electron Boltzman distribution of characteristic energy of approximately 1 eV.

The broadband TV observations allowed a table to be made with a basic grouping of similar phenomena based on TV images, which was presented by *Desroschers* et al. [1995]. This table is reproduced in Figure 1.4. Besides sprites, jets and starters, this table also included "airglow enhancements" which are now known as halos. In the wake of some sprites, *Desroschers* et al. [1995] presented a phenomenon occurring after sprites which they termed "palm tree." Lastly, "candles," or columniform-sprites in current terminology, were also listed.

In 1995, Japanese researchers joined the summer field season and brought with them a multi-anode photometer. Using this instrument, they identified "elves," an acronym for "Emission of Light and VLF perturbation from EMP [electromagnetic pulse]" [*Fukunishi* et al., 1996a], predicted earlier by *Inan* et al. [1991].

Table 1.4. Summary of known MeTLEs in 1995, as presented by *Desroschers* et al. [1995] at the 1995 Fall AGU Meeting. Wih current terminology, "airglow enhancements" would be referred to as halos, and "candles" are columniform sprites.

	Sprite	Jet	Starter	Airglow	"Palm Tree"	"Candle"
Altitude	87	40	22	—	57	—
Lightning Association	Strong Pos.	Weak Neg.	Weak Neg.	Strong Pos.	Strong Pos.	Strong Pos.
Number Obs.	100s	40+	30+	100s?	1	100?
Duration(ms)	< 17	200-300	??	< 17	< 17	< 17
ELF/VLF	Yes	No?	No?	Yes	?	Yes?
Optical	N_2 1P	?	?	?	N_2 1P?	N_2 1P
Color	Red	Blue	Blue	Red	Red	Red
Assoc. with		Hail	Jets		Sprites	

1996-1997

The summer of 1996 proved to be bountiful in observations. The multichannel photometer data by Japanese researchers showed that sprites start with downward moving tendrils, followed by upward moving branches for the case of carrot sprites [*Fukunishi* et al., 1996b; *Takahashi* et al., 1996]. Other groups included both broadband and filtered cameras and photometers to try to get a handle on the energetics of sprites.

Analysis of one sprite spectrum captured in 1996 led *Morrill* et al. [1998] to conclude some ionization is occurring, as the best modeled fit to the spectrum required emission from an ionized state of nitrogen. *Armstrong* et al. [1998] and *Suszcynsky* et al. [1998] used a blue filter to show sprites emit in the blue, however, their filter did not discriminate between ionized nitrogen emissions and upper-level neutral nitrogen emission, both occurring in the blue part of the spectrum.

At the same time as spectral observations, additional broadband images of "candles," now termed "columniform" sprites, allowed *Wescott* et al. [1998b] to triangulate the altitude

Table 1.5. Sprite campaigns in 1996. NMT is New Mexico Institute of Technology; Stanford is the Stanford Univ. group [Umran Inan]; Tohoku is the Univ. of Tohoku, Japan group [Fukunishi, Takahashi], U of Otago is a New Zealand group [R.Dowden], and Creighton University in Nebraska includes professor Dean Morss.

Sprite campaigns in 1996				
Group	Platform	Location	Instruments	Campaign
UAF	ground	Jelm Mt.	TV imager, spectral	Sprites'96
NMT	ground	Langmuir	TV imager, broadband E	
Tohoku	ground	Yucca	optical, 16-channel photometer	Sprites'96
USU	ground	Yucca	TV imager, filtered (red,blue) video imager, filtered CCD	Sprites'96
Stanford	ground	Yucca	TV imager, Fly's Eye photometer	Sprites'96
FMA	ground	Yucca	TV imager	Sprites'96
U of Otago	ground	Yucca	VLF	Sprites'96
Creighton	ground	US Midwest	TV imager	

of the columns, and found the altitude to range from ~76 to ~86 km. At the 1996 Fall AGU meeting, *Stanley* et al. [1996] presented what they originally termed "sprite-jets." The "sprite-jet" phenomena appeared to occur after sprites, as a jet following sprite tendril channels back up from cloudtops. Since the phenomenon is neither a sprite nor a jet, later researchers called the same phenomena "fingers" (extending upward from clouds), "trolls," and "embers"[9].

High speed images of sprites were first obtained in 1997 by the New Mexico Institute of Technology [*Stanley* et al., 1999]. The 1000 - 3000 frames per second images showed that sprites initiate at ~75 km altitude and move both downward and upward from this altitude [*Stanley* et al., 1999]. The velocities of the tendrils were consistent with streamer velocities measured in laboratory conditions.

---

[9]The term fingers was used by Moudry et al. in June 1999 at a CEDAR conference. Trolls was used by Lyons in December 1999 [*Lyons* et al., 1999]. Embers was used in *Stenbaek-Nielsen* et al. [2000].

Table 1.6. Sprite campaigns in 1997.

Sprite campaigns in 1997				
Group	Platform	Location	Instruments	Campaign
NMT	ground	Kennedy SC	TV imager, KSC LDAR, NMT Intf/broadband E	
NMT	ground	Langmuir	TV imagers, high speed imager, broadband E/B, photometer	
FMA	ground	Yucca	TV imager	
Stanford	ground	Langmuir	TV imager, Fly's Eye photometer	
U of Otago	ground	~Darwin, AU	TV imager	

1998

From 1998 data, *Heavner* [2000] showed the presence of the upper-level neutral nitrogen emission, cascading to a lower level, as well as a very weak ionized emission. *Heavner* [2000] also showed that intersystem collisional transfer occurring between two nitrogen molecules could account for observations of some spectra, which would otherwise be quenched (collisionally deactivated) before spontaneous emission would occur. *Bucsela* et al. [2002] have suggested that energy pooling may account for the spectral data they present.

Barrington-Leigh and Inan [1999] presented observations of the outward expansion of elves predicted by the model of *Inan* et al. [1996a], using a multi-channel photometer ("Fly's Eye photometer"). Elves associated with both +CGs and -CGs were identified. In addition, the first observations of a sprite associated with -CGs [*Barrington-Leigh* et al., 1999b] constrained some developing theories of sprites.

An intriguing event was captured on video in 1998 when a meteor was captured on video, with a sprite closely following (~300 ms) the disappearance of the meteor behind a cloudbank, and a jet following the sprite some 60 ms later. Meteors had been suggested to be triggering sprites in 1995 [*Muller*, 1995], and the event captured in 1998 provided another hint of this possiblity.

In addition, more details of sprite structure became visible with new images captured by a camera mounted on a Dobsonian telescope [*Gerken* et al., 2000]. These images allowed the

Table 1.7. Sprite campaigns in 1998. NRL is Naval Research Lab group [Carl Siefring, Jeff Morrill, and others]; AFRL is AirForce group [Jeremy Winnick].

Sprite campaigns in 1998				
Group	Platform	Location	Instruments	Campaign
UAF, NRL, AFRL	airborne	U.S. Midwest	TV imager; color; NIR, 427.8 nm and NUV filtered cameras	EXL'98
UAF	ground	Jelm Mt.	TV imager, spectral, photometer	
UAF	ground	Mt. Evans	TV imager, spectral	
FMA	ground	Yucca	TV imager	Sprites'98
Stanford	ground	Langmuir	TV imager, Fly's Eye photometer, telescopic imager	
NMT	ground	Langmuir	TV imager, broadband E	Sprites'98
USU	ground	Yucca	Filtered (red,blue,white) video imager, filtered CCD	Sprites'98
Tohoku	ground	Dodaira; Sendai	TV imagers, 16-channel photometer	Sprites'98

estimation of the diameter of smaller-scale structures in sprites, based on their proximity to parent lighting. The tendrils imaged were shown to be tens to hundreds of meters in diameter.

1999 - present

In video observations, unstructured emissions sometimes occurring with sprites have been referred to as elves [*Lyons*, 1996], until 1999 when both *Wescott* et al. [1999] and *Barrington-Leigh* et al. [1999a] have presented evidence that they are not the same phenomenon. Those emissions readily visible with TV imagers are now referred to as a (sprite) halos. All literature presenting TV images of elves before that time is, in the new terminology, most likely showing images of halos.

Deployment of a high speed (1 ms) imager by the University of Alaska Fairbanks has provided the best resolved 1 ms images of upper atmospheric phenomena [*Stenbaek-Nielsen* et al., 2000]. Most of the observations presented later in this thesis were obtained with

Table 1.8. Sprite campaigns in 1999. UH is Univ. of Houston group [Edgar Bering III]. ISAS is Institute of Space and Astronautical Sciences in Japan [Hajime Yano].

Sprite campaigns in 1999				
Group	Platform	Location	Instruments	Campaign
Tohoku	ground	Dodaira; Sendai	TV imagers, 16-channel photometer	
UH	balloon	Ottumwa,IO	photometer, $\vec{E}, \vec{B}$ field sensors,...	'99 NASA
UAF	ground	Jelm Mt.	TV imager, spectral, photometer, high speed imager	Sprites Balloon
UAF	ground	Bear Mt.	TV imagers	Campaign
FMA	ground	Yucca	TV imager	
Stanford	ground	Langmuir	TV imager, Fly's Eye photometer, telescopic imager	
USU	airborne	Mediterranean	TV imager	Leonids'99
ISAS	airborne	Mediterranean	HDTV imager	Leonids'99
NMT	ground	Lemitar,NM(1.1km)	Broadband E	
Tohoku	ground	Maebashi (Japan)	TV imagers, red (380-500 nm) and blue (560-800 nm) filtered 116-channel photometer	

this instrument. Other observations included un-intensified observations of gravity waves emanating from the thunderstorm, with sprites sporadically appearing in the same images [*Sentman* et al., 2003]. These observations were in support of a balloon campaign measuring electromagnetic signatures of sprites and parent lightning [*Bering III* et al., 2002].

The 1 ms images provided a useful tool for differentiation between multiple phenomena, both sprites, phenomena independent of sprites such as elves and halos, and phenomena following sprites. Most are summarized in the abstract of *Moudry* et al. [2001]. Some, as yet not well documented phenomena, are further presented in *Lyons* et al. [2001].

Table 1.9. Sprite campaigns in 2000. DMI is the Danish Meteorology Institute group [Torsten Neubert].

Sprite campaigns in 2000				
Group	Platform	Location	Instruments	Campaign
Tohoku	ground	Maebashi (Japan)	TV imagers, red and blue filtered 16-channel photometer	
DMI	ground	Midi-Pyrenee	TV imager	First European Sprites Campaign
Stanford	ground	Yucca	TV imager, telescopic imager	
NMT	ground	Burlington, CO	TV imagers, broadband E, NMT LMA, NMT Intf	STEPS 2000
USU	ground	Yucca	Filtered (blue) video imager	
FMA	ground	Yucca	TV imager	

1.4.5 Theoretical Developments

Modelers trying to explain sprites started attacking the subject from three fronts: modeling optical emissions due to electromagnetic pulses from lightning return strokes; modeling optical emissions due to quasi-electrostatic fields from lightning continuing currents; and modeling optical emissions due to runaway electrons accelerated by quasi-electrostatic fields.

EMP approach: electromagnetic pulse

Models of lightning influence on the upper atmosphere were initially developed in the ELF/VLF community in order to see whether some of the electromagnetic signatures observed in their data could be explained. *Inan* et al. [1991] used a wave propagation technique to attack the issue. Using the portion of the wave absorbed by the medium, they calculated the perturbation to the electron collision frequency, which in turn allowed an estimate of the electron kinetic energy and temperature to be made. Considering only electrons with energy greater than the ionization energy of nitrogen, they also estimated the amount of ionization produced by the heated electrons. *Taranenko* et al. [1992] used the *Inan* et al. [1991] model and included not only terms describing electron impact ionization, but also

Table 1.10. Sprite campaigns in 2001. Penn is Penn State Univ. group [Victor Pasko], Cheng-Kung Univ is a Taiwanese group [Han Su]. Acronym LSO stands for "Lightning and Sprites Observation"

Sprite Campaigns in 2001				
Group	Platform	Location	Instruments	Campaign
Penn	ground	Arecibo (0.3 km), PR	blue TV imager	
NMT	ground	Dominguito (0.2 km), PR	broadband E	
Stanford	ground	Vieques Island, PR	VLF receiver	
Stanford	ground	Midi-Pyrenee, France	photometer	Conjugate
Stanford	ground	SAAO, South Africa	photometer	Sprites
DMI	ground	Midi-Pyrenee, France	TV imager	campaign
Cheng Kung	ground	Ali Mnt., Taiwan	TV imager	
Tohoku	ground	(Japan)	TV imager	
France, Russia	orbital	Int'l Space Station	nadir directed imager	LSO

excitation of electronic states of nitrogen and oxygen. The model included quenching and spontaneous emission possibilities and gave predictions for the altitude profile of the optical emissions.

Taranenko et al. [1993a] used the plasma approach described very briefly in Section 1.3.7, where sources included inelastic collisions resulting in vibrational excitation, rotational excitation, optical emission, dissociation, attachment and ionization. The electron distribution function was written in the form of zeroth- plus first-order approximations. The model included the altitude range 70-120 km. An EM wave was injected at the lower boundary with a specified amplitude, and allowed to propagate through the simulation domain. Subsequently *Taranenko* et al. [1993b] used the same model to calculate the optical emissions, and they included a discussion about radiative transfer. Their model allowed partial reflection of the wave off the ionosphere.

Rowland et al. [1995] used an analytical approach to calculate far-field values for an electric field pulse launched by a high-amplitude short-duration current. The approach was similar to that described in Section 1.3.6. A 2-1/2 dimensional model (two spatial dimensions and three velocities) was used. Within the grid, the fields were solved using

Table 1.11. Some of the locations for ground-based sprites observations in US and elsewhere.

Name	Full name, location	State	Coord (° N, ° E, km)			Notes
Bear	Bear Mt.	SD	+43.88	-103.75	2.15	fire lookout
Jelm	Wyoming Infrared Observatory (WIRO)	WY	+41.10	-105.98	2.94	astron. obs.
Kennedy	Kennedy Space Center	FL			0	NASA
Langmuir	Langmuir Lab	NM	+33.98	-107.18	3.2	national lab
Evans	Mt. Evans Observatory	CO	+39.58	-105.63	4.05	astron. obs.
O'Brien	O'Brien Observatory	MN	+45.18	-92.77	0.15	astron. obs.
Yucca	Yucca Ridge	CO	+40.67	-104.93	1.65	private
Ali	Ali Mnt.	Taiwan	+22?	+121?	2.4	observatory
Dodaira	Dodaira Astr. Obs.	Japan	+36.0	+139.2	0.8	astron. obs.
Midi	Observatoire Midi-Pyrenee	France	+42.9	+0.15	2.8	astron. obs.
Sendai	Sendai	Japan	+38.3	+140.9	~sea	university
SAAO	South African Astronomical Observatory	South Africa	-32.4	+20.82	1.8	astron. obs.

Maxwell's equations, other quantities were calculated using swarm results[10], Ohm's law, and the ionization rate. *Rowland* et al. [1995] found that the lightning electric field can exceed breakdown field in altitudes of 80-95 km, and that the electromagnetic pulse waves may be reflected off the ionosphere. *Fernsler and Rowland* [1996] included both an analytical and numerical approach for the EMP and QE fields. The analytical approach was outlined in Section 1.3.6. The numerical model showed that the enhancement in the electron density due to the EMP occurs at higher altitude and earlier than the enhancement due to the QE. Optical emissions were not calculated.

Inan et al. [1996b] modeled a return stroke of a lightning flash by assuming the current to be a function proportional to hyperbolic secant of time. From the current, the scalar and vector potential in free space were determined in order to find the electric field at 70 km

[10]Swarm results are laboratory based electron collisional cross sections, independent of (or rather, averaged over) angle of incidence, from which effective ionization rate can be tabulated. *Rowland* et al. [1995] write "Swarm results incorporate all details of the velocity distribution and associated air chemistry."

altitude. Between 70 and 100 km, Maxwell's equations were solved using a gridded mesh, including conduction current, ionization and attachment rates. Optical emissions were solved as in *Taranenko* et al. [1993b]. The model showed optical emissions to occur in an expanding ring centered on the lightning current, with a hole in the center. Integrated over television-rate fields, the model predicted donut-shaped emissions. A year later [*Inan* et al., 1997] showed that the modeled expanding-ring optical emissions due to electromagnetic pulse corresponds well with signatures in photometer observations.

Valdivia et al. [1997] modeled the intracloud portion of a return stroke as a fractal, and propagated the resulting radiative fields self-consistenly upward. The electron distribution function was calculated from the fields using a Fokker-Planck code. The distribution function is convolved with excitation cross section, giving the excitation rate. It is assumed that all excited molecules decay by emitting a photon without quenching. The resulting optical emissions would be highly structured due to the underlying fractal lightning.

Instead of a fractal lightning, *Cho and Rycroft* [1998] and *Cho and Rycroft* [2001] modeled a simple lightning path with an oscillating current. The model used a finite difference time domain method to solve Maxwell's equations. Swarm data were used to express electron temperature, and ionization and attachment rates as a function of E/n (see Section 1.3.3). The electromagnetic pulses, temporally dependent on the shape, size, and temporal function of the current, are reflected both off the ground and the ionosphere, and create temporally varying patches of constructively interfering electric field, and of enhanced electron density. Their results show the enhanced electron density is a strong function of the various parameters.

Veronis et al. [1999] used a cylindrical box and a finite-difference model to calculate the electric and magnetic fields given a source return-stroke current including continuing current. Other approximations were taken similar to those described by *Pasko* et al. [1997] for QE fields, including ionization and attachment rates for electrons, electron and ion profiles and conductivity. The source current included both a fast transition and a slower tail to account for both EMP and QE fields. The optical emissions were calculated and showed the combination of the two types of fields. This model was later used by *Barrington-Leigh* et al. [2001] to differentiate between elves, due to EMP, and halos, due to QE, and appears to match both of those emissions relatively well.

QE approach: quasi-electrostatic field

Most extensive modeling of QE fields due to large amounts of charge removed by lightning has been done by Victor Pasko, initially at Stanford [*Pasko* et al., 1995, 1996, 1997, 1998, 1999]. The model uses a cylindrical coordinate system with the ground and the ionosphere taken to be perfectly conducting surfaces with ambient neutral and electron density profiles appropriate to typical nighttime conditions. The charge is allowed to build up within a thundercloud and then discharged with specified temporal periods. The electric field, charge density and conduction curent are calculated from Maxwell's equations assuming the quasielectrostatic approximation holds, *i.e.* the electric field is the gradient of a scalar potential, neglecting the vector potential. Ionization and attachment coefficients are taken to be dependent on E/n (see Section 1.3.3). The E/n dependent ionization and attachment result in the modification of electron density when electric field is applied. The rate of change of nitrogen in an upper electronic state is taken to be due to electron impact excitation, spontaneous decay, and cascading, and the optical emissions are calculated from the spontaneous decay term. The size and strength of the optical emissions depends on the amount of charge grown and removed.

As mentioned in Sections 1.3.6 and 1.4.5, *Fernsler and Rowland* [1996] made a partly analytical and partly numerical model for the emissions resulting from an EMP and a QE. They estimated breakdown to occur if the lightning charge dipole moment exceeds several hundrd C-km. They also estimated that some sprite tendrils, assuming field enhancement occurs at their tips, may propagate down below 50 km altitude. Their numerical model showed optical emissions due to QE occur lower and last longer than those due to EMP.

Ernstmeyer and Chang [1998] created a multiple fluid quasi-electrostatic simulation of the atmosphere above a thunderstorm in the altitude range 20-90 km. The simulation box was cylindrical. The top (ionosphere) at 90 km and bottom (ground) at 0 km were taken to be perfectly conducting. Charge was introduced at 15 km and then discharged. Multiple processes were solved simultaneously, including transport, collisional effects, chemical interactions, densities, drift velocities and temperatures. While a Maxwellian electron distribution is used in the momentum and the energy transport equations, the processes with a high energy threshold, such as ionization rates and dissociative attachment, use a Druyvestein distribution. *Ernstmeyer and Chang* [1998] find a significant charge at strato-

spheric altitudes during a +CG but not during a -CG, though both types of CGs increase the total conductivity in the same region by an order of magnitude 10 s after the discharge.

Two groups started focusing on a streamer mechanism for conventional breakdown. *Pasko* et al. [1998] modeled in cylindrical coordinates a streamer propagating under an applied electric field using a flux-corrected transport code. The streamer propagation is governed by an equation showing the dependence of streamer head radius, curvature, and streamer velocity on the electric field in the background and in the streamer head. They identified three regions in their sprite model: a diffuse region above 85 km characterized by electron avalanches without streamers; a streamer region below 75 km altitude characterized by avalanches evolving into streamers; and a transition region between the two. They also found that a streamer too large in diameter will split into smaller ones as it travels into the lower-pressure region where the large-diameter streamer cannot be supported.

Independently, *Raizer* et al. [1998] made a 1D model of the streamers under a static field from a charge at some altitde and its image charges from the conducting ground and ionospheric reflections. The streamer velocity is related to the effective ionization frequency, given by the difference between ionization and attachment rates. All of these quantities are electric-field dependent. *Raizer* et al. [1998] provided another relation describing the dependence of streamer radius and the maximum electric field in its head to the potential inside the streamer and the background. Their results showed a streamer originating at 80 km altitude takes approximately 7 ms to propagate down to its stopping altitude of ~48 km. The velocity in that time varies from 10^6 m/s to slightly above 10^7 m/s.

Following the observations of *Suszcynsky* et al. [1999] showing a sprite possibly being triggered by a meteorite, *Symbalisty* et al. [2000] created a numerical multifluid model simulating the effect of a lower-conductivity meteor trail under the presence of a quasi-electrostatic field. The meteor trail persists on the order of one hour, and the lightning may occur at any point within that hour. From the simulations giving the electron density, the optical emissions are calculated, and these are shown to be greatly enhanced in the meteor trail.

REL approach: runaway electron models

Finally, one approach to modeling sprites involves high energy (keV to MeV) electrons accelerated by the quasi-electrostatic fields from the lightning. Electrons of adequate energy and under a sufficiently strong applied electric field experience less frictional drag, liberating additional electrons, which also gain high energy, and develop into an avalanche. Having a large enough population of initial high energy electrons, the runaway breakdown can occur under electric fields an order of magnitude smaller than those required for conventional breakdown [*Roussel-Dupré and Gurevich*, 1996]. The lower required electric field, together with possible optical emissions at lower altitude than those due to conventional QE breakdown and the possiblity of creation of gamma rays such as those observed originating in thunderstorms [*McCarthy and Parks*, 1992], explain the popularity of RELs with some modelers.

Bell et al. [1995] constructed a 1D model using similar parameters as *Pasko* et al. [1995] but included transport and continuity equations for RELs. The source of the runaways are energetic cosmic ray secondary electrons. Ionization rates are calculated together with electron impact excitation of various nitrogen and oxygen electronic states, resulting in optical emissions. The model predicts optical emissions down to 45 km altitude.

Similar calculations submitted for publication 10 days later came from *Roussel-Dupré and Gurevich* [1996]. For 20-100 km altitudes, *Roussel-Dupré and Gurevich* [1996] calculate the total optical output, gamma ray flux, and the ratio of blue to red optical emissions. Similar to the observations of *Sentman* et al. [1995], they have blue emissions dominating in lower parts of their "sprites" while the red dominates above.

Lehtinen et al. [1997] expanded the 1D model of *Bell* et al. [1995] to two dimensions. Their model used the *Pasko* et al. [1997] model to calculate pre-discharge electric fields, and then included the runaways in the calculation of the discharge fields. Transport and density equations give the populations of electrons in space and time. In terms of optical emissions, the *Lehtinen* et al. [1997] model includes both the conventional breakdown QE optical emissions together with a beam of emissions reaching lower altitudes. While the runaway electrons move upward, the optical emissions appear to expand downward as more electrons from lower regions become runaway under the applied electric field.

The model of *Roussel-Dupré and Gurevich* [1996] was expanded by multiple researchers

[*Taranenko and Roussel-Dupré*, 1996; *Roussel-Dupré* et al., 1998; *Yukhimuk* et al., 1998, 1999] to calculate the optical characteristics and temporal evolution of the optical emissions. *Yukhimuk* et al. [1999] used more realistic (lower) ionization rates, and put the discharge at a lower altitude, still getting strong optical emissions.

Current status of theories

At present, the *Veronis* et al. [1999] model combining the EMP model of *Inan* et al. [1997] with the QE model of *Pasko* et al. [1997] appears to predict elves and halos well, as was shown by *Barrington-Leigh* et al. [2001]. Future modeling efforts need to expand more qualitatively on the streamer mechanism models of *Raizer* et al. [1998] and *Pasko* et al. [1998]. Some intermediate modeling efforts of streamers have been presented by *Liu* et al. [2002], so far without any calculations of velocities. The runaway-electron models have been disproved by observations of sprites triggered by negative cloud-to-ground lightning [*Barrington-Leigh* et al., 1999b], showing that at least some sprites involve a different mechanism. New modeling efforts in this direction involve both the runaway and conventional breakdown, and preliminary results were presented by *Triplett* et al. [2002]. As with the streamer model [*Liu* et al., 2002], the results were preliminary and did not include a calculation of expected velocities, which will be useful for a comparison with observations.

1.5 Comparison of Different Types of Luminous Events in Terrestrial Atmosphere

A comparison of different types of luminous events occurring in the terrestrial atmosphere can be made based on energy input, processes, atmospheric density, duration, etc. Some can qualify as transient, some do not. Table 1.12 shows the comparison of auroral optical emissions with MeTLEs, day/nightglow, artificial airglow induced by ionospheric heaters, and meteors. The major difference for each of these optical emissions is the source of energy, and whether it lies above or below the region of interest. Likewise, the process by which molecules and ions are excited, as well as whether there is any ionization, varies from one luminous event to another. Other categories listed include the duration, which in all cases is dependent on the duration of the input source. Lastly, the altitude range for most common

Table 1.12. A list of atmospheric luminous phenomena, both transient and longer duration. For each event, the energy input is specified, whether the energy source lies above or below the event; excitation process; relative importance of ionization; duration, which is mainly input dependent; altitude range in which the event occurs; and main components of spectra.

	Aurora	MeTLEs	Dayglow	Nightglow	Artificial airglow	Meteors
Input	Electrons	Tstorm DC $\vec{E}$-field	Solar	chemistry, gravity waves	HAARP AC $\vec{E}$-field	Meteor
Lies ...	above	below	above	local/below	below	above
Excitation mechanism	electron impact	electron impact	photon excitation	chemical reaction	electron impact	ablation, shock
Ionization	Yes	Some	Yes	No	No	Some
Duration	ms-hours	ms	hours	hours	s	s to min
Altitude	100-250	30-100 km	80-200 km	80-130 km	250-350	70-130 km
Spectrum	O, O_2, N_2	N_2, O_2	H, O_2, NO, OH	OH, O_2, Na	O, N_2^+	metals, atmospheric species

occurrences, and components of spectra are also listed in the Table.

Of luminous events occurring in the atmosphere, only MeTLEs span the range below the thermosphere towards lower atmospheric regions. Optical emissions from aurora and MeTLEs are similarly due to electron impact on the background atmosphere. The difference is that the energy for the electron excitation comes from above for aurora, but from below for MeTLEs. In aurora, the electrons are accelerated at higher altitudes and precipitate downward; in MeTLEs, local electrons are accelerated by electric field from the underlying thunderstorm. This difference accounts for the different altitude regimes of aurora and MeTLEs: auroral electrons become increasingly likely to collide in lower altitudes and the aurora does not extend below 85 km altitude. Similarly the electric fields from thunderstorms cannot propagate into region with high electron density and MeTLEs occur below

the ionospheric electron density ledge near 100 km altitude.

There is likewise a similarity between MeTLEs and artificial airglow excited by iono-spheric heaters such as HAARP (High frequency Active Auroral Research Program[11]). Both have their energy source near the ground - in one case, the source is the thunderstorm, in the other case, it is the ionospheric heater. In both cases the propagating electric field accelerates electrons, which collide with other atoms or molecules, exciting them. The main difference is that in one case, the electric field is due to a DC current, whereas in the other case it is due to AC current(resulting in RF - radio frequency fields). This accounts for the different altitude regions where each emission occurs.

The other luminous events occurring in the atmosphere are listed simply for compari-son. Dayglow is excited from solar radiation and occurs during daytime. Chemiluminescence accounts for nightglow in the absence of solar input. Often nightglow is modulated by verti-cally propagating gravity waves, which modulate the ambient medium and the temperature of the chemical reactions that produce the nightglow. Meteors also provide occasionally spectacular displays of luminous events. The light from meteors comes from particles ab-lating from the meteor body as well as the resulting shock wave exciting local atmospheric species.

---

[11]http://www.haarp.alaska.edu/haarp/

Chapter 2

Instruments and Data

2.1 The NASA 1999 Sprites Campaign

The sprite group at Geophysical Institute of the University of Alaska Fairbanks (UAF) mounted sprite campaigns from 1993 to 1999 every one or two years. In each of the campaigns, TV-rate low-light-level cameras were used for broadband, filtered, or spectrographic imaging of the phenomena. These systems, in particular the filters and spectrographs used in conjuction with the cameras, are described in detail in *Heavner* [2000]. The campaigns were listed in Tables 1.2 to 1.10.

The principal data set used in this thesis was obtained during the NASA 1999 Sprites Balloon Campaign [*Bering III* et al., 2002]. The University of Alaska deployed a variety of cameras into the field for this campaign. Two sites were operated by UAF - one on top of Bear Mountain near Custer, South Dakota, and the other at the University of Wyoming Infrared Observatory (WIRO) on Jelm Mountain, southwest of Laramie, Wyoming. At the Wyoming site, instruments included a TV-rate camera, a 1000 fps high speed imager (HSI) [*Stenbaek-Nielsen* et al., 2000], and a 16-channel high speed photometer [*McHarg* et al., 2002].

The primary goal of the balloon campaign was acquisition of electromagnetic signatures of sprites measured from a balloon floating at stratospheric altitudes in the visinity of a thunderstorm, together with the corresponding optical observations measured at the ground stations. The balloon campaign moon-down window extended over the latter half of August,

1999. The data for the primary scientific goal related to EM emissions were obtained on August 21, 1999, and are described in *Bering III* et al. [2002], including 1 ms images. This data includes images from the high speed imager. Sprite observations were obtained on other nights, when the conditions were not favorable for balloon launch. In particular, the night of August 18 Universal Time (August 17 Local Time), a mesoscale convective system developed over Nebraska. On average, the storm was 500-700 km from our site in Wyoming. High speed imager data of sprites and other phenomena occurring over this storm system constitute the majority of the images presented in this thesis.

2.2   High Speed Imager

In 1999, the high speed imager (HSI) was a newly developed, computer controlled, low light-level, 1000 frames per second ("high speed") intensified CCD imager. A 105 mm, f/0.9 lens provides for a 6.4×6.4 degree field of view. The CCD resolution is 256×256 pixels at 8 bits (256 gray levels), arranged into four quadrants of 128×128 pixels each. Each quadrant of the CCD is read out in parallel through separate electronics, and consequently, individual images often show slight differences between quadrants. The end-to-end spectral response of the system is 500-900 nm with maximum sensitivity near 700 nm. The high speed imager has been intensity calibrated using stars of known spectral characteristics. Saturation (gray level 255) is 3 MR, and minimum detectable enhancement above system noise is of the order of 20 kR. Intensitifier phosphor decay time is measured to be ~0.8 ms, giving some persistence in the data.

During data acquisition, the high speed imager data are continuously read into a 4096 frame (~4 s) circular buffer. When a sprite or other bright event is observed visually on a scene camera boresighted with the high-speed imager, we save by a keyboard command the buffer, or part thereof, to disk. The save operation typically requires a few 10s of seconds.

The August 18, 1999 storm was 500-700 km from our site in Wyoming, a distance ideal for the 6.4×6.4 degree field of view of the high-speed imager since a sprite of several 10's km vertical extent would subtend an appreciable fraction of the image. All full-sized 1 ms images presented in this thesis have an equivalent vertical extent of ~ 60 to ~ 70 km at the range of the events. Twenty six events were recorded by the imager, with examples of elves, halos

and sprites all being imaged. The events ranged from single halos or sprites to complex events with multiple elve/halo/sprite sequences, but few had all three types simultaneously occurring in the same event. Elves were observed only in association with halos and sprites. We did not identify any solitary elves in our data, but, our manual triggering on visually bright phenomena would tend to preclude the acquisition of the solitary elves, which are very dim.

2.3 TV-rate Camera

The scene camera is an ICCD-TV with a 10×14 degree field of view and 640×480 pixel resolution. The camera is similar to those used in earlier sprite campaigns [*Sentman*, 1998]. The camera operates at regular TV framing rate (60 fields per second) giving ~17 ms time resolution. The video is recorded continuously on tape with a GPS timestamp and look-angle information (azimuth and elevation) included on each field. The time stamp and azimuth are used during subsequent analysis to determine the most likely causative lightning strike as registered by the National Lightning Detection Network (NLDN) [*Cummins* et al., 1998]. The timestamped TV images were also used to provide timing for the HSI, with a ± 17 ms time uncertainty.

2.4 Interpreting HSI Data

The HSI images reflect the source emissions of the sprite as modified by radiative transfer effects and the effects of instrument response. In the direction of the sprite, atmospheric Rayleigh scattering of photons decreases the optical intensity.

A schematic of the high speed imager without any optics components is shown in Figure 2.1. Light enters from the left into the intensifier, which increases the signal, and the intensified image is captured by the CCD.

The intensifier works by converting incoming photons into electrons at the photocathode. The photocathode needs to have its electrons replenished, and in cases of extremely bright signals, sometimes the electrons are not replenished sufficiently fast due to a limiting current supplied to the photocathode. This may result in a "delayed ghost" of a feature from an
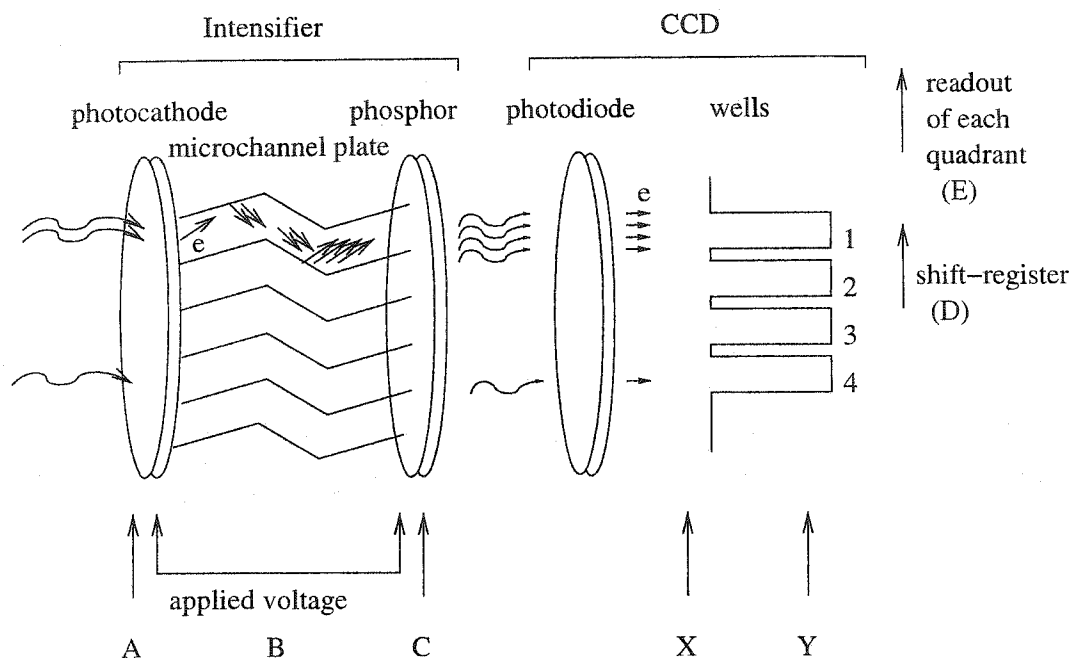
Figure 2.1. Sources of instrument artifacts for the high speed imager

earlier image occurring in immediately following images. In Figure 2.1, the location of possible introduction of a "delayed ghost" is denoted as "A," and an example is shown in Figure 2.2.
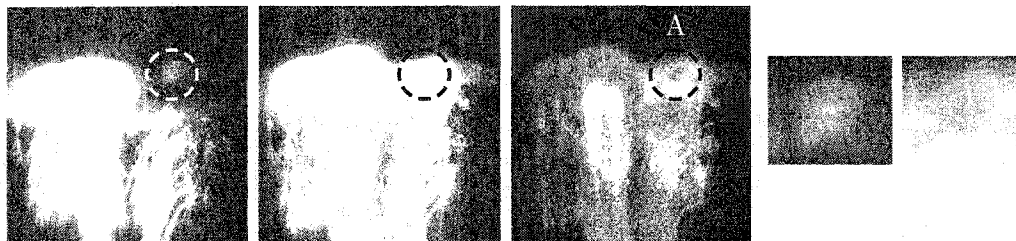

Figure 2.2. Example of instrument artifact A: "delayed ghost."

Figure 2.2 shows an example of a limiting current to the photocathode for a sprite at 05:45:05 UT. The three images are 1 ms apart. A "burger" feature is circled in the first image, shown magnified at right. The next image shows a sprite which saturates a large portion of the imager, including the "burger." One ms later, much of the sprite brightness continues to be visible, but the "burger" is reversed and dimmer than the surrounding region

(circled, also shown at extreme right). The reversed-burger indicates the photocathode, being starved by the extreme saturation during the middle field, could not resupply electrons to the region first depleted of them.

The photoelectrons created at the photocathode are accelerated in an applied electric field into the microchannel plate, where they create an electron avalanche through subsequent collisions with the walls. The current gain in the avalanches is controlled and limited to prevent damage to the micro-channel plates. The location of the gain control is denoted by "B" in Figure 2.1. An example of the data exhibiting this artifact is shown in Figure 2.3.
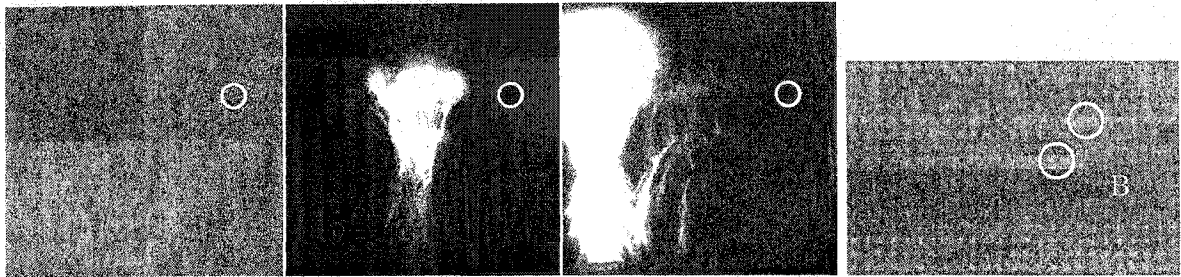

Figure 2.3. Example of partial intensifier shutdown, designated as artifact B in Fig.2.1. The left image shows a circled star (image has greyscale modified); center two images show two sprites at 05:10:38 UT. On the right, a timeseries of the star is given in 16 rows of 25 ms, for a total of 400 ms (greyscale modified). Circled are the times of the two sprites. After the second sprite, the intensifier reduced gain (label B equivalent to B of Fig.2.1), and the star is not visible for approximately 100 ms.

The example in Figure 2.3 presents data showing the reduction in gain to the intensifier for two sprites occurring at 05:10:38 UT by tracking a star over 400 ms as two sprites occurred. First image shows a greyscale modified starfield, with one star circled. In the next 200 ms, two sprites occurred, shown in the two middle images. The second sprite triggered the current limitation. This can be seen in the timeseries, at right, of the star circled in the first image. The timeseries shows 16 rows of 25 ms each, top-to-bottom, with greyscale adjusted. The temporal locations of the two sprites are circled. After the second sprite, the intensifier voltage was limited, visible as four dark lines not showing the star following the second sprite, labeled B. Note that the star was never along the line-of-sight of the sprite. The brighter background in the time series at the time of the second sprite is due to photons emitted by the sprite region in all directions, some of which were

Rayleigh-scattered by the intervening atmosphere back towards the detector.

Returning to processes in Fig. 2.1, the electron avalanche created in the microchannel plate of the intensifier hits a phosphor screen, which emits photons. The phosphor has a decay time of approximately 0.8 ms [Hans Nielsen, private communication]. Thus, an image will be effectively spread to an exponential decay, introducing a "fading ghost" at the phosphor. The location of introduction of the artifact is labeled as "C" in Fig. 2.1. An example of a combination of real signal and the fading ghost in actual images is shown in Figure 2.4, which shows the same sequence as Fig. 2.2. The circled region is saturated in the first two images, and the real+artificial signal due to a finite decay in the phosphor is visible in the circled region in the last image.
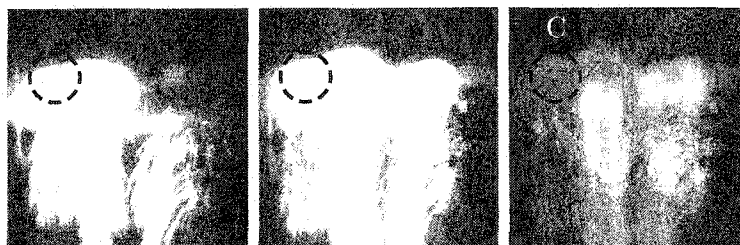

Figure 2.4. Example of instrument artifact C: "fading ghost."

The image on the phosphor screen is relayed via optics to the CCD, where at the photodiode the photons are again converted into electrons. These electrons accumulate in a capacitor, discharging it. The capacitor is known as a "well." After accumulating electrons for 1 ms, the electrons in the corner well (well 1 in Fig. 2.1) are read out, giving value for pixel 1. The neighboring well (2) gets shifted to (1) before getting read out as pixel 2. Similarly well 3 is shifted to well 2 then to well 1 before being read out as pixel 3. All the wells are thus read sequentially in several μs, a time short compared to the integration period.

If the signal is very strong at well 1 at the moment of the readout, the influx of electrons into well 1 will increase the values of pixel 2 and all subsequent pixels passing through the location of that well during the readout process. This introduces artificial scan lines above and below very bright sources. The location of source of this artificial signal is shown as "D" in Fig. 2.1, and two examples are shown in Figure 2.5.
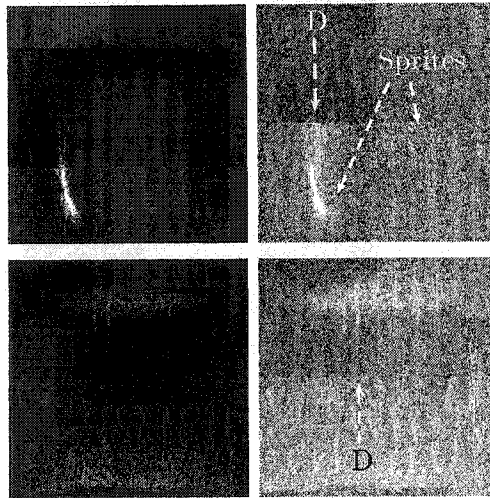
Figure 2.5. Examples of instrument artifact D: artificial signal due to photons entering during readout scan.

Top line of Figure 2.5 shows an image of a sprite at 06:30:14 UT, the original images (left) as well as a contrast-enhanced image (right). In the contrast-enhanced image two sprites are visible. For the brighter sprites, as the pixels in the lower quandrant of the CCD were read out, the ones located above the sprite received extra signal during the readout, resulting in the readout scan-lines. A similar artifact for the top quadrants is shown in the lower example. The bottom row of Figure 2.5 shows three sprites at 05:17:16 UT. The original (not modified) image is shown at left, together with the same image with greyscale modified at right. When the greyscale is contrast enhanced (right), the readout line scan from the sprites becomes visible (label D). Since the sprites occurred in the upper quadrant, the first readout scan lines appear below them, in contrast to the readout lines shown in the top row.

The CCD consists of 4 quadrants of pixels, each of which is read out through different electronics for a faster readout. This introduces a slightly different base signal level for signal from each quadrant, making the four quadrants visible in the greyscale-modified images. Source location of this instrument artifact is shown as E in Figure 2.1, and example is shown in Figure 2.6. The figure shows an image 1 ms after the image shown in the top row of Figure 2.5. As before, the image is presented in the original form (left), and also

contrast-enahnced (right). With contrast enhancement, the slightly different background levels of each of the four quadrants of the CCD are visible.
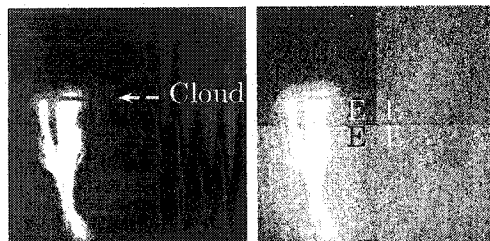

Figure 2.6. Examples of instrument artifact E: different background for each of the four quadrants of the CCD due to readout through separate electronics.

Other sources of signal in images taken by the high speed imager are not artifacts of the instrument but rather artifacts of radiative transfer. For example, there are many photons emitted by both lightning and sprites in every which direction. Some of the photons emitted initially not in the direction of the instrument may be scattered into the field of view of the instrument due to Rayleigh scattering with the intervening atmosphere. These rayleigh-scattered photons appear as a glow around a bright object. Two examples are shown in Figure 2.7. Both of these examples were shown previously in Figs. 2.6 and 2.5, and include brightness due to the rayleigh scattered photons emitted by sprites and lightning.

In addition to these known instrument or atmospheric artifacts, there are two additional artifacts so far not mentioned which are important under different conditions. These are: dark current in the CCD, denoted as X in Figure 2.1, and incomplete well readout, denoted as Y. Dark current refers to the process by which even if the CCD is left in complete darkness, due to blackbody radiation, some sporadic electrons will be created and stored in the wells. Over time, these can constitute a significant amount in comparison with the signal itself. For the 1 ms integration time used with the HSI, though, the dark current is insignificant. The other artifact not significant is the incomplete well readout (Y in Fig.2.1), where only part of the accumulated electrons in the well is read out.
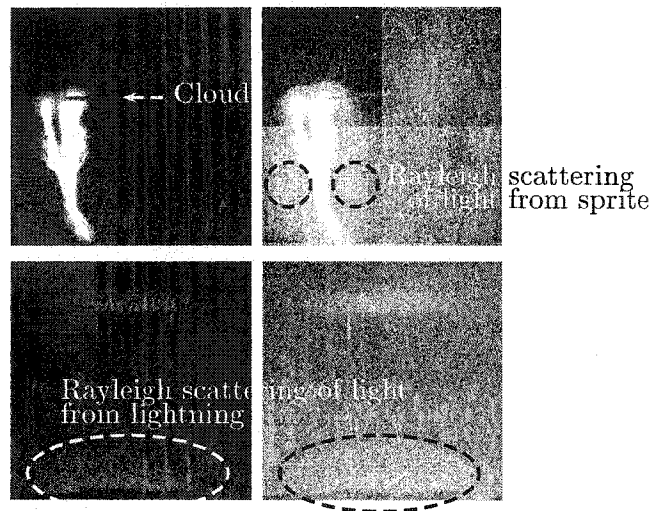
Figure 2.7. Example of Rayleigh Scattering of sprite and lightning emissions

Chapter 3

Imaging of Elves, Halos and Sprite Initiation at 1 ms Time Resolution

Elves, halos and sprites were observed during August 1999 with a 1 ms high speed imager. The higher time resolution compared to conventional television cameras (17 ms for NTSC or 20 ms for PAL) allowed excellent images of the three phenomena temporally separate from each other to be obtained. Analysis of images of elves and halos indicates that the causal lightning-generated electromagnetic pulse and quasi-electrostatic fields are nearly homogeneous and any small-scale (sub-10 km) structure, if visible, most likely derives from a structured atmosphere. Observations of sprites initiated to the side of a halo, without a halo, and from beads left over from a previous sprite, respectively, all suggest sub-pixel (<0.5 km) background structures in atmospheric pressure or composition as being the dominant factors in determining the sprite "seed" location, or site of sprite initiation. In this chapter[1], dim structures accompanying the initiation of large sprites are described, together with description of details of sprite development not previously reported, in particular, very dim tendrils ultimately forming large sprites.

---

[1]This chapter is a modified version of a paper accepted by *Journal of Atmospheric, Solar- Terrestrial Physics*: Moudry, Stenbaek-Nielsen, Sentman and Wescott, Imaging of elves, halos and sprite initiation at 1 ms time resolution, *J. Atm. Solar-Terr. Physics*, 2002, in press. The work presented is work done by Dana Moudry, using data of Hans Stenbaek-Nielsen.

3.1 Elves

3.1.1 Models of Elves

As outlined in Section 1.4.5, elves are modeled to be due to the EMP from a lightning return stroke; a vertical cloud-to-ground lightning current [*Inan* et al., 1997], and should appear as a ring of light in the ionosphere expanding radially outward at apparent speeds greater than the speed of light, lasting less than 1 ms. The outward expansion and short duration of elves has been observed with photometers [*Barrington-Leigh* et al., 2001]. Integrated over 1 ms, the expanding disk smears out to a uniform diffuse emission in the high speed images.

Valdivia et al. [1997] propose that the structure in "sprites" arises from the positively/negatively interfering EMPs from intracloud fractal lightning following a cloud-to-ground discharge. The model was applied to the intracloud portion of lightning discharge in order to allow for the observed delays between NLDN-recorded return strokes and sprites. In this model, the intracloud lightning was taken to be a fractal radiating antenna, yielding spatial interference patterns in the mesosphere. These in turn produce horizontally structured regions of optical emissions varying by as much as 30 dB, over scale distances of 10 km for the parameters used by *Valdivia* et al. [1997]. For CG flashes, the model can also be applied to the intracloud portions of the lightning very close (spatially and temporally) to the channel leading to ground, since 1) peak radiative electric fields from lightning occur within 25 μs of onset [*Uman*, 1987, p.197], and 2) peak return stroke currents occur within less than 200 μs for 95% of positive cloud-to-ground strokes (+CGs), and within less than 18 μs for 95% of -CGs [*Uman*, 1987, p.124]. The resulting fields/emissions in the mesosphere would have relatively both small spatial and temporal separation from those of the return stroke. Here, this model is called the modified fractal antenna model, modified in the sense that only a small amount of temporal delay (itself unspecified in the model) would be expected from the return stroke for the conditions described here.

A comparison of observed structure in elves with that predicted by the straight-lightning channel model [*Barrington-Leigh* et al., 2001] and by the modified fractal-antenna lightning model [*Valdivia* et al., 1997] as described above, allows us to estimate the degree of homogeneity of the EMP fields in the mesosphere created temporally close to the return stroke.
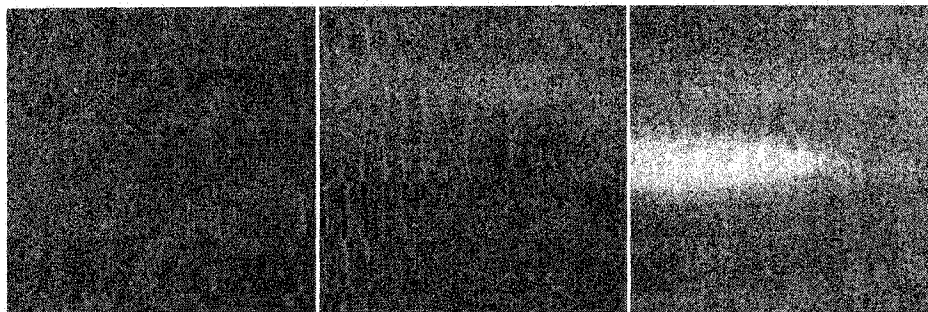
Figure 3.1. Elve followed by a halo. Example of three successive images 1 ms apart, showing background, elve and halo. Event is at 06:04:18 UT on Aug. 18, 1999.

It should be noted that variations in atmospheric composition may also be expected to play a role [*Stenbaek-Nielsen* et al., 2000].

3.1.2 Observations of Elves

Figure 3.1 shows three images 1 ms apart of an event at 06:04:18 UT on Aug. 18, 1999. The first image, with a contrast enhanced greyscale to bring out dim features, shows the background. Several stars are visible. On the second image, an elve is visible in the upper quadrants, followed 1 ms later (third field) by a halo near the center.

In the high-speed images, elves are observed associated with halos and sprites in 9 of the 26 events. Of the 9 events where halos were entirely in the lower 60% of the image, all but 1 had elves visible in the top part of the image, indicating that we were looking too low to see elves the rest of the time. It is not possible to estimate the height of the elves without assuming some shape and extent for the emissions. No solitary elves have been identified. Elves last less than 1 ms, are considerably less luminous than halos, and as indicated earlier would generally not be visible in the video (30 frames per second) used to trigger a save action of the high-speed imager. Post-campaign laboratory analysis of the video (TV rate) data did not produce any elves that could be identified as such. However, this does not necessarily preclude the possibility that elves may occur as solitary events. There are many unidentified, short-lived events in the photometer records that could be elves (G. McHarg, private communication, 2001). Similarly, on the ballooon payload there appear to be many events possibly linked to solitary elves (E. Bering, private communication, 2001; *Bering*

et al. [2001]). This clearly warrants further investigation, but is beyond the scope of the present paper.

3.1.3 Analysis of Elve Observations

In order to check for horizontally-alternating quasi-periodic strong/weak emissions predicted by the modified model of *Valdivia* et al. [1997] described above, horizontal strips (both 20 and 64 pixels wide) were selected across the elve in the image. The pixels in the rows selected were summed into a single horizontal profile to increase signal, on which a Fourier transform was performed. No strong periodicities were detected at the 95% confidence level. The same analysis was performed on four other elves with similar results. No indication of structure was found in any of the 5 events analyzed.

This analysis indicates that there is no strong quasi-periodic interference pattern of the EMP in the lower ionosphere, and that the EMP affecting the mesosphere lacks spatial structure, as can be expected from a vertical lightning discharge. In turn, this uniformity of elves has implications for sprite initiation, as discussed below.

3.2 Halos

3.2.1 Halo Models

Halos are brighter, but spatially smaller than, elves, and last several ms. They appear in an image as diffuse emissions in the shape of a "pancake" up to $\sim$70 km in diameter near 75 km altitude. Most early models of "sprites" employing the quasi-electrostatic field from lightning return stroke (e.g. *Pasko* et al. [1997]) now appear to be good models of halos instead. Recent work by *Barrington-Leigh* et al. [2001] shows that emissions from the interaction of the QE field with the background atmosphere at mesospheric heights match the altitude, size and duration of halos well. So far no models predict structured halos.

3.2.2 Observations of Halos

There were 23 halos imaged by the high speed imager on August 18, 1999, of which 20 had an obvious parent cloud-to-ground stroke in the NLDN data, as determined by spatial
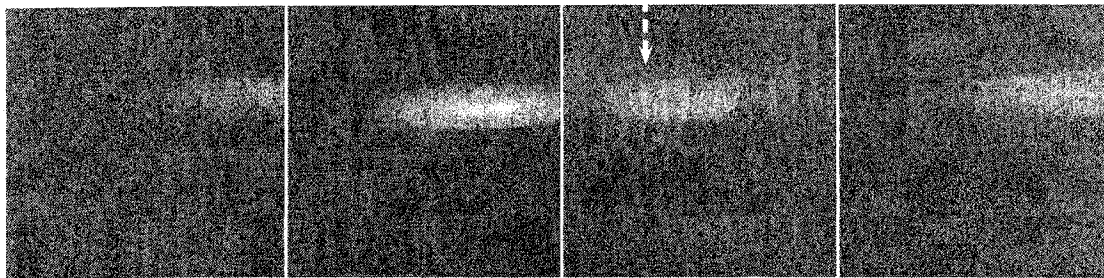
Figure 3.2. Examples of unstructured halos. Events are, from left to right, at 04:38:42, 05:02:05, 06:15:07 and 06:32:07 UT on Aug. 18, 1999. The bottom edge of the second halo is at the same elevation angle as an intervening cloud closer to the observing site, visible as a dark band. A sprite is visible in the third halo.

proximity and $< 1s$ temporal precedence. The other halos may still be associated with CG flashes, as the NLDN does not record all +CGs, especially those of complex forms. The halos tended to fall into two distinct categories with respect to their spatial structure. Figure 3.2 shows single images from four different halos that are fairly representative of approximately half of the 23 halos observed on Aug. 18, 1999. These halos are smoothly varying spatially, with no discernible structures. A small sprite onset originating from a halo is visible as a thin vertical line in the third example of Figure 3.2, indicated by an arrow.

The other half of all halos in the dataset for Aug. 18, 1999 are represented by the examples shown in Figure 3.3. In contrast to the halos shown in Figure 3.2, the halos in this group are structured to various degrees. The first halo in Fig. 3.3 has a lobe (a large-scale structure) to the left of, and separate from, the main portion of the halo. The second halo has some structure on its left side but is otherwise rather uniform (also a large-scale structure).

The third image of Figure 3.3 shows the most structured halo in the dataset. The structure is not due to intervening clouds, as is clear from images of the subsequent sprite. There is Rayleigh-scattered light above the clouds at the very bottom of the image (top row, 3rd image). One ms later, two larger sprites appear (not shown), one each from the two brightest "beads" within the halo, near the centerline of the CCD. The brighter of the two comes from the dimmer bead. One ms later they form a single carrot sprite (not shown). Note that the outline of this halo is still in the shape of a "pancake."
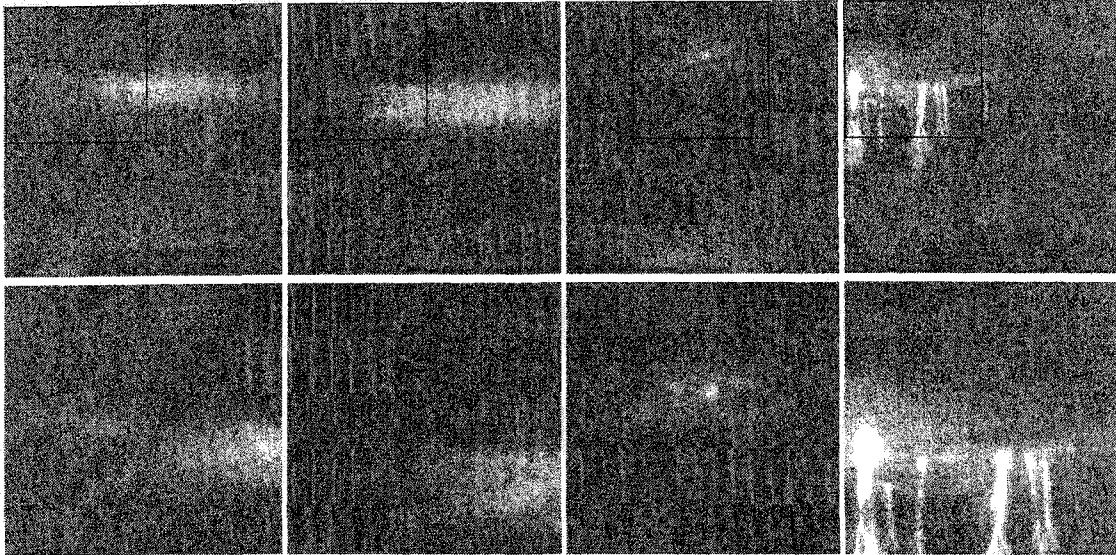
Figure 3.3. Examples of structured halos. From left to right, events occurred at 04:36:09, 04:41:10, 05:24:22 and 06:32:07 UT on Aug. 18, 1999. Top row shows the entire image of the four halos. The region indicated by a square in each field is expanded directly below it, in the bottom row.

The fourth halo in Fig. 3.3 shows a complicated image with both a halo and sprites. The halo started 2 ms earlier, and sprites 1 ms earlier than the image shown. The halo appears uniform and dim in the 1st ms (not shown), develops some apparently horizontal striations in the 2nd ms (not shown), which brighten in the 3rd ms (shown). These striations are visible around the brightest of the sprites and the two smaller sprites to the right of it. Note that the one darker stripe immediately "above" the second brightest sprite is an intervening thin cloud close to the observing site.

3.2.3 Analysis of Halo Observations

The same spatial Fourier analysis as was performed on elves (Section 3.1.3) was performed on four "unstructured" halos to search for evidence of periodic structure. Several horizontal image rows were chosen intersecting the halo. These were summed into a single horizontal profile, which was Fourier transformed. As with elves, no periodic structure was detected at the 95% confidence level. The other half of halos were structured, most with large scale non-periodic variations (Fig. 3.3 columns 1,2), and a few with small-scale variation (Fig. 3.3
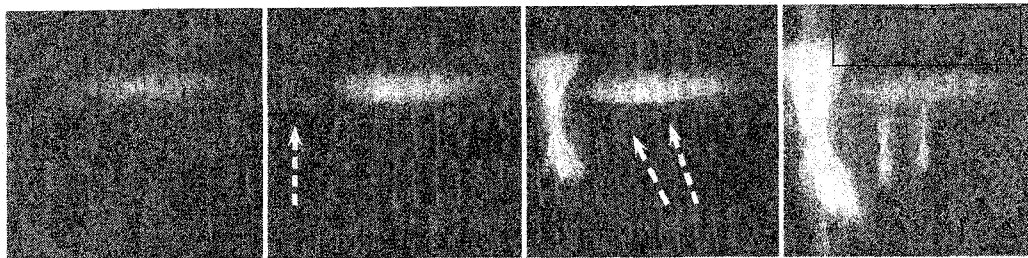
Figure 3.4. An example of a sprite initiating outside of a main halo. The sprite group occurred at 04:36:09 UT, and four consecutive fields 1 ms apart are shown. Arrows indicate the initiation sites of the three sprites. Multiple small clouds close to the observer are visible at the top of the last field (in box). The vertical streak above and below the left sprite are readout artifacts of the CCD.

column 3). Summarizing, half of the halos have no detectable small-scale spatial structure, and most of the structured ones possess large scale variations.

3.3   Sprite Initiation

Figure 3.4 shows the moment of initiation of several sprites occurring at 04:36:09 UT on August 18, 1999. The sequence shows 4 ms of data. The first image of a halo is the same image shown in Fig. 3.3 (first halo). One ms later, a thin sprite column appears by the side lobe of the halo (indicated by an arrow), while the main part of the halo becomes brighter. On the third field, the sprite by the side lobe has developed both extensive downward tendrils and upward branches. The main halo has brightened slightly from the previous field. Also, small, barely visible beads appear "below" the main halo (indicated by arrows in the third field). These beads are separated from the halo, but it is not possible to tell whether they are in front, behind or below the halo. In the 4th field, the leftmost sprite has developed into an even larger form, saturating the imager. Downward tendrils and small upward branches have developed from the two beads. By the next ms, not shown, both of the sprites on the right form large "carrot" sprites.

Figure 3.5 shows a sprite initiating in field 1 with a very dim tendril (indicated by an arrow). In fields 2-8, the tendril brightens a stationary bead while propagating downward. By field 9, the tendril is visible as a thin line, and the stationary bead continues to glow.
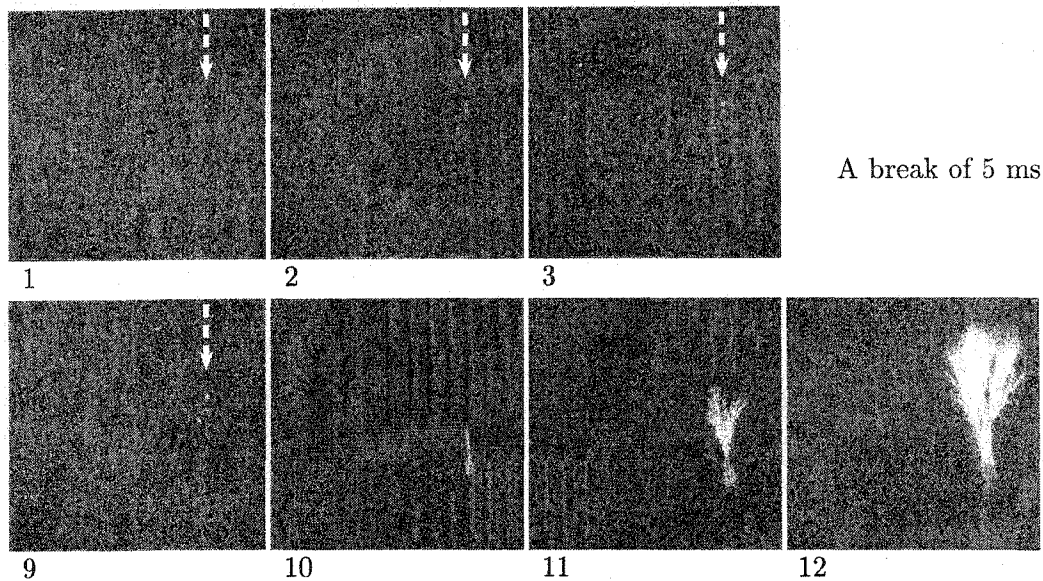
A break of 5 ms

Figure 3.5. Examples of sprite initiating without a sprite halo. This event occurred at 04:58:14 UT on August 18, 1999. Arrows indicate the initially very dim tendril location. Fields 1-3, 9 have greyscale enhanced with respect to 10-12 in order to show detail. As before, the vertical lines below and above the sprite on field 12 are instrumental.

The speed of the tendril remains nearly constant throughout the first 9 fields, on the order of 1×10^6 m/s.

In the following ms (field 10), with neither Rayleigh-scattered light near the horizon nor a visible halo, the tendril brightens and speeds up, then forms upward branches (field 11) and becomes a well developed "classic carrot" sprite (field 12). This large sprite forms without any associated halo. The average downward speed of the tendrils between fields 9 and 10 is on the order of 1×10^7 m/s. From the Aug. 18, 1999 dataset of 26 sprite/halo events imaged by the high speed imager and often consisting of multiple sprites, a total of seven sprites develop in similar manner. Many (> 10) sprites follow development similar to fields 1-9 of Fig. 3.5 but then disappear instead of forming a large sprite.

Finally, in Figure 3.6 an example of a complex event exhibiting a variety of effects is presented. The series in Figure 3.6 consists of two groups of sprites. In the first group, a single sprite initiates with a very slow and dim tendril, like the sprite in Fig. 3.5. After 13 ms, the tendril suddenly brightens, and forms a large carrot in the 14th ms. This sprite
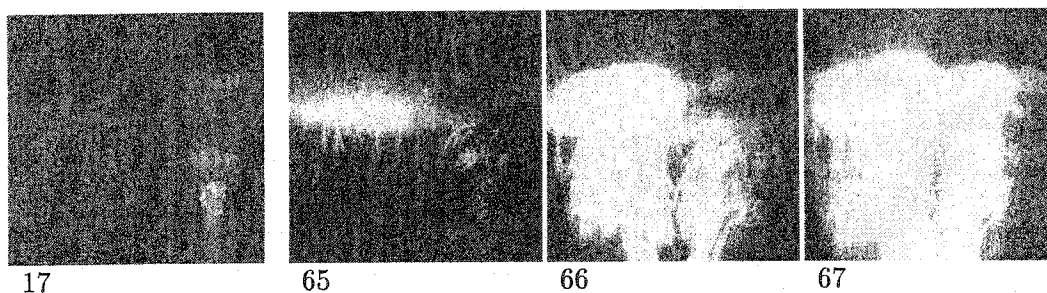
17   65   66   67

Figure 3.6. Examples of sprite initiation from beads left over from a previous sprite, at 05:45:05 UT. This event was discussed by Stenbaek-Nielsen et al. 2000.

saturates the imager. In order to show the details of the sprite structure, Fig. 3.6 shows field 17 (17 ms after sprite onset, or 3 ms after largest extent of the sprite) by which time the brightness has started to decay. The sprite body includes many beads and remains the brightest portion of the sprite. The tendrils are not very large below the body, and extensive branches lead to a diffuse glow above. It is the beads in the body that persist the longest, but even they disappear below the detector threshold by field 30. Starting with approximately field 50, some of the original beads seen in field 17 brighten again. On field 64 (not shown), an elve appears in the top of the image. One ms later, on field 65 the beads brighten extensively (field 65, right side). In addition to brightening, some of these beads also initiate tendrils to the side. At the same time, a halo brightens to the left of the beads, and small tendrils are visible emanating downward from the halo.

All of the tendrils visible in field 65 continue their development over the next two fields, creating an immense sprite group that saturates more than half the CCD image. This example shows both sprites initiating from beads left over from a previous sprite and those starting "within" halos.

3.4 Discussion

In the mesosphere and lower ionosphere, elves and halos appear as diffuse glows, while sprites appear as very structured discharges. By examining the elves, halos and sprites as observed by the high speed imager, some conclusions about sprite initiation can be formed. In particular, the spatial structure, or lack thereof, of elves and halos may indicate the structure of the causative electric field.

The emissions making up elves and halos have been proposed to be due to the interaction of electric fields from return strokes, either electromagnetic pulse or the quasi-electrostatic field, with the mesosphere and lower ionosphere [*Inan* et al., 1997; *Barrington-Leigh* et al., 2001]. The structure of the emission thus depends on both the structure of the electric field (the field coming from the lightning and interactions with its own reflections from the ionosphere), and the structure of the local atmosphere due to pressure or compositional perturbations. Sprites have been proposed to be due to the interaction of quasi-electrostatic fields from the return stroke with the mesosphere, launching streamers [*Pasko* et al., 1998; *Barrington-Leigh* et al., 2001], and also to the electromagnetic pulse from the subsequent intracloud portion of the lightning discharge [*Valdivia* et al., 1997], also possibly launching streamers [*Raizer* et al., 1998].

3.4.1 Elves Discussion

Starting with the elves, *Barrington-Leigh* et al. [2001] modeled a homogeneous electromagnetic pulse from the return stroke/vertical portion of the lightning interacting with a homogeneous atmosphere, which resulted in unstructured emissions when averaged over 1 ms. The modified theory of *Valdivia* et al. [1997] described in Section 3.1, where the electromagnetic pulse comes from the intracloud portion of the lightning discharge very close to the return stroke channel, would result in spatially structured optical emissions with only a small delay (<1 ms) from the unstructured emissions due to the EMP from the return stroke. These emissions would be at the same altitude as the unstructured emissions. Since a horizontal current is a better radiator into the mesosphere than a vertical current [*Valdivia* et al., 1997], these structured emissions, if present, should be brighter and readily visible. The absence of any discernible structure in the elves (Section 3.3) implies that the electromagnetic pulses creating elves is also relatively unstructured.

3.4.2 Halos Discussion

An argument similar to that of elves can be applied to halos. Halos have been modeled to be due to a quasi-electrostatic field interacting with the mesosphere [*Barrington-Leigh* et al., 2001]. Those results appear to match observations of unstructured halos. The emissions making up structured halos are governed by the interaction of a quasi-electrostatic field

with the atmosphere, and again, either of those two could be structured. To date, no model for a structured field has been published, but *Pasko* et al. [1997] have explored the influence of neutral density depletions, yielding stronger emissions in the depleted regions.

Thus, a QE field may create spatially structured emissions by either a structured field from the underlying lightning or a structured background in the ambient atmospheric composition/densityor by some combination of these effects. A structured QE field of a small scale-size may be difficult to create in the mesosphere. Consider a lightning strike which drains multiple charge regions within a thundercloud (which is known to occur for sprite-producing lightning [*Stanley*, 2000]). In an elementary approach, each of the charge regions can be treated separately to set up a QE field, and contributions from each summed to obtain the total field. In the simplest case, in the far-field approximation, the quasi-electrostatic field at a distance r from a charge Q residing at a height h above the ground is proportional to $\frac{M}{r^3}$ where M=hQ is charge moment [see for example eq. 12,13 of *Rowland*, 1998]. This $\frac{1}{r^3}$ dependence makes it difficult to create structured fields in the mesosphere. Adding the contributions of multiple charge structures will yield only a large-scale variation in the field.

We turn to the second way of creating structured optical emissions, by way of inhomogeneities in the mesospheric composition/pressure. Recall that most of the halos are unstructured or possessing large-scale structures. If there are small scale variations in the halos, they should be observeable in the images. Make an assumption that the halo model of *Barrington-Leigh* [2000] is a good approximation for the general shape of halos (as it appears to be), and also that there are small-scale (0.5-10 km) large-amplitude (for example, three times brighter than the surrounding region) variations superimposed on top of this general shape. Consider the case that this variation is superimposed on the brightest part of a halo, which is perhaps $\frac{1}{4}$ the size of the entire halo [*Barrington-Leigh*, 2000, Fig.5-6], and the halo does not saturate the imager. In this case, the fainter contributions from the dimmer outer edges of the halo along the line of sight can be ignored, and the variation should be discernable in the image. If, on the other hand, the variation is in the dimmer edges instead of the bright core of the halo, it should be possible to see this variation on the side of the halo in some of the cases (depending on the viewing geometry). No small-scale variations in either the core or the sides of the 20 halos examined were detected. The remaining 3 halos from a dataset of 23 from the night of Aug. 18, 1999 have small-scale

structure.

The EMP from fractal intracloud lightning model [*Valdivia* et al., 1997] or from the intracloud portion of CG lightning, since most of the halos had a parent CG flash, could also be potentially interpreted as causing structured halos. However, zero-to-peak risetime of electric fields from +CGs range from 4 to 25 μs [*Uman*, 1987, p.197]. Any change in the mesosphere due to these fields will have a peak variation at these timescales (plus time-of-flight), i.e. would occur at the same time as EMP from vertical dipole when observed with a 1 ms temporal resolution instrument, and decrease in magnitude thereafter. In the high speed imager, there is a definite delay [of $\sim$ 0.8 ms in our data, on average] between elves and halos, suggesting halos and their variations are not due to EMP.

Most (20 of 23) of the halos imaged have no detectable small-scale spatial structure, and most of the ones with some structure possess large-scale variations. The unstructured halos can be explained well by the model proposed by *Barrington-Leigh* et al. [2001]. In the case of halos with large-scale spatial structure in their emissions, it is not possible to say whether they are due to QE field variations, large-scale background atmospheric composition/pressure variations, or both. In the case of structured halos with small-scale variations, it is proposed that these are due predominantly to compositional/pressure effects. In particular, examples showing small scale variations (Fig. 3.3, image 3), would be very hard to create with quasi-electrostatic fields due to their $\frac{1}{r^3}$ dependence.

The observations thus indicate that both the incident electromagnetic pulses (EMPs) from lightning causing elves and the quasi-electrostatic (QE) fields causing halos tend to be uniform on 10 to 0.5 km length scale and 1 ms time scale. These observations thus appear to favor the vertical stroke model (for both electromagnetic/radiation and quasi-electrostatic fields) of *Barrington-Leigh* et al. [2001] over the fractal radiation model of *Valdivia* et al. [1997] for elves and halos, respectively.

3.4.3   Sprites Discussion

Sprite nucleation has been proposed to be either due to the quasi-electrostatic fields that also create the halo [*Pasko* et al., 1998], or due to the EMP from the intracloud portion of a cloud to ground lightning discharge [*Valdivia* et al., 1997]. *Valdivia* et al. [1997] proposed that since the intracloud part of lightning can continue for 10's, if not 100's of ms, their model easily

explains the often-observed [*Lyons*, 1996] delay between sprites and the parent lightning. In addition, a horizontal discharge radiates stronger EMP in the vertical direction than a vertical discharge. This horizontal fractal lightning results in very structured emissions, of about 10 km scale size for the values used by the authors (with an adjustment of the model parameters, the scale of these patches can presumably be increased or decreased). Patches at those length scales are not visible in the data. *Raizer* et al. [1998] used the Valdivia model as a pre-conditioning of the atmosphere, assuming that under the application of an quasi-electrostatic field these patches of enhanced ionization formed streamers. *Cho and Rycroft* [2001] suggest that EMP from horizontal (intracloud) discharge forms localized peaks of electron density in the altitude range 75-85 km, from which streamers could develop under QE. Their model included inhomogeneous EMP on very large length scales, ~100 km, which were not observeable with the imager at the distance of the storm due to the relatively narrow (6.4 × 6.4°) field of view.

Raizer et al. [1998] proposed sprites to be streamers propagating downward in the mesosphere. Their theory predicts streamers developing under QE from packets of enhanced ionization, such as predicted by the *Valdivia* et al. [1997] model. As was shown, the strong structure in emissions predicted by the *Valdivia* et al. [1997] model is not observed, either immediately after elves or at later times. The *Raizer* et al. [1998] streamer model predicts a range of velocities from 10^6 m/s at the beginning of the streamer to a maximum of 10^7 m/s near time $= 4$ ms for the charge used. The sprite in Fig. 3.5 shows a slowly developing sprite moving with nearly constant speed (10^6 m/s) which suddenly speeds up after 10 ms to 10^7 m/s. This speedup could be caused either by the streamer moving into an atmosphere with a different composition, or by an increase in electric field strength since streamer velocity increases with external field [*Raizer*, 1997, p.336].

The question of whether EMP from intracloud portion of a cloud-to-ground lightning is important in sprites merits further discussion. As is presented in *Valdivia* et al. [1997], a horizontal antenna radiates efficiently upward. The theory predicts very bright patches of emissions, with some unspecified delay from the return stroke. Such patches are not visible in the data. However, the idea of accounting for the time delay from a return stroke to a sprite by using the intracloud portion of lightning may be appealing. It is possible that the structured EMP fields from the intracloud discharge help heat the structured regions of the

mesosphere, albeit not to the level of optical emissions visible by the instrument, and in turn facilitate the initiation of streamers. Combining the Lightning Mapping Array (LMA) system of New Mexico's Institute of Mining and Technology with high speed observations of upper atmospheric flashes would help answer this question.

We now ocnsider streamers initiated by the QE field. *Pasko* et al. [1998] write that under an applied quasi-electrostatic field, "... a streamer can develop from an avalanche initiated by a single electron." This electron is one of many freed by the QE fields interacting with the mesosphere to form a halo. Under an appreciable field, most of the electrons attach dissociatively to O_2 to form O^- and O. The maximum rate for this attachment is 1 kHz at 80 km and 10 kHz at 60 km [*Barrington-Leigh*, 2000, Fig. 1-1 and p.9]. The attachment rate is slow enough that there would be many free electrons left after 1 ms, and within any halo the streamers should initiate in abundance. The observation of sprites initiating outside of halos (Fig 3.4) would seem contradictory to this theory, at least in its simplest form. Applying the theory to a height structured atmosphere with density fluctuations may prove more promising.

Barrington-Leigh [2000] has further suggested that the bottom of a halo, where the electric field is the strongest, could launch a streamer (a sprite tendril). This theory is contradicted by the images in Fig. 3.4 where a sprite is initiated well to the side of the main halo. However, with these exceptions, the halo theory appears to predict halos and halo characteristics in the high speed images very well.

There have been a number of suggestions for an external trigger of sprites. *Suszcynsky* et al. [1999] have presented possible evidence for a sprite initiated by a meteor and a model using the meteor trail for pre-conditioning of the atmosphere was presented by *Symbalisty* et al. [2000]. Based on the spatial separation of triangulated locations of sprites and their parent lightning *Wescott* et al. [2001] have likewise suggested meteors to be the possible trigger of sprites. Similarly, *Zabotin and Wright* [2001] have suggested micrometeors to be responsible. None of these suggestions can be discounted by the image data. In fact, the idea of a random trigger is especially appealing for events like that in Figure 3.5, where a large sprite forms without any associated halo. However, the image data also suggest that there may be other types of sprite "seeds." In Figure 3.6, sprites are clearly initiated from beads persisting from a previous sprite. These beads are at altitudes up to 80 km, where the

electric field relaxes in less than 1 ms, according to the relaxation time scales published by *Pasko* et al. [1997] and [*Barrington-Leigh*, 2000, Fig. 1-1]. The long duration of the beads (10's ms) suggest that factors other than simple electrical relaxation, such as chemical processes or ambipolar diffusion, may be responsible for determining their relatively long lifetime. Either way, the beads, being luminous, are obviously different in some aspect from the background atmosphere, and can provide initiation sites for subsequent sprites.

Overall, elves and halos can be thought of as mappings of the EMP and QE fields, respectively, from the return stroke and associated charge distribution within a thundercloud into the upper atmosphere. The mainly relatively spatially unstructured character of both phenomena suggests the underlying electric fields associated with them similarly lack significant small-scale spatial structure. The observations of sprites triggering outside of a main halo (Figure 3.4), without a halo (Figure 3.5) and from small scale features left over from a previous sprite (Figure 3.6), respectively, when considered together with the unstructured fields discussed above, suggests sprites are triggered at sites of localized inhomogeneities in the mesospheric medium. These could be inhomogeneities persisting from a previous sprite, as proposed by *Stenbaek-Nielsen* et al. [2000], or could be the effects from other pressure or composition perturbations, including but not limited to the previously suggested meteors and/or micrometeors, or gravity wave turbulence such as described by *Yamada* et al. [2001].

3.5 Summary and Conclusions

Images of elves and halos obtained with a 1 ms high speed imager were analyzed. The main conclusions are: (1) Most of these events are relatively featureless on 0.5-10 km length and 1 ms time scales. (2) It is concluded that the EMP and QE fields from return stroke of lightning reaching the mesosphere and lower ionosphere to form elves and halos, respectively, similarly lack small-scale large-amplitude structure. Any structure in the emissions is interpreted to be due to background inhomogeneities in atmospheric composition or pressure. (3) Sprites are most likely not initiated in patches of strongly enhanced electron density created by electromagnetic pulses from either vertical or horizontal lightning channels, nor exclusively by the enhanced quasi-electrostatic field on the bottom side of halos, as evidenced by sprites that appear outside of halos, or without accompanying halos. Sprites are

most likely initiated principally in regions of localized pressure or chemical perturbation of the background atmosphere at sites most conducive to streamer formation. Such perturbations include beads left over from a previous sprite, or other sources such as gravity wave turbulence. Meteors or micrometeors could also act as triggers in some circumstances.

Chapter 4

Varieties of Sprites

The spatial forms of sprites as recorded in CCD images loosely fall into distinct categories that have been dubbed columniform sprites, carrot sprites, or jellyfish sprites. Examples are shown in Figure 4.1. Columniform sprites, or c-sprites (pronounced "see-sprites"), consist of a bright column with tendrils often extending below it [*Wescott* et al., 1998b]. Carrot sprites are reminiscent of a bright carrot topped by more diffuse leaves, with the tendrils (the roots of the carrot) appearing to hang down from the main carrot body. An image of a jellyfish sprite consists of a bright oval (the bell of the jellyfish) below which many sprite tendrils (tentacles) are visible. All of these sprites may include bright small patches, termed beads and balls, often visible near the region of sprite body [*Sentman* et al., 1996].
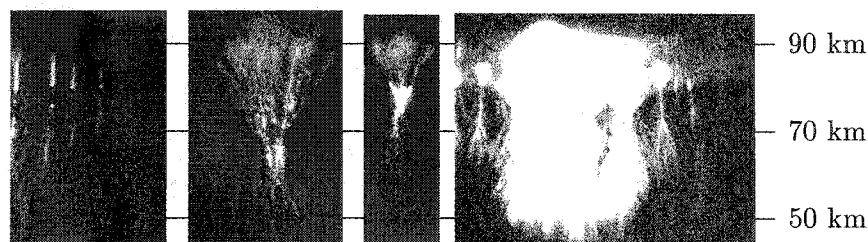

Figure 4.1. Commonly-used descriptions of sprites include columniform sprites (left), "carrot" sprites (both sprites in the middle), and "jellyfish" sprite group (right). Altitudes are approximate based on parent lightning location. The events occurred at (L to R) 05:57:16 UT, 04:58:14 UT, 05:17:16 UT and 06:15:07 UT on August 18, 1999, respectively. Images were integrated over 1 ms.

Takahashi et al. [1996] and *Fukunishi* et al. [1996a] have shown, using a multi-anode, high speed photometer, that sprites initiate between 70-80 km altitude with downward tendrils. In the case of carrot sprites, *Takahashi* et al. [1996] have shown that the downward tendrils are followed a short time (<2 ms) later by upward branches. Similar observations carried out with a high speed camera were presented by *Stanley* et al. [1999]. Both the downward tendrils and upward branches have been suggested to be streamers [*Raizer* et al., 1998; *Pasko* et al., 1998; *Stanley* et al., 1999].

In addition to the sprite types described above, in this chapter the development at 1 ms temporal resolution of a wide range of sprite types is described, ranging from the smallest, most basic, and dimmest forms, to the largest and brightest forms. A discussion about the variety of glows forming sprites follows. Based on our images, sprites are separated into two basic categories: those without and those with upward branches. Sprites without upward branches appear to be smaller than those with upward branches. Groups of sprites are shown, which are often mixtures of more than one type of sprites of similar form, as recorded with both the 1 ms imager and TV-rate ($\sim$ 17 ms) cameras. Based on these observations, the characteristics of different optical emissions within sprites are described, separating optical emissions into dynamic and stationary forms based on dynamical behavior across several successive images. Dynamic forms include downward tendrils and upward branches, and have been suggested to be streamers. Stationary forms include 1) beads occurring within upper parts of tendrils and lower parts of branches, 2) thin columns, thick columns and elongated "not-quite-column" features termed here as "quasicolumns" occurring in the central part of sprites, and 3) puffs occurring above branches. Within groups, most complex sprites are in the center of the group, with simpler sprites generally occurring on the edges of the group. It is proposed that once a sprite is initiated, its shape and form are largely determined by the temporal form and magnitude of the driving electric field emanating from the underlying thunderstorm.

4.1 "Regular" Sprites at 1 ms and TV-rates

"Regular" sprites generally last less than 30 ms, in contrast with "unusual" sprites presented in a later section.

4.1.1 Single Sprites Without Branches at 1 ms Temporal Resolution

Sprites without branches exhibit many forms. The dimmest and smallest form of a sprite consists of tendrils only. A sprite of this form may develop a bead along its tendril. A bead is a brightness feature that is not elongated in our images in any direction. Beads are spatially not resolvable at the high speed imager resolution (300 m). The bead continues to glow following passage of the tendril. Other examples exhibit multiple beads, columns, or thick columns that brighten. Examples of each of these forms are shown in the order described.

A tendril-only sprite

Figure 4.2(a) shows an example of a sprite consisting of tendrils only. It shows the same small section cut from 12 successive 1 ms images and stacked side-by-side, effectively creating a time series of the development of the tendril. The width of one single image, or field, within the time series is equivalent to the 1 ms time integration of each image. The time is shown below the images. To the right of the images is shown a bar whose length is equivalent to 5 km. The greyscale has been reversed and contrast-enhanced. A downward propagating tendril in this presentation is visible as a downward sloping line. In this case the tendril is barely visible, so an unmarked diagonal line to the right of the images has been added to help guide the eye. Rotating this page and tilting it so as to look down this indicated line reveals the downward moving signal in the data. The speed of this tendril is on the order of 10^6 m/s. This sprite occurred temporally (within 20 ms) and spatially (in the field of view) near a group of larger sprites. This example and other sprites consisting only of tendrils are dim, but are readily visible when the 1 ms data is played in succession as a movie. They are difficult to see in TV-rate data.

A tendril-and-bead(s) sprite

Sometimes a downward moving tendril develops a bead during its descend. An example of this type of sprite is shown in Figure 4.2(b). The Figure shows a 16 ms sequence of 1 ms images of this "tiny sprite" stacked side-by-side, forming a time series. The time is shown below the images, and a 5 km bar is indicated to the right. The gray scale has been
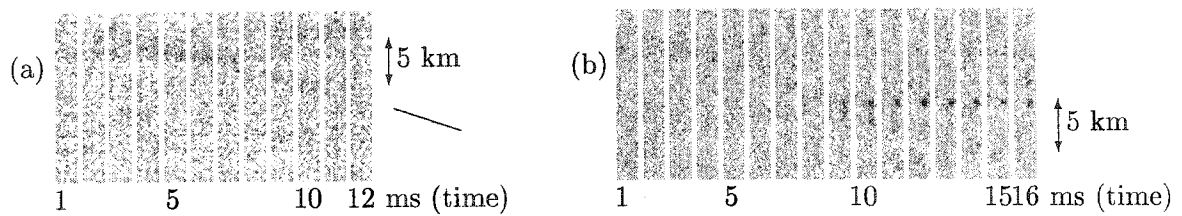
Figure 4.2. Examples of sprites without upward branches 1. Grey scale has been reversed and contrast-enhanced in all examples: (a) A 12 ms time series of a tendril-only sprite at 04:41:10 UT. (b) A 16 ms sequence showing a beadand-tendril sprite at 05:17:16 UT.

reversed and contrast enhanced to bring out the dim details. Visible in the time series is a brightened bead near the center of the image (field 9), and this bead persists for more than 5 ms. The tendril is visible apparently descending from the bead, but if the page is rotated, one may see that the dimmer tendril in fact starts at a higher altitude than the bead. Tendrils are dynamic and short lived phenomena, whereas the beads are static phenomena, with an apparent lifetime of 5-10 ms or even longer. The bead is not necessarily at the top of the tendril, *i.e.* it does not occur at the location where the tendril initiated. This "tiny sprite" occurred temporally separated from any other sprite by nearly 400 ms, and was recorded purely by chance. This leads one to believe that current observations are likely missing much low-level optical activity occurring above active thunderstorms.

In general tendrils are dimmer than beads, but many beads triggered by a passing sprite tendril may enhance the brightness of a sprite. In Figure 4.3(a) is shown a sprite that includes many beads. Shown are 13 ms of data stacked side-by-side, with time since the first image indicated below, and a 5 km scale shown at right. The figure shows a tendril that moves steadily downward from field 1 to field 4 with a bead brightened at the top. The tendril then speeds up slightly (fields 5-6) and brightens multiple beads, with a definite time delay between the passage of the tendril and the brightening of a bead. The tendril finally slows down and dims. Nine milliseconds after the start of the time series, the sprite tendril is no longer visible but multiple beads remain, strung along the region passed by the tendril. The lifetimes of the beads are longer than 10 ms. It appears as if the central/brightest beads need to "turn on" before the beads above can brighten. This is indicative of a feedback mechanism, *e.g.*, there exist cases when a tendril passage is a necessary but not a sufficient condition to brighten beads.
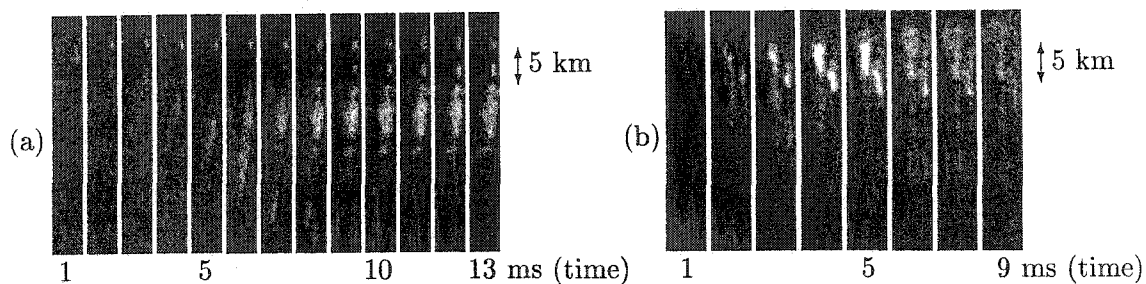
Figure 4.3. Examples of sprites without upward branches 2. (a) A sprite with multiple beads, at 04:41:10 UT. Right column: (b) "Quasicolumn" sprites, occurring at 05:05:47 UT.

A "quasicolumn" sprite

The beads brightened by a tendril occasionally expand and form a structure that is almost a continuous column. An example of "quasicolumn" sprites is shown in Figure 4.3(b). In the first field a tendril is barely visible near the top. It brightens, together with a bead and another tendril, in fields 2 through 4. Both of the sprites form somewhat short and stocky columns. These short, thick columns expand both upwards and downwards. However, they are shorter and more structured than the "columniform" sprites originally described by *Wescott* et al. [1998b] (shown next). Thus, these forms, together with the tendrils are classified as "quasicolumn" sprites.

Columniform sprite

In some cases, as a sprite tendril descends, its top end increases in luminosity, resulting in a nearly uniform column brighter than the tendril itself and forming a so-called columniform (or c-) sprite. One such example is shown in Figure 4.4(a). Eight successive 1 ms images are shown side by side. A dim tendril is barely visible in the second image, and is of nearly uniform brightness at all altitudes. One ms later, in the third image, the tendrils are topped by a bright column, which remains luminous for a few ms. The tendril also brightens two beads in lower altitudes.

After two ms the column itself appears slightly wider and brighter near the bottom than at the top. As it decays, its lower end remains brighter than the upper end. The two beads are visible below the column even as the tendrils decay below instrument sensitivity. Note
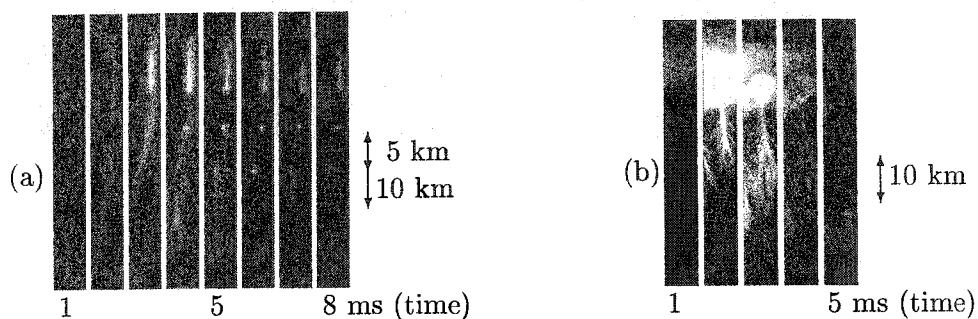
Figure 4.4. Examples of sprites without upward branches 3. (a) A columniform sprite occurring at 05:57:16 UT. (b) Five ms in the wide-columned sprite occurring at 06:15:07 UT.

that based on the examples given before, the beads within tendrils, in this case below the columns, do not indicate a special feature of columniform sprites.

Angel sprites

Some sprites develop into thicker forms than that of a simple column, including formation of a bulb-shape at the top of the tendrils. These have been previously called "angel sprites" by *Stanley* et al. [1999]. One such example is shown in Figure 4.4(b). The Figure shows five successive 1 ms images. In the first image, a halo is visible near the top, brightening in the second field. Below the halo, sprite tendrils develop downward. In the third field, after the brightness of the halo has subsided, a bulbous shape is visible where the halo previously existed, while the tendrils continue their downward propagation. In the fourth field, the apparent darker region within this bulb is probably an instrument artifact. By the fifth field, most of the brightness has subsided.

In most respects the angel sprite appears similar to c-sprites, with the exception of the shape of the bright emissions at the top. These, instead of being a column, appear as a bulb. Otherwise, as with all previous sprites, the tendrils develop downward, and bead(s) within the tendrils may brighten.

The angel sprites conclude our section on sprites without upward branches. These sprites, consisting of tendrils only, tendrils brightening a few beads, tendrils brightening many beads, and column and angel sprites, are similar to an intermediate form sprites, which ultimately form branches, go through.

4.1.2   Single Sprites With Branches at 1 ms Temporal Resolution

Tendril to carrot formation

Upward branches of sprites appear to occur in two distinct classes, which will be called large and small. Large branches are generally longer than 10 km, with large ($\geq$ 2 km) diffuse puffs or hair on top. Small branches are smaller than 10 km, with small ($\leq$1 km), diffuse puffs on top if they occur at all. Small branches often develop slower than large branches, and tend to be displaced to the side of the main vertical form, but the distinction is usually not as sharp as is presented here. Both types of branches develop upward, but only the large branches ultimately form the extensive "carrot" sprites. Several examples of sprites are presented that start their development similarly to those already presented, but ultimately form branches.

Figure 4.5(a) shows a case in which a dim tendril forms a carrot sprite. The figure shows two parts of a 12 ms sprite sequence. The numbers below each field show the time, in ms, and at right is shown a 10 km length scale. Fields (or ms) 1-9 were grey scale adjusted to show dimmer detail, and arrows indicate the location of the dim sprite tendrils and a bead.

In field 1 a dim bead is visible below the arrow, and a star is below it. (In the previous field, not shown, only the star is visible.) In subsequent fields, a tendril propagates downward from this bead, with speed on the order of 1×10^6 m/s. Up to this point the sprite is indistinguishable from a sprite consisting of tendril only.

In field 10, the downward tendril suddenly speeds up to order of 10^7 m/s (covering in 1 ms the same distance it covered over the previous 9 ms), brightens, and starts to split. The original bead continues to be visible, but is much dimmer than the tendril itself, and another bead is visible in the (new) bright tendril. In the next two ms (fields 11-12), extensive upward branching develops from this new bright tendril reaching past the location of the original bead.

This example shows that the initial development of sprites can persist over a relatively long time, in this case more than 10 ms, before the "final" form is reached. In its initial
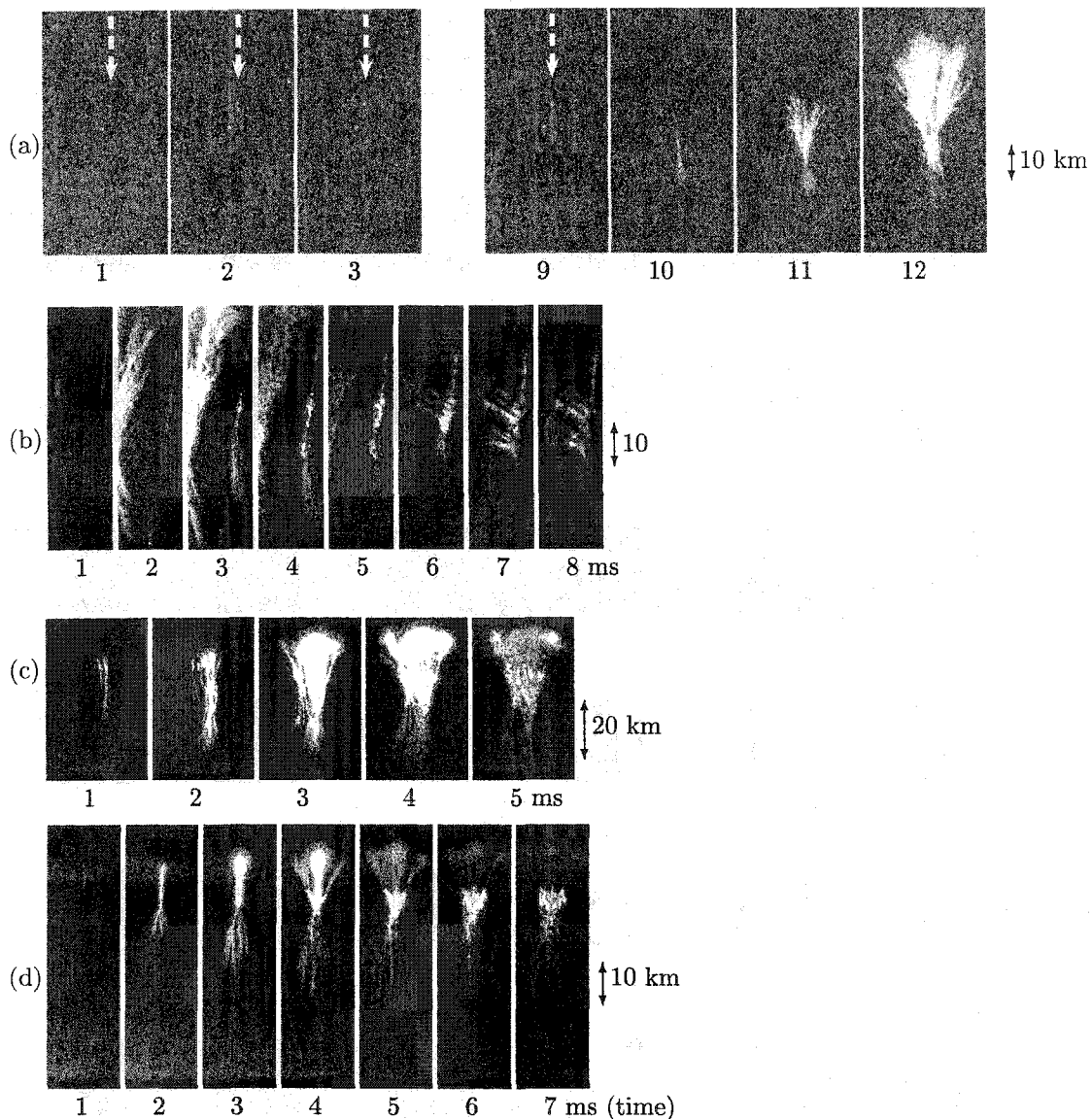
Figure 4.5. Examples of sprites with upward branches. (a) Example of a carrot sprite initiating from a tendril. This event occurred at 04:58:14 UT on August 18, 1999. Arrows indicate the initially very dim tendril location. Fields 1-3, 9 have greyscale enhanced with respect to 10-12 in order to show detail. Example was presented in *Moudry* et al. [2003]. (b) A sprite consisting of beaded tendril, forming branches. The sprite was one in a group occurring at 05:24:22 UT on August 18, 1999. (c) Branching from a "quasicolumn" in the sprite occurring at 05:10:38 UT on August 18, 1999. (d) A columniform sprite whose column widens before forming upward branches from the bottom of the column. The sprite occurred at 05:17:16 UT.

form, the sprite is indistinguishable from a "tendril-and-bead" sprite. Two things then occur: i) the tendril speeds up and brightens (field 10), and ii) upward branches appear (field 11). The two are only slightly dependent on each other; while branches appear to form only in cases when the speed of sprite tendrils exceeds 10^7 m/s, the "jellyfish" sprites presented later include fast tendrils but no extensive branching. The downward tendrils in the final form are small, yet at the same time the upward branches of the sprite develop into an extensive form.

Branching from beads formed in tendrils

In the previous example branches developed from the tendril but not from the bead(s). A case is now presented in which branches do form from the beads. Figure 4.5(b) shows an 8 ms cropped sequence of one of the sprites occurring at 05:24:22 UT on August 18, 1999. Contaminating the left part of fields 1-4 is another sprite, that starts in field 1 (left side), and is nearly fully developed one ms later (field 2), decaying after field 3. Ignoring this sprite on the left, on the right side, starting with field 1, a downward moving tendril. In field 3 this tendril develops extensive beads, which brighten over the next three ms by some unknown secondary processes. These secondary processes result in the multiple structures visible along the tendril path in field 5 (for example, top-most part of the tendril) which were not present in fields 1-3. In fields 5 - 8, branches form from the middle beads in the direction of the "contaminating" sprite.

The (small) branches then reach out sideways, appearing initially as uniform and dim structures. The branches appear to reach exactly to the outermost reaches of the "contaminating" sprite visible in fields 2-4. Within a few ms of the branch formation beads develop within the branches.

Branching from quasicolumn sprite

Next are presented examples of branching from sprites which are of the "quasicolumn" form in the intermediate state. As with other sprite types, these can also form upward branches, as shown in Figure 4.5(c). The first field shows several beads and tendrils, the two brightest ones on the right side and one on the left. In field 2, the two tendrils on the right brighten and expand, as does to a lesser extent the one on the left. The most

intense development occurs in field 3, resulting in a massive carrot sprite with large upward branches, which saturates the imager. The branches include bright diffuse emissions at the top. One branch, perhaps originating from the left tendril, is to the left of the branch, and it, too, forms a diffuse luminosity in field 4. Note the second set of tendrils coming from halfway down the right side of the sprite in fields 4 and 5. These are probably responsible for multiple developments of beads and columns in the body of the carrot sprite, accounting for the largest extent of the sprite in field 4. As the imager decays from saturation in field 5, some structure of the sprite becomes visible, in particular the complicated body of the sprite, above which are multiple branches, topped with diffuse puffs or hair.

This sprite also highlights a problem in terminology. In fields 4 and 5, the structure appears to be one single sprite. Yet, in field 1 there are at least three relatively distinct tendrils moving downward, plus a host of smaller ones (not visible at this scale). It is not clear if this is one sprite, or three sprites merged together. Ultimately, the final form of a sprite does not give any information as to how many independent tendrils initiated it, or if they occurred spatially and temporally close together.

Column-to-carrot sprite formation

In addition to the formation of upward branches from "quasicolumns" presented in the previous section, branches can also form from the bottom of columns. A sprite that starts out as a simply columniform sprite is shown in Figure 4.5(d). The sequence is 7 ms long. In the first two images, a halo and columniform-like sprite are visible. The sprite column brightens and widens extensively in the third ms. Note that this is not an instrumental saturation effect. The thickness of the column is greater near the top than near the bottom. The top of the column is diffuse. The tendrils continue downward. In the fourth ms, oblique upward branches form from the bottom of the bright column. As with the previous examples, the upward branches expand in diameter as they travel up and end in diffuse puffs at the top. These puffs are longer-lived than the branches that created them and are still visible in field 7.

Note also that the shape of the light-emitting region has changed from field 4 to field 7. In particular, the puffs are separated from the body of the sprite, and the branches have retracted to form shorter columns. This reshaping of emitting regions occurs with the

development of secondary tendrils, which move downward from the body in fields 4-7 (at the resolution shown perhaps best visible in field 6).

4.1.3 Several Other Examples of Sprites at 1 ms Temporal Resolution

Figure 4.6 shows some additional examples of sprite dynamics. At upper left, a sprite is shown that develops small branches in fields 4 and 5, with small puffs (not visible at this resolution). The small branches originate near the bottom of the column, as with all the other examples presented here. However, the branches do not reach any extensive proportions, and the sprite remains relatively dim.

In the upper right of Fig.4.6 is an example of a sprite that develops a few large branches from a generalized brightness which cannot be classified as a column, but the branches form predominantly to one side, away from a group of sprites on the right (not shown). In the lower parts, the branches transform into a series of beads.

In the bottom panel is shown a sprite that forms a few large branches and can be classified as a carrot sprite. Initially, only a small amount of brightness near the top is visible (if the contrast is enhanced, the tendril is visible also). On field 3, a second brightness becomes visible lower down. As the top brightness slowly progresses downward and the bottom brightness upward, the sprite becomes reminescent of that shown later in Fig.4.10a. The similarity continues in field 8: as the two bright sections come together, first one large branch develops upward, then in the next field a second branch appears. Together with the two branches, the body of the sprite brightens as additional secondary processes (such as additional column and bead formation) occur. The top part of the large branches decays, leaving only a puff, while the bottom part of the large branches remains luminous from persistent beads.

4.1.4 Sprite Groups at 1 ms Temporal Resolution

Of the sprite forms described in the Introduction, carrot and columniform sprites (individual sprites) were presented, but not jellyfish sprites (a group of sprites). Multiple sprite groups are presented next, first at 1 ms, then also in 17 ms resolution in order to show the variety of delays of sprite initiations within a group and the variety of sprite forms. In most sprite groups, the sprites appear within 1-20 ms of each other.
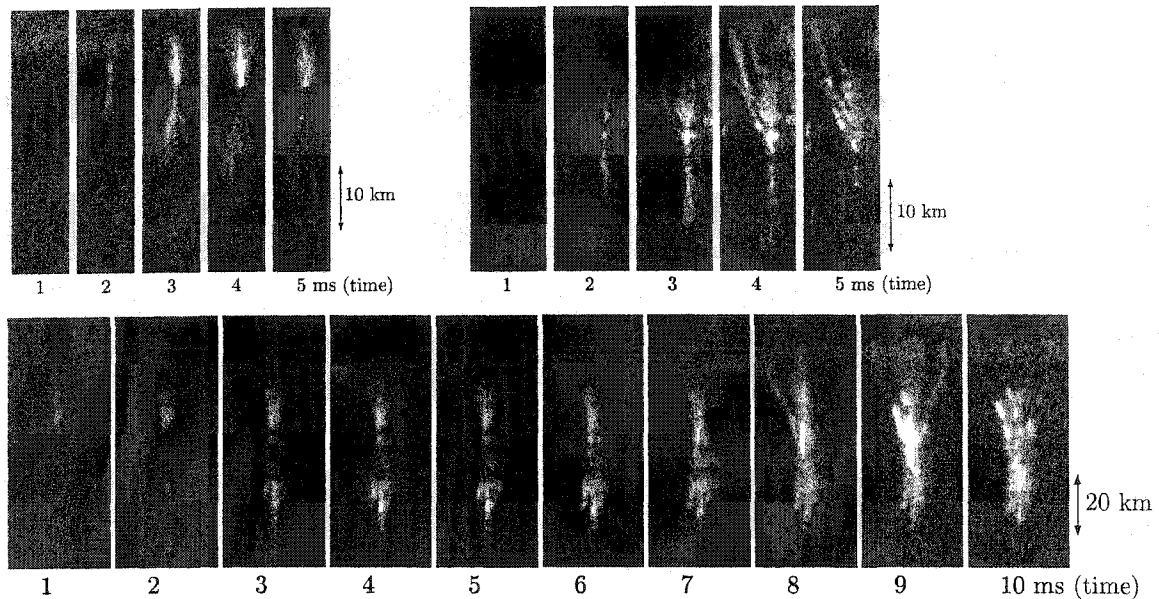
Figure 4.6. Additional examples of sprites with small branches. (upper left) Sprite with small branches occurring at 06:32:07 UT. (upper right) Sprite with a few large branches only to one side, occurring at 04:38:42 UT. (bottom) Large branches developing after extensive pre-branch activity in one of the sprite occurring at 07:05:26 UT on August 18, 1999. This sprite may be similar to that shown later in Fig.4.10a but occurring on a shorter timescale.

Figure 4.7 shows images of groups or individual sprites at 1 ms time resolution. The Figure shows six sequences of sprite events, all with preceding halos. The images are shown in reverse grey scale and have been contrast enhanced to bring out the features of interest. The first image in each sequence shows the background without any halo, though there is the faint suggestion of an elve. The second image in each sequence shows the first image with any discernible halo, though the halo may not be visible in the printed Figure. The sequences all terminate with fully developed sprites, and are time-aligned based on the greatest spatial extent of the sprites, shown in the box.

In some of these sprite groups, in particular in jellyfish sprites, the sprites appear nearly instantaneously, *i.e.* within less than 2 ms of each other and of the halo that precedes them. Two such examples are shown in the two top rows of Figure 4.7. In both of these groups, the greatest extent of the sprites is within less than 2 ms of the first indication of a halo. In the second row, the halo is visible by itself for 1 ms, indicating that jellyfish sprites are composed of a halo and multiple sprite tendrils. The similarity to the shape of a

jellyfish is what gave the name to sprite groups of this form. While not shown here, jellyfish sprites in their later stages are observed to be composed of columns somewhat thicker than columniform sprites, possibly with small developing branches extending obliquely upward from the bottom of the thick column of the central sprites in the group. From these limited observations, it appears that a typical jellyfish sprite, or more accurately, a halo and multiple sprites, consists of simple sprites without extensive upward branching. This could indicate that branches require a longer time to develop compared to tendrils.
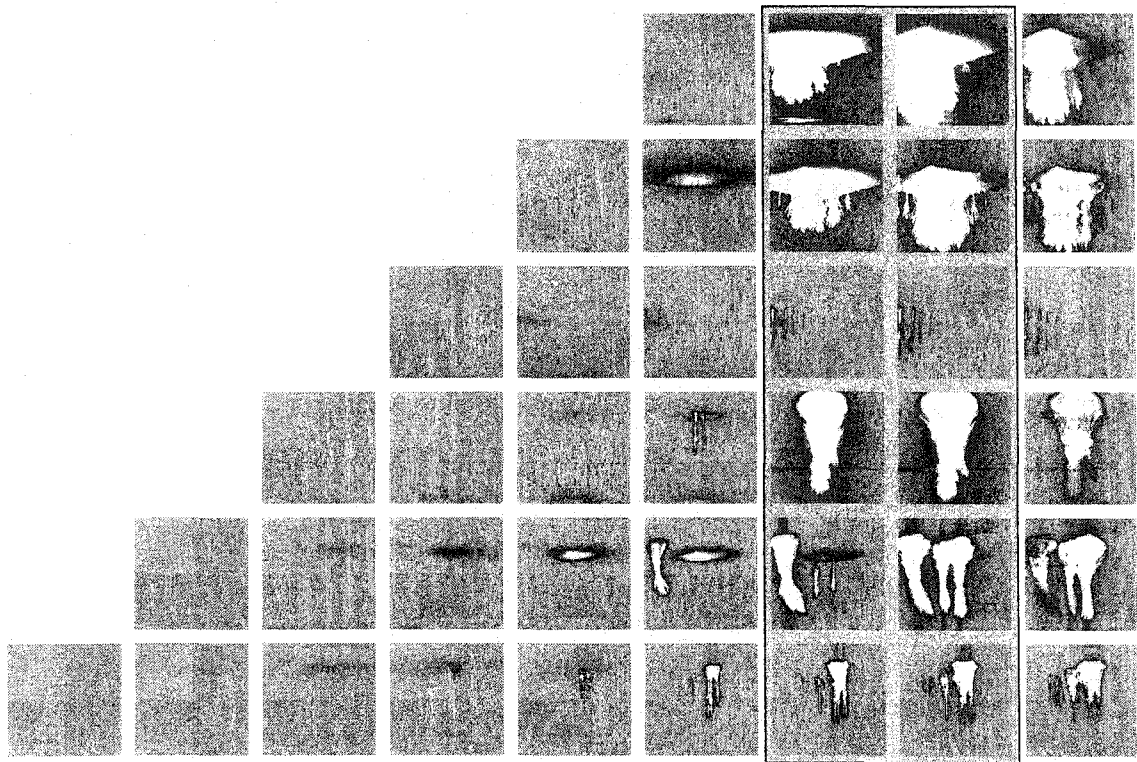

Figure 4.7. Examples of sprite groups. Six groups of halos and sprites shown at 1 ms time resolution. The images have the grey scale reversed and adjusted. The first field shows the background image, next image shows the first indication of a halo, with following sprites. The sequences are approximately aligned based on the greatest spatial extent of the sprites.

In contrast to the fast development and short time delay between sprite initiations of the jellyfish sprites shown in the two top rows of Fig.4.7, the other rows show groups of sprites which develop over a longer period of time. In the third row are shown a group of columniform sprites, that do not develop any branches, and are brightest 2-3 ms after halo

initiation. The fourth row shows a carrot sprite with upward branches (not well visible due to saturation) which lasted 3-4 ms from first indication of a halo. The second-to-last row shows a group of sprites shown by [*Moudry* et al., 2003, Fig.4], which take 4-5 ms to develop into the large form from the initiation of the halo. The sprites within the group do not appear at the same time.

The last row shows another group of sprites which takes longer than $\sim$5 ms to develop. The first sprite is visible only on field 4, and brightens and expands in subsequent images. To the left of it, a small sprite becomes visible on field 6, and likewise expands. On field 7 (first field in the box), more sprites become visible to the left of the two described.

There are several points to notice regarding these groups of sprites. Sprites within a group can, but do not necessarily, all start at the same time. Those that do often form a jellyfish sprite (group). Within a jellyfish or other groups, most often the first and/or center sprites (with respect to a halo, if any) develop the fastest and into the largest forms, while those off to the side or later ones are smaller.

4.1.5 Sprites and Groups of Sprites at TV-rates

The difference a camera makes

Before delving into a gallery of sprites observed at television-rate time resolution, we wish to show in Figure 4.8 images of two separate sprite events taken by three different cameras with different fields of view. The top row shows a carrot sprite, and the bottom row a group of undeveloped sprites. The first two images in each row show the sprite events as observed by two University of Alaska Fairbanks cameras at a range of approximately 600 km, the last image is of the same sprite event as observed using a Xybion camera, kindly provided by Walt Lyons, at a range of approximately 500 km.

Figure 4.8 shows that the apparent shape of a sprite depends on the characteristics of the camera used to obtain the images, in particular its field of view and response. The first image in each row, in comparison with the other two images, shows that sometimes a less sensitive camera provides unsaturated images and better information. Thus, the carrot-sprite of the first row appears to have a body mainly composed of beaded structures; this structure is not visible in the other two images. Unlike the bright sprite body, which
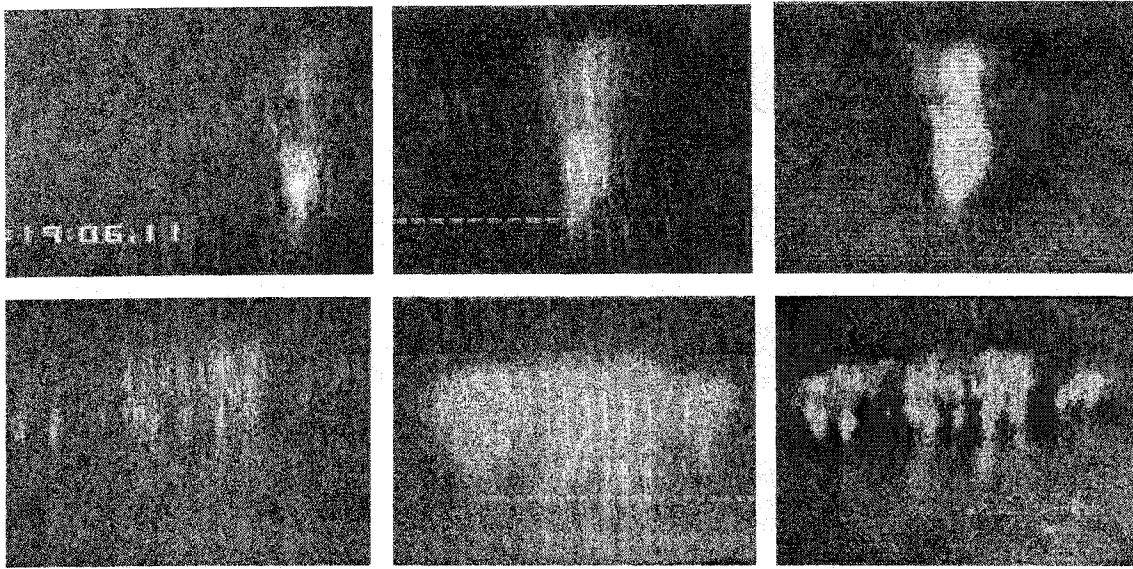
Figure 4.8. Examples of two sprite events seen by three different cameras. A part of a time stamp and of dashed line used to indicate field of view of a slit spectrograph are visible in three of the images. The images were cropped to show the sprite events at a similar field of view.

is best visible in the first camera image, the diffuse parts above the bright body are most visible in images from the two other cameras. A similar observation is shown in the bottom row: while a camera with a limited sensitivity provides detail of the bright central part of sprites (first column), cameras with increased sensitivity allow one to see the dimmer sprite tendrils below the body. The shapes of the sprites also differ slightly.

In summary, for saturated sprites images, the shape of the sprite is dependent on the camera. In images where the sprites are not saturated, the dimmer regions are missing. In order to see the details of all the light-emitting regions within sprites, ideally two cameras would be used: a more sensitive one to observe the dimmer elements, and a less sensitive one to observe the central core region of sprites which often saturates the imagers. Alternately, a camera with a greater dynamic range would also provide better images.

TV-rate sprite gallery

We present a gallery of TV-rate sprite images in Figure 4.9 showing the wide range of forms the different sprite types take. Since these forms depend on many variables, they vary in

detail from the ones presented at 1 ms time resolution section. The sprites in the four rows of the gallery are loosely grouped to show: (1) complex sprites with some upward branches; (2) developing sprites (sprites beginning to develop upward branches); (3) groups of mostly simpler sprites, some forming jellyfish sprites groups; and (4) simple sprites without upward branches, including angel sprites and columniform sprites. The images were obtained in field campaigns in 1996 and 1998. In the multiple images, part of a time or azimuth/elevation stamp is visible in the shown region; or a dashed line which indicated the field of view of a spectrograph slit. The spectral data were presented previously by *Hampton* et al. [1996] and *Heavner* et al. [2000]. The images are not necessarily to the same scale. We compare and contrast the details of these images to illustrate the variety of forms that occur within the various classes of sprites.
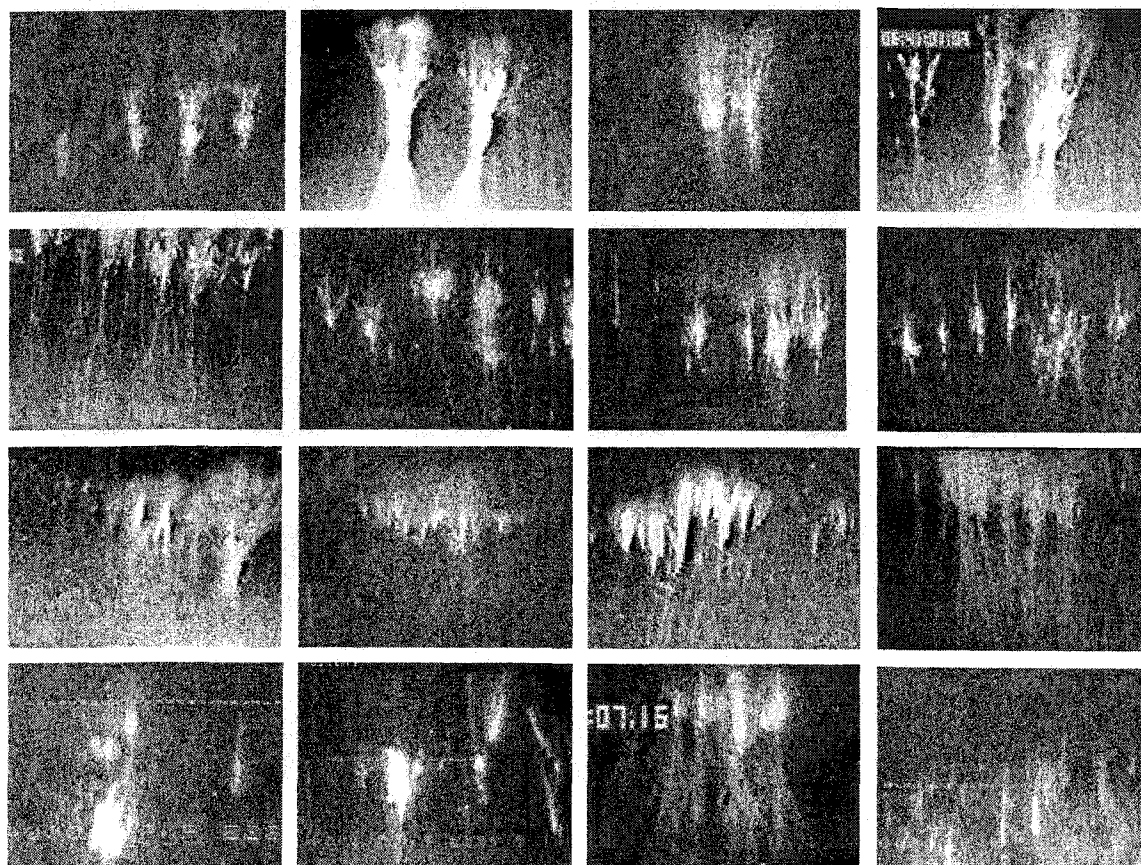
Figure 4.9. A gallery of TV-rate sprite images.

In the *top row* of Figure 4.9 are shown four sample snapshots of carrot sprites. The first image shows a group of carrot sprites taken with a less sensitive camera. The dominant emission comes from the central region of the sprites, the sprite body. Diffuse puffs are visible above the bright central region, separated from it by a darker region. Tendrils below the central core are not visible.

The second image in the top row stands in contrast to the first image - the tendrils are well visible as a downward diverging triangle, the body of the sprite is saturated in the image and no internal structure is visible, the puffs are visible above the body, and also several branches coming off the right-most sprite are visible at increasingly greater angles from the vertical.

The third image in the top row of Figure 4.9 shows two carrot sprites, less saturated than the previous image. Tendrils are better visible than in the first image, but not saturated unlike the second image. Branches visibly connect the body of the sprite with the diffuse puffs above.

The last example in the top row shows that sprites within a group can be of differing complexities - the sprite on the right is the most developed, the sprite in the center is smaller but still has upward branches and some diffuse puff at top, the sprite at left has no fully developed branches but some which started to develop off to the side.

In the *second row* of Figure 4.9 are shown more examples of sprites with developing, but not fully developed, branches. Sprite tendrils are best visible in the first image in that row. In comparison with the tendrils of the carrot sprites, the tendrils of the developing sprites are not as divergent.

In the second image, the developing sprites show a main column, with the developing branches diverging upward from the bottom of the column.

In the third image, the sprites are similar, with fewer developing branches, and diffuse puffs are visible at the top of main column. Within the group, the most complex of the developing sprites are near the center, and the simpler ones, without developing branches, are near the (left) side.

In the last image, diffuse emission tops the central columns, and the developing branches that form the bottom part of the column are very small.

In the *third row* of Figure 4.9 are shown groups of simpler sprites. In the first image,

a carrot sprite is visible at right with multiple upward branches, with simpler and smaller sprites to the left of it. The simpler sprites immediately to the left of the carrot appear as thick columns with tendrils and some diffuse emission above. The sprites furthest to the left appear simply as beads. In the second image is visible a jellyfish group of sprites. Extensive diffuse emission, a halo, tops the sprites. The sprites themselves appear as short thick columns, decreasing in size from the middle of the group. A few of the central sprites do have one or two developing branches from the bottom of the column.

The third image in the third row shows a group of thick-column sprites with simple downward tendrils with very little divergence. Again, the central sprites are the largest and brightest compared with sprites to the side of the group. To the right of the main group, a group of seven smaller sprites is visible. These smaller sprites have likewise simple tendrils when compared with those of carrot sprites in the top row. Since the groups of smaller and larger sprites appear at the same elevation angle, they are at approximately the same distance from the observer. The columns of the smaller sprites are shorter by a factor of 2-3 that the larger sprites, indicating the columns of sprites do not have any characteristic length.

In the last image of the third row is shown another jellyfish sprite group, similar to that in the second image of this row. The tendrils of the sprites are divergent, the halo is relatively bright, the columns of the sprites are wide and possibly have developing branches. A few tiny sprites appear to either side of the group.

In the *fourth row* of Figure 4.9 is shown a melange of sprites. The first two images show simpler developing sprites, some of which resemble the tree structure described by *Gerken* et al. [2000]. The third image shows a group of angel sprites, with thicker columns than classic columniform sprites, and divergent tendrils. In the last image of the fourth row is shown a group of columniform sprites, demonstrating that the sprites come in different sizes, and the columns may be curved.

Overall, the following may be noted with respect to Figure 4.9: within a sprite group, either all sprites reached the similar stage of development, or the sprites near the center are the most complex, with sprites of similar type but decreasing complexity to the side. Note that a group of sprites of these characteristics (largest sprites in the center) in 3D, projected onto a 2D surface (the image) will still yield a group of the same characteristics

(largest sprites in the center). Often there is a definite separation between sprites within a group (e.g. examples in second row), indicating there are preferred locations for sprite initiation or occurrence. The brightest optical emission often comes from the central portion of the sprites, equivalent to the stationary sprite features mentioned in the Discussion. Simpler sprites tend to have less divergent tendrils in comparison to carrot sprites, which are considered complex.

4.2 Sprites with More Complex Dynamics

Some sprites which do not quite fit into the categories presented in the 1 ms section include a long duration sprite occurring at 05:10:39 UT on August 18, 1999. Selected fields are shown in Figure 4.10(a). Downward tendrils are visible in fields 1-3, multiple beads brighten in the region passed by the tendrils, and these appear to join together into a uniform column in field 10. For the next 60 ms or so, the column remains nearly unchanged, then around field 70 new beads brighten in lower region, and move upwards. At the same time, the column expands down. As the upward moving beads and downward expanding column meet, a branch shoots upwards and becomes bright while the column disappears (field 87-91). Unfortunately field 91 is the last field of the high speed imager record. From the TV record, this event resulted in another carrot sprite. The TV images are shown in Figure 4.10(b), with time ± 4 ms labeled in 17 ms increments. While this event started with downward tendrils as all other sprites presented in this paper, it was unusual due to its very long (∼100 ms) lifetime and its very complex dynamics.

A second example of an unusual sprite is shown in Figure 4.10(c). This is an example of a long-duration sprite. Unlike the previous example, multiple sets of downward tendrils are visible in this case (not shown). Multiple (short) upward branches form in the upper portion of the sprite, topped with small diffuse emissions. For dynamics of tendrils of this sprite, please see Figure 5.5.
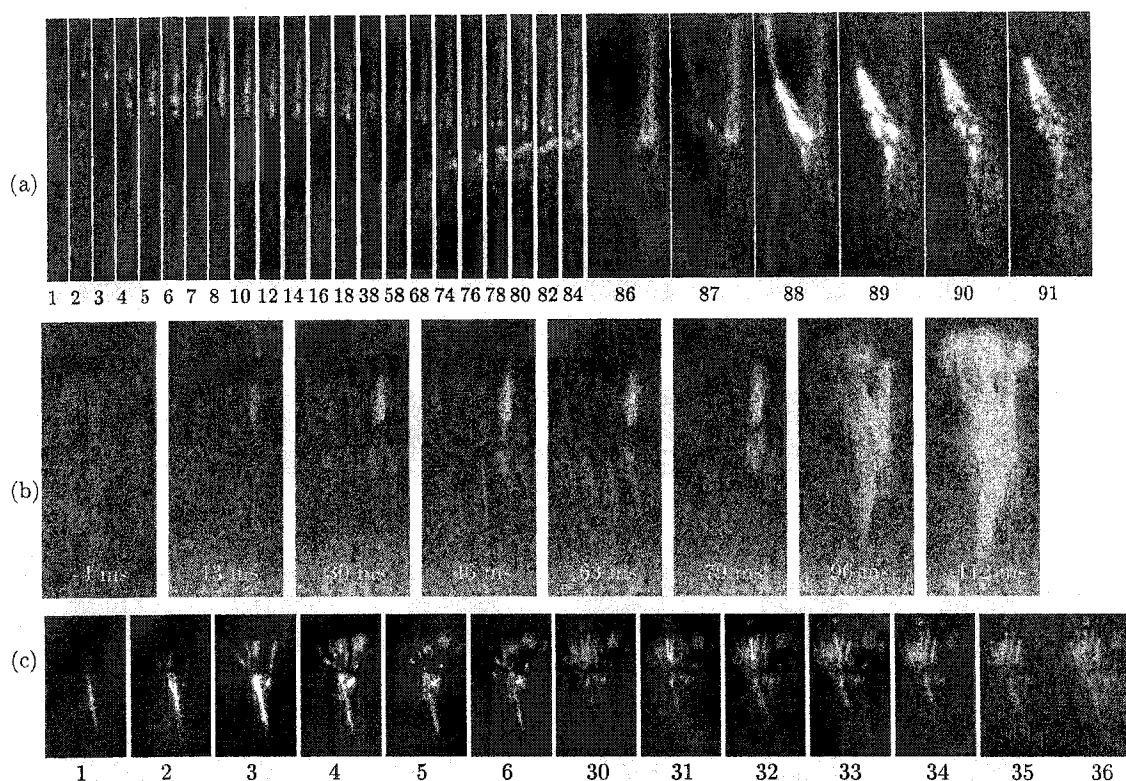
Figure 4.10. Examples of unusual sprites. (a) Unusual sprite occurring at 05:10:39 UT on August 18, 1999. The vertical extent of the images is 30 km. The greater spacing between fields indicates longer time period between those fields, up to the greatest period (20 ms) between fields 18, 38,and 58. (b) TV-rate images of the same sprite partially shown in part (a). Time ±4 ms is shown. On first field only a star is visible, near the center of the image. (c) Unusual sprite occurring at 04:23:31 UT on August 18, 1999. The vertical extent of the images is 34 km.
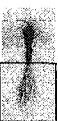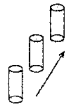
4.3 Discussion
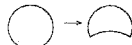
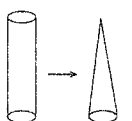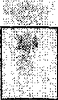Sprites assume a variety of forms. The following definition of a sprite, encompassing all of the sprite forms presented here, is proposed: *A sprite is a transient optical phenomenon occurring above active thunderstorms, initiated in the upper mesosphere by underlying lightning, with one or more relatively narrow tendrils propagating downward from the point of initition with speeds on the order of* 10^5 *to* 10^7 *m/s.* This definition differentiates sprites from elves and halos [*Wescott* et al., 2001; *Barrington-Leigh* et al., 2001], and allows for the inclusion within "sprites" of the spatially smallest luminous structures that appear similar

to those leading up to large sprites.

4.3.1 Types of Features

Sprites include a number of glow regimes. A list is presented in Table 4.1. The glows are divided into "dynamic" and "stationary" features. Within dynamic features, there are the downward-propagating tendrils, which occur in all sprites, and upward-propagating branches, which occur in only some sprites. Tendrils extend from the upper part of the sprite body (if it exists) downward. Branches, if formed, occur from the bottom of the sprite body and extend upward. Thus the region of a sprite body can, at different stages of the sprite development, support both tendrils and branches in addition to the stationary glows. Dynamic features have been suggested to be streamers [*Pasko* et al., 1998; *Raizer* et al., 1998; *Stanley* et al., 1999].

Table 4.1. Summary of glows and discharges within sprites. Typical geometries and spatial orders of magnitude are included. Speeds are indicated in m/s; dimensions are D=diameter or L=length, in meters; and durations are in ms.

| **SPRITES: DYNAMIC FEATURES** | | | | (Durations are < 1 ms at any altitude) | |
Name	Structure	Speed	Dimensions	Range	Summary
Tendrils		10^5-10^7 down	D:100m, L:10,000m		Common to all sprites. Basic sprite consists only of tendril(s). Sprites may have multiple temporally-separate sets of tendrils. Sprite brightness and tendril speed appear related. Modeled as streamers.
Branches		10^6-10^8 up	D:100m, L:10,000m		Two sizes, $>\sim$ 10 km and $<\sim$ 10 km. Often form puffs, beads. May 'retract' into columns. Suggested to be streamers, not yet modeled.
SPRITES: STATIONARY FEATURES				(Speeds of brightness propagation < 10^5 m/s)	
Name	Structure	Duration	Dimensions	Range	Summary
Puffs		2->30	D: 100-1000m		May appear at tops of both long branches (large puffs) and short branches (small puffs). Relatively long-duration. Diffuse. Not halos! Not yet explained or modeled.
Columns, fat-columns, not-quite-columns (central stationary form of the sprite)		2-> 100	D:100-1000 L:10,000 m		Longer duration emissions, either in shape of a column or less elongated. May slowly transform into different shape. Not yet explained or modeled.
Beads		2->100	D:100m?		In central portion of sprites. Long duration, small extent (wrt tendrils/branches). Appear 1-10 ms after passage of tendrils/branches. Not yet explained or modeled.

Stationary features visible within sprites move at less than 10^5 m/s and in the 1 ms high speed images appear to be stationary, thus the proposed name. They include columns, quasicolumns, and thick columns, such as shown earlier in this chapter. All of these occur within the body of a sprite, and have a longer lifetime than the tendrils or branches. Other stationary glows visible within sprites include beads and puffs. Beads occur within the body of the sprite or below, and are smaller than the pixel resolution of the imager, $\sim$ 300 m. Puffs, such as those seen in Figs. 4.5c-d, appear above branches, often persisting for 10s ms. Typically a branch shoots upwards and may form a puff. The top part of the branch then decays, leaving a short (stationary) column in the body part of the sprite with a small but definite separation from the puff above it. One example of shorter columns is visible in the body of the sprite in Fig. 4.5d field 7. A shorter branch and a puff with the same behavior can be seen in Fig. 4.10c; in field 31, the brightest short column includes a small puff above it, whereas in the previous field only a solid branch is visible in the same location.

From the examples presented in this chapter, sprites have a minimum of one tendril, and may be accompanied by an assortment of other glows. The variety of glows observed within sprites are believed to depend on both compositional fluctuations of the atmosphere and electric field variations. It is the "stationary" features that often yield the brightest emissions, as can be seen in the gallery of TV images - Figures 4.9. There, the tendrils of the sprites are often dimmer than the main parts of the sprites.

4.3.2 Flow Chart

A simple description of the temporal evolution of sprite elements is as follows: Most large-form sprites start out with the formation of a tendril that moves downward (primary process - dynamic)

- One or more of the following then occurs (primary processes - stationary):

  - no other process occurs.

  - one or more bright, longer-duration beads form in the tendril channel, which may then expand, forming a larger region of brightness.

  - larger irregular-shaped brightness forms near the top of the tendril, which may then transform in shape.

- a bright column or other regular-shaped brightness forms at the top of the tendril.

• One of the following then occurs (primary processes - dynamic):

- no other process occurs.

- smaller branches form, which may be followed by puffs.

- larger branches form, often followed by puffs.

- branching from progressively lower altitudes.

• Finally, one of the following may occur (secondary processes - both stationary and dynamic):

- additional tendrils form.

- additional branches form.

- additional beads, columns, etc. form, or transform into other forms.

A smaller subset of the sprites described above is shown in Figure 4.11. Only carrot sprites are shown, together with sprites ending before large branching starts. As always, the first process occurring is the initiation and development of tendrils. Once tendrils start moving downward, sprite development can proceed in many ways, as is indicated by the multiple lines from the tendrils box. The multiple lines of development start with either simple tendrils, tendrils brightening one or multiple beads along the way, tendrils whose tops brighten into short, fat, or simple columns; each indicated by a box in Figure 4.11.

At any of the boxes, the development splits into three parts (1) the development terminates (examples shown in first column), (2) upward branching can occur from these forms (examples shown in second column), or (3) the forms can undergo reshaping into another form, as indicated by a downward arrow leading to the next box. As an example of this last development, consider the "unusual" sprite shown in Figure 4.10a. In that example, tendrils lead to beads which expanded and formed a nearly uniform column.

Implicit in the branching cases is the possible formation of either small or large branches. Large branches often result in secondary processes (secondary tendrils and secondary small branches), ultimately forming a complicated sprite body.
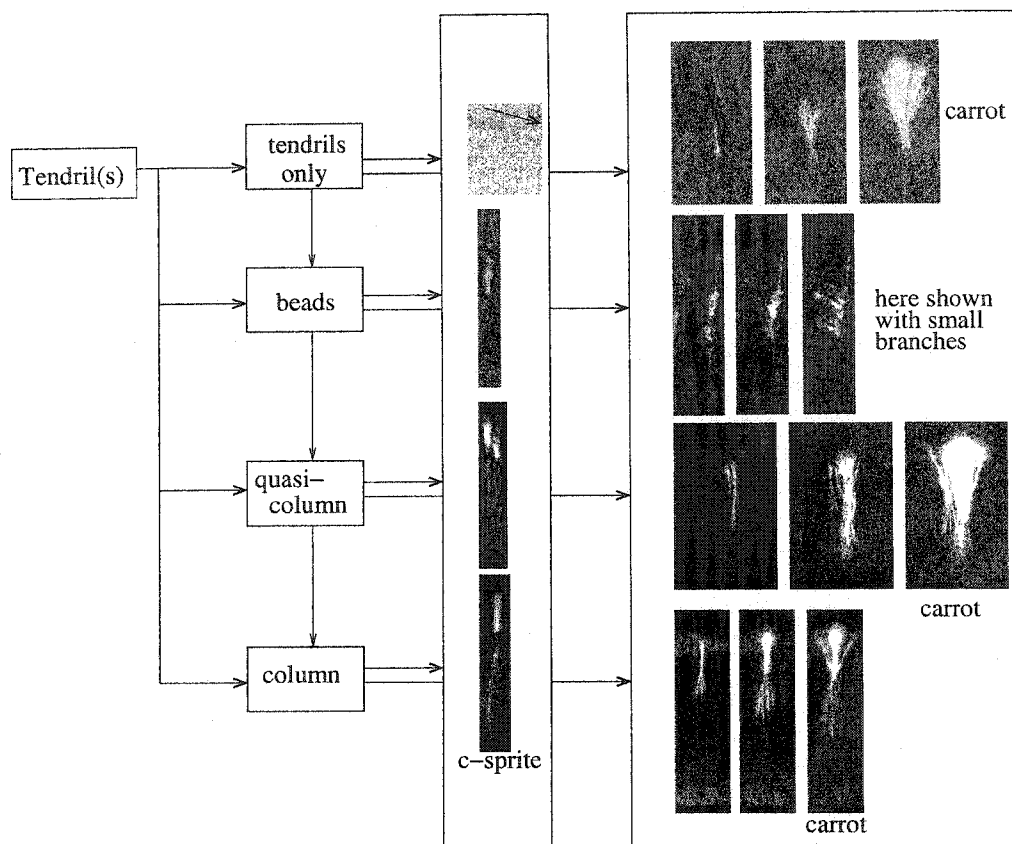
Figure 4.11. A chart showing a few specific examples from a subset of sprite types from the list in the text, mainly carrot sprites, and sprites similar to an intermediate stage of carrot sprites.

4.3.3 A Grid: $\vec{E}$ Field Strength/Duration vs Sprite Type

The examples presented in this chapter, and especially those of the sprite groups, lead to several additional conclusions. First, simply because tendrils start their downward propagation does not mean a large sprite will form. This indicates that the local electric field initiating sprites must be of some minimum duration, magnitude, and shape before significant tendrils and/or branches will form. This is equivalent to the idea of *Hu* et al. [2002], who find that a lightning with a charge-moment change of >1000 C km in <6 ms has a 90% probability of initiating a sprite. As sprite tendrils have also been suggested to be streamers [*Raizer* et al., 1998; *Pasko* et al., 1998], this is consistent with the condition that streamers cannot propagate in the absence of an external electric field [*Raizer*, 1997, p.353].

Overall, it is expected that an electric field of certain characteristics (minimum duration and magnitude thresholds) is required for the development of large sprites.

Second, since the model of *Barrington-Leigh* et al. [2001] appears to explain halos well, we can correlate the brightness within a halo to the quasi-electrostatic field causing it. Then we can correlate sprite development within different parts of the halo with the probable causative field. In particular, in two top rows of Fig. 4.7, we see that the fastest sprite tendrils occurred near the center, and the slower sprite tendrils occurred towards the side of the halo. In addition, the sprites to the side had a simpler head than the ones in the center; either they consisted of tendrils-only, or had a "quasicolumn" or an angel head. Thus, based on the simple proxy of halo brightness and its probable relation to the causative electric field, we note that sprite tendril speeds are larger in greater electric fields. This behavior is similar to that in streamers [*Raizer*, 1997, p.336]. Likewise, sprites near the center of a group form a larger stationary feature, as seen in some examples of Figure 4.9.
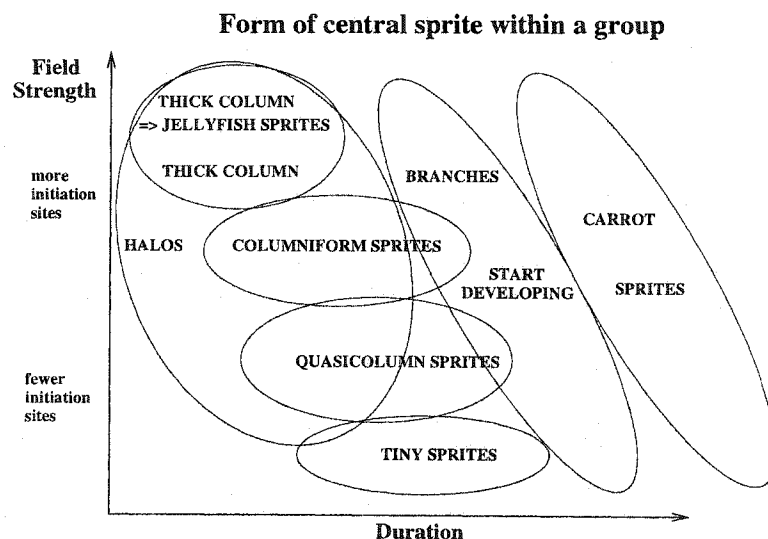

Figure 4.12. Dominant sprite within a group as a function of electric field strength and duration.

The form of the largest stationary feature within a sprites group, together with halo brightness as a proxy of the electric field strength, can be used to make an outline of sprite type as a function of electric field strength and its duration. This is shown in Figure 4.12. The grid of electric field strength vs duration is rough and is only used for illustration;

there is no scale assigned to either axis. Thick column sprites occur at shortest time delay and brighest halos, followed by c-sprites and quasicolumn sprites. Each region is shown as simple non-overlapping oval for clarity. The diagonal displacement of the above-described ovals and the diagonally-sloping ovals indicating beginning of branches, and carrot sprites, reflect both our observations (Fig.4.7) and the ideas of *Cummer and Stanley* [1999] and *Hu et al.* [2002], indicating a threshold requirement for sprite initiation and further development.

In particular, Figure 4.12 shows that with the least time delay from the first indication of a halo, and with the brightest halos observed, are the jellyfish sprites. With a longer time delay from the beginning of the observable halo, and a lower electric field strength columniform sprite groups are formed. Some tiny sprites occur without observeable halos, as is indicated near the bottom of the Figure.

The sprites within a jellyfish group are composed of thick columns in center, with angel sprites and tiny sprites to the side. The central sprites within a group may form partly developed branches with continuing electric field, or may perhaps form complete branches. An example of sprite forming branches out of a barely visible tendril was shown in Figure 4.5(a), indicating that a stationary sprite feature is not a requirement for branches to form.

If the basic form of the grid shown in Figure 4.12 is verified by subsequent studies, regimes of stationary-form development and branch development within sprites can begin to be constrained in order to help identify the processes involved. The equivalent processes in laboratory discharges may be identified. Likewise, potential consequences of sprites on the long-term composition of the mesosphere, if any, can begin to be estimated.

It needs to be noted that electric field strength alone is not sufficient to account for the observed forms; also required is some spatial inhomogeneity in the atmospheric dielectric (see discussion in *Moudry* et al. [2003]). Without such inhomogeneity, sprite initiation would not be expected to occur for events such as the carrot in Fig. 4.5a. Likewise, beads, such as the isolated tendrils-and-bead sprite shown in Fig. 4.2b, may similarly be due to inhomogeneous structure and the interactions with, and within, the passing tendril front.

Observations clearly indicate the operation of secondary processes in sprites. They involve both secondary tendrils and columns, and other stationary features. These, together with the multiple beads excited, are important for the long duration (>5 ms) of optical

emissions in the central body of sprites. It is not clear what requirements need to be satisfied for these processes to occur.

4.4 Summary

Sprites occur in many forms, but all of the brightness features start with downward propagating tendril(s). The tendrils may lead to the formation of a number of relatively bright stationary features, such as beads imbedded within them, columns at the top, or other bright features at the top, all of which may slowly evolve in time. Any of these tendrils, including ones without any other features, may lead to an upward branch formation, often culminating with the stationary puff at the top of the branch, as the branch possibly transforms into a stationary column. The final appearance of a carrot sprite does not necessarily correlate with the sprite form in its intermediate stage. For example, we have presented multiple carrot sprites, some of which started from one single tendril, some from multiple tendrils. Beads do not necessarily indicate the initiation location. Branches, if initiated from columns, do so from the bottom of the column. Secondary processes within sprites, such as new tendrils and branches, are important for reshaping the light-emitting regions.

We have also presented a gallery of sprites observed at TV-rate time resolution. We show a few examples where having an additional observational (camera) system with a smaller gain may be beneficial in order to see the stationary features of sprites, which are often in the region saturated from the bright but brief sprite tendrils or branches. Lower gain allows one to see the longer-duration features without saturating the imager with the shorter-duration tendrils. Ideally, however, one would use CCD imaging systems with wider dynamic range than afforded by the older systems.

The long lived stationary features within the decaying remnants of sprites account for much of the total optical emissions. To date, no suggestions have been made as to the mechanisms behind these stationary processes.

Chapter 5

Velocities of Sprite Tendrils

As described in the previous chapter, the spatial development of sprites was first measured by *Takahashi et al.* [1996] and *Fukunishi et al.* [1996], who showed that sprites are initiated near 75 km altitude with downward tendrils moving with velocities on the order of several times 10^7 m/s, followed by the creation of upward branches. The first high speed imaging observations of sprites were obtained by *Stanley et al.* [1999], who used a 1000-3000 frames per second (fps) low light level television camera. *Stanley et al.* [1999] measured the velocities of sprite tendrils on the order of 10^7 m/s. *Stanley* [2000] subsequently extended the observed range of sprite tendril velocities downward to several times 10^6 m/s. These velocities correspond to velocities of streamers, as proposed by *Pasko et al.* [1998] and *Raizer et al.* [1998]. *Raizer et al.* [1998] modeled a streamer in the mesosphere, with resultant velocities undergoing a 10^6 to 10^7 to 10^6 m/s (slow-fast-slow) progression over the lifetime of the streamer, with the maximum velocity being attained in $\sim$ 4 ms following initiation.

In this chapter[1], representative examples of sprite tendril behavior from high speed imager observations are shown, velocities of sprite tendril development are derive, and examples that show that sprite tendrils sometimes include horizontal component of expansion in their slow phase, and show that multiple tendrils can occur for a single sprite, are presented. It is also shown that individual sprite tendrils include multiple velocity regimes.

---

[1] A modified version of this chapter has been published as the article Moudry, Stenbaek-Nielsen, Sentman and Wescott, Velocities of Sprite Tendrils, *Geophys. Res. Lett.*, 29(20), p.53, doi:10.1029/2002GL015682, 2002. The work presented is work done by Dana Moudry, using data of Hans Stenbaek-Nielsen.
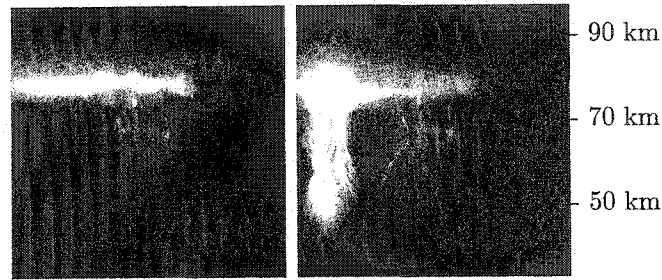
Figure 5.1. Two images 1 ms apart showing a fast sprite, at 05:10:38 UT on Aug 18, 1999. The sprite was shown previously by *Stenbaek-Nielsen et al.* [2000], their Fig. 3.

Downward tendril development occurred at velocities that varied by more than two orders of magnitude, ranging from $\sim 10^5$ to $\geq 3 \times 10^7$ m/s. In several cases the tendrils progressed through multiple velocity regimes, typically in the order fast-slow or slow-fast-slow. Examples are presented of multiple sets of temporally distinct tendrils that develop from the same sprite event and tendrils that have a horizontal component of expansion.

5.1   Velocities of Sprite Tendrils

Sprite tendrils develop and propagate with a wide range of velocities. In this section, examples of fast (10^7 m/s), slow (10^5 m/s), and intermediate velocities, respectively, are presented.

5.1.1   Fast: Order of 10^7 m/s

In Figure 5.1 two images are shown, 1 ms apart. The first image shows a bright and horizontally extensive halo, together with multiple beads that have persisted from an earlier sprite. A halo is an unstructured emission modeled to be due to quasi-electrostatic fields from lightning [*Barrington-Leigh et al. 2001*]. The second field 1 ms later shows the same halo and beads, but also a large sprite with extensive downward tendrils. The minimum velocity of propagation, assuming the sprite initiated from beads immediately below the halo in the first image (not visible at this resolution), is 3×10^7 m/s. It has further been assumed that the sprite started at the beginning of the 1 ms integration time. This is the fastest-developing sprite identified in the high speed imager data, close to the velocity
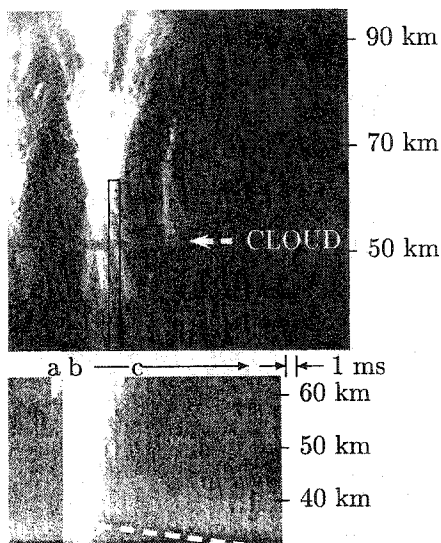
Figure 5.2. A sprite with slow tendrils is shown in its entirety at top. A rectangle shows the region cropped into the time series, shown at bottom. The time series shows 25 ms of data. The slow phase of the tendrils is propagating steadily downward after the initial sprite brightening, at a speed of 4×10^5 m/s (label "c," also dashed line). This sprite occurred at 05:24:22 UT on Aug 18 1999 and was shown previously by *Stenbaek-Nielsen et al.* [2000], their Fig. 4.

detection limit of the imager. This event was also observed with a multichannel photometer by *McHarg et al.* [2002] (their Figs.3,4), yielding similar velocities. The downward velocity of the tendrils is the same order of magnitude as measured by previous researchers.

5.1.2 Slow: Order of 10^5 m/s

Downward propagation

After the initial phase of fast-moving tendrils, such as those seen in Figure 5.1, sprite tendrils always slow down as they continue to propagate. Most often sprite tendril brightness decreases beneath instrument threshold within <5 ms after deceleration. The sprite shown in Figure 5.2 includes, in contrast, long-lasting tendrils. The sprite itself is shown at top, together with a thin black rectangle, indicating the region of interest. This region was cropped from 25 successive images, and stacked side-by-side, giving effectively the time series of the brightness within it. The contrast-enhanced time series is shown at the bottom
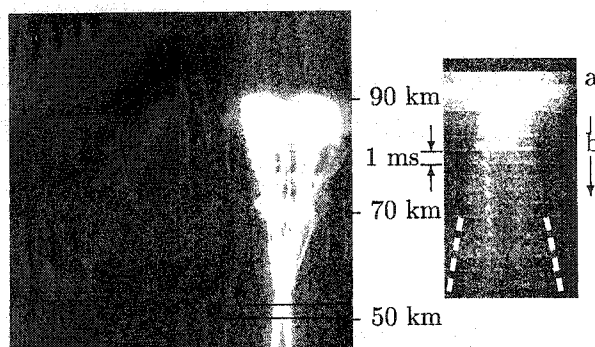
Figure 5.3. A sprite event with a horizontal component of tendril expansion is shown a left. The rectangle shows the region selected and shown as a top-to-bottom time series (18 ms of data) at right. The horizontal component of the expansion is visible in the timeseries during label "b" (see guiding dashed lines), with a speed of 3 to 4 $\times 10^5$ m/s. The sprite occurred at 05:45:05 UT on Aug 18 1999.

of Figure 5.2. The width of a 1-ms "slice" is shown above the altitude labels of the time series. Visible in the time series are the tendrils coming in from the top (label "a"). At time "b," the tendrils are bright and emit sufficient light in all directions, that the light scattered by the intervening atmosphere back towards the detector raises significantly the background noise level of the detector (equivalent to the full-moon effect). With contrast enhancement to show dim features at a later time, at time "b" the tendrils thus falsely appear to reach the bottom of the image, instead of the actual altitude reached of approximately 40 km. During the next $\sim$20 ms, a dim brightness is visibly descending downward ("c" and dashed line) into the lowest quarter of the image. This downward moving brightness feature indicates that the tendril, having decayed in brightness and velocity, nevertheless continues its downward motion. The velocity is 4×10^5 m/s downward.

Horizontal component of expansion

In addition to continuing downward propagation following their fast phase, sprite tendrils may also include a horizontal component of expansion, as is shown in Figure 5.3. On the left is the sprite marked with a rectangle showing the region of interest. This region was cropped from 18 successive images 1 ms apart, and these were stacked into a top-to-bottom time series as shown to the right. The time series again includes a section with much
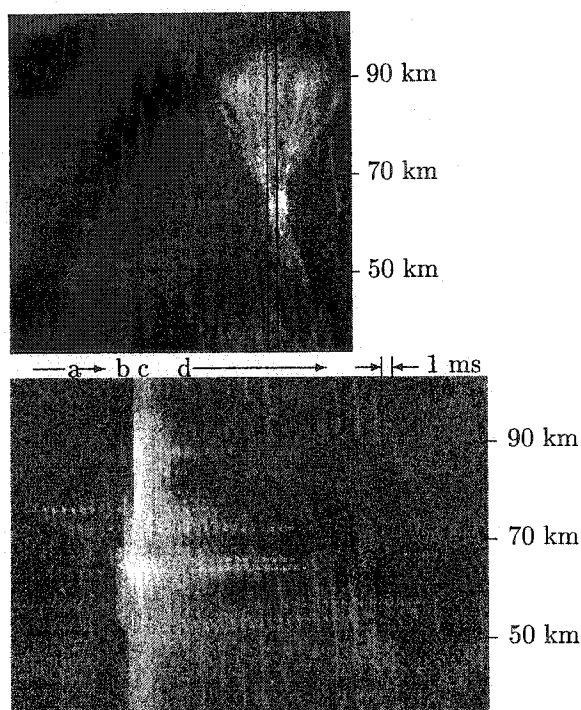
Figure 5.4. A sprite with tendrils going through multiple velocity regimes is shown at top. The rectangle shows the crop from which a time series, bottom, was made. Shown are 50 ms of images. The sprite tendrils have initially a slower speed before accelerating, then decelerating again. The sprite occurred at 04:58:14 UT on Aug 18 1999.

scattered light (label "a"). After this period, the high speed imager was able to pick up the slower and dimmer outward expansion ("b" and guiding dashed lines). The speed of this horizontal component of expansion is 3×10^5 m/s towards the left, and similar towards the right.

5.1.3 Intermediate and Multiple Velocities

The downward propagation velocity often varies in time within individual tendrils. An example of this is shown in Figure 5.4. At the top of Figure 5.4 a sprite is marked with a region indicated by a black rectangle, and at the bottom the time series for that region is shown. The time series shows 50 successive 1 ms images. The cropped region includes the sprite initiation, which is visible in the beginning of the time series (label "a"), as a bead

brightened by a passing tendril. The bead is visible as a horizontally dotted line due to its long lifetime. Further down from this, but still in "a" another dim bead appears. In the first 12 ms, the velocity of the tendril is, on average, 9×10^5 m/s. There is a sudden brightening of the tendril, and an increase in velocity by an order of magnitude, that appears as the first vertically extensive brightness on the 13th field ("b"). The velocity, based on the distance traveled in the 1 ms, is at least 1.3×10^7 m/s. Following the acceleration of the tendril, there occur upward growing branches observed as a brightness extending vertically into the upper half of this time series. There is enough light scattered to increase the background level of the next two crops ("c"). During this same interval the tendrils slow down to near original level.

Figure 5.4 also illustrates a common characteristic of many complex sprite events, namely that the tendrils and branches tend to be much brighter, but of shorter duration than the beads. The sprite duration, based only on branches and fast tendrils, is less than 5 ms, but beads brightened by passing tendrils and branches ("d") may persist > 20 ms.

5.2 Multiple Sprite Tendrils Within a Sprite

The examples presented above include only one set of tendrils per sprite. Other events exhibit more complex tendril structure. Multiple tendrils occurring sequentially result in longer sprite durations, as well as more complex sprite shape. One such example is shown in Figure 5.5. In the upper right is the sprite image, with two rectangles showing the regions of interest, one oriented vertically to show the downward motion and one horizontally to show the horizontal component of expansion explicitly. Two time series are constructed as before. At the left of Fig. 5.5 the time series is shown for the horizontal rectangle, with 51 successive 1 ms images. At the bottom the time series is shown of vertical rectangle region, covering the same time interval.

The two time series in Figure 5.5 show multiple downward-propagating tendrils (arrows in bottom time series) that may also be seen expanding horizontally (arrows in left time series). The horizontal component of expansion has speeds of 4×10^5 and 1.5×10^5 m/s, respectively. The downward speeds vary by an order of magnitude. The tendrils visible in the first three fields of bottom time series (first arrow) start with velocities of 7×10^6 m/s,
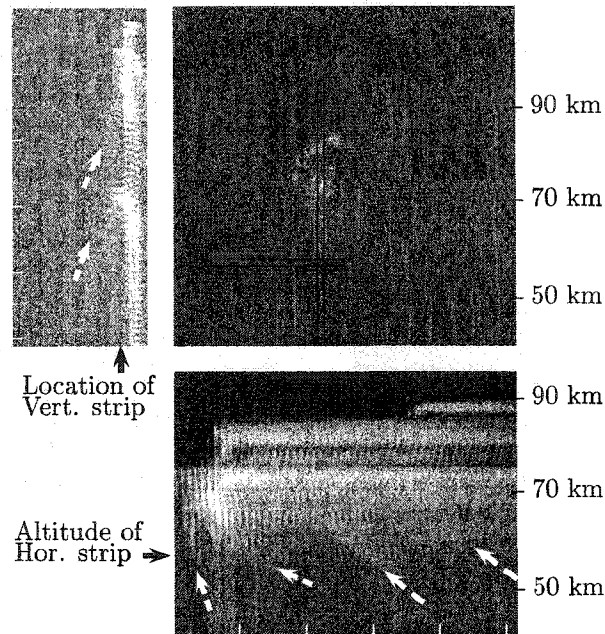
Figure 5.5. A sprite event with multiple temporally-distinct sets of tendrils is shown at upper right. The two rectangles show the areas cropped into 51 ms long time series. The horizontal rectangle shows the region cropped to show the widening of the sprite tendrils, at left. The vertical rectangle shows the region cropped to show the multiple sprite tendrils occurring within this sprite event, on the bottom. Tick marks in both series indicate every 10 ms. The sprite occurred at 04:23:22 UT on Aug 18 1999.

then slow immediately to 3×10^6 m/s and lower velocities. The second wave of tendrils has velocities near this smaller value, then slows to 6×10^5 m/s. The third wave of tendrils, once it leaves the bright region, has velocities around 10^6 m/s. Other downward propagating tendrils are (barely) visible at later times. The multiple tendrils within the sprite result in emissions which persist much longer than those of the sprites shown previously. Due to the multiple tendrils, the sprite shape does not fit into the basic sprite forms.

5.3 Discussion

Sprite tendrils have been suggested to be streamers [*Raizer et al.*, 1998; *Pasko et al.*, 1998]. The velocity of 10^5 m/s corresponds to the low end of velocity regimes in which streamers are known to exist when overvoltages are small and pressures high [*Pasko et al.*, 1998].

The slow streamer, at small overvoltage and a high pressure, appears to be the most likely explanation for the slow downward velocities of the tendrils seen in the data. Distinguishing between the two effects is difficult since they are related - at lower altitudes the breakdown electric field is higher, and a given external electric field will have a smaller overvoltage over the breakdown field.

Two questions may be posed about the slow downward propagation of the tendrils shown in Figure 5.2. First, the downward speed of sprite tendrils appears to be nearly uniform for intervals exceeding 10 ms. In terms of streamer lifetime, this is a long time. The electric field from lightning can be sustained for this long period due to a long relaxation time at lower altitudes [*Pasko et al.*, 1997]. However, *Raizer et al.* [1998] have shown with their constant electric field model that once sprite tendrils reach their maximum velocity approximately 4 ms from their onset, the sprite tendril velocity continuously decreases from that moment on, and the sprite tendrils are practically stopped 4 ms later. Thus, in order to have a near-constant velocity of propagation for the slow downward tendrils shown in Figure 5.2, if these brightness structures are streamers, the electric field would need to be increasing in order to sustain their propagation.

Secondly, the emissions in label c of Figure 5.2 do not have the characteristic shape expected to be created by streamers. Most of the energy deposition in streamers occurs at the head [*Pancheshnyi et al.*, 2000]. For example, *Stanley et al.* [1999] observed sprite tendrils with a 0.3 - 1.0 ms resolution high speed imager and showed that in many of their examples, the sprite tendril brightness extends down to a certain altitude on one field, and continues from that altitude downward on the following field. This indicates that most of the emissions come from a relatively narrow region propagating downward. In contrast, the spatially-extensive emissions behind the front of the slowly-propagating tendrils in Figure 5.2 would not be expected with a streamer mechanism alone.

The slow tendrils (both downward and horizontal component) of a sprite always appear very dim, and as a wavefront rather than as individual structures. At present it is not clear whether the wavefront is real or whether it is only an apparent feature due to insufficient spatial resolution of the instrument. Based on the horizontal component of tendril expansion shown in Figure 5.3, which occurred in a region where the tendrils initially had a nearly exclusively vertical component, it is suggested that at least in that case, the wavefront is

truly an expanding front and not multiple, dim, horizontally-propagating tendrils.

The observations of the time evolution of tendril velocity, *e.g.*, Figure 5.4, are consistent with the basic slow-fast-slow characteristics of the model presented by *Raizer et al.* [1998] (their Fig.3) for some sprites. Their model uses a laminar conductivity profile and an electric field created by a single vertical cloud to ground discharge to compute the atmospheric response and streamer position at successive times. However, not all tendrils exhibit this slow-fast-slow behavior; other sprites have a fast-slow evolution of sprite tendril velocity instead.

Figure 5.5 shows a sampling of sprite dynamics observable at 1000 fps imagery. Here, a single sprite may have multiple tendrils with beads, and that upward development of the set of branches follows the development of downward tendrils. The beads do not brighten with each downward tendril, but they tend to persist for longer times than the tendrils. It is presently unknown what initiates successive streamers, or whether a single seed is associated with these events.

Finally, comparison of tendril velocities with the associated sprite shows that the maximum tendril velocity appears to be correlated to the brightness and the overall extent of the sprite. The brightest sprites tend to have tendril velocities above 10^7 m/s, while smaller and dimmer sprites tend to have slower tendril velocities (e.g. Figures 5.1 and 5.5).

5.4 Summary

The detailed view of sprite dynamics observable in 1000 fps imagery has revealed numerous new features that challenge the understanding of the effects of lightning on this region. The dynamics of tendril propagation in several sprites were presented. The principal conclusions of this work may be summarized as follows:

1. Very slow downward tendril velocities have been identified in sprites, on the order of 10^5 m/s.

2. Horizontal component to propagating sprite tendrils has been identified in some sprites, expanding with speeds $\sim 10^5$ m/s.

3. Sprite tendrils do not develop at constant velocity, but rather pass through multiple

regimes. Typically they follow a fast-slow pattern. Some sprites follow a slow-fast-slow pattern, similar to that predicted by *Raizer et al.* [1998].

4. Sprites may possess multiple downward-propagating tendrils.

5. The duration of beads within a sprite is typically much longer than that of either tendrils or branches.

Chapter 6

Crawlers: Dynamical Optical Phenomena in Optically Decayed Sprite Tendrils

As has been described in previous chapters, electrical effects of thunderstorms extend into the mesosphere and lower ionosphere to produce optical emissions termed "elves," "halos," and "sprites." Often optical after effects occur following sprites, and are termed "crawlers," subsets of which include "palm trees," "embers/trolls" and "smooth crawlers" (see below for a more detailed description of after effects and references).

Occasionally there occur upward-moving discrete patches of brightness in the decaying phase of sprites. These phenomena collectively take the name "crawlers" to indicate their relatively slow (compared to sprites) upward speed. Within crawlers, three specific subgroups can be distinguished based on their apparent vertical extent compared to sprite tendrils in television-rate imagery. "Smooth crawlers" appear as small beads of brightness moving upward, with a small vertical extent, without any connection to cloudtops. Previously they were described simply as crawlers by *Moudry* et al. [2001]. The adjective "smooth" given to them here is used to indicate the nature of their dynamics at higher time resolution in comparison to other crawlers, as will be shown later. On the opposite end of the size spectrum of crawlers lie "palm trees" [*Desroschers* et al., 1995; *Heavner*, 2000], which are vertically extended emissions consisting of a single stem coming up from

the cloudtop and spreading out into a wider crown near 60-70 km altitude, hence the name. Lastly, a phenomenon with a stem emanating from cloudtops, but without a crown, has been given multiple names in the past: "sprite-jets" by *Stanley* et al. [1996] since the phenomena appeared as jets moving back up the sprite tendrils; then "fingers" by *Moudry* et al. [1999] and *Siefring* et al. [1999] to indicate their relatively thin nature and multiplicity, as if someone's fingers were extending upwards from the clouds; at the end of 1999 they were given the name "trolls" by *Lyons* et al. [1999]; and lastly "embers" by *Stenbaek-Nielsen* et al. [2000] due to the irregular dynamics of the phenomenon when observed at 1 ms time resolution, similar to embers in a dying campfire which flare up irregularly. All of these terms refer to the same phenomenon. Due to the slight awkwardness of the original term "sprite-jets," since the phenomenon is neither a sprite nor a jet, the term "ember" will be used in this chapter instead.

The three types of crawlers appear 30-100 ms after sprites in our limited number of observations, though it may be possible that sprites are not a necessary requirement for crawlers to appear. For example, the "blue jet" reported by *Pasko* et al. [2002] has a single stem extending up from a thunderstorm and may be a crawler, yet was not preceded by a sprite. In our observations, when sprite tendrils have decayed, the crawlers brighten and appear to move upward with speeds on the order of $10^4 - 10^5$ m/s based on TV-rate imagery.

In this chapter we first present examples of these various events as recorded by television-rate cameras to indicate their respective distinguishing characteristics. We then perform a detailed analysis of the dynamics of "smooth crawlers" and "embers" as viewed with 1 ms time resolution imagery. Smooth crawlers appear as beads of slowly-varying luminosity moving upward with speeds on the order of 10^4 m/s, without any apparent connection to cloudtops. An ember typically develops and brightens over ~ 1 ms as a small (< 2km diameter) bead within decayed sprite tendrils at an altitude < 60km. The bead then decays in brightness while remaining stationary, but initiates a secondary, downward-propagating patch of luminosity towards the cloudtop that moves at a speed on the order of 10^6 m/s. This speed corresponds to the characteristic speeds of streamers under similar E/p ratios observed in laboratory discharges [*Suzuki*, 1977]. After 1 to 30 ms, another bead may brighten and initiate the downward-moving brightness, either from the same location, higher, to the side, or sometimes even lower than the original one, although the average position of successive

beads is higher than its predecessor. Multiple beads appearing and decaying in succession may encompass a time span of several tens of ms to more then 100 ms. Since the period between successive brightenings is irregular, the average apparent upward speed is not constant, but varies from event to event. With standard TV-rate (16-33 ms) cameras, the downward motion of the individual embers is blurred and only the average upward motion is visible. To date, no models have been presented to explain the observed characteristics of these three types of crawlers. Embers possess some similarities to lightning K-events or M-events, and may be stratospheric analogs of these lower lying phenomena. They may also be the smaller versions of "palm trees." Palm trees have not yet been observed at 1 ms resolution.

6.1 Television-rate Images of Crawlers

Figure 6.1 shows examples of the three types of crawlers presented here. Images within each series are separated by $\frac{1}{60}$ s, ~17 ms, and the first image is not necessarily the beginning of the sequence. In the top series of Figure 6.1 is shown an example of a smooth-crawler following a sprite. Part of the frame stamp extends into the region near the top (a frame consists of two interlaced fields). The sprite appears in the first two images, extending into the next several fields partly due to the persistence of the intensifier phosphor. Blooming is also visible in the bottom part of the images due to scattered light from lightning within the clouds. After the sprite tendrils have decayed, smooth crawlers (circled in one field) appear within the previously smooth region as beads that move upward. There is no apparent connection between the beads and the bottom of the image, which distinguishes smooth crawlers from other crawlers. We show in a later section that at 1 ms time resolution, smooth crawlers appear to be beads that move smoothly upward.

In the middle series of Figure 6.1 is shown an example of embers following sprites. Part of the time stamp is visible at the top of the images. As before, the first images of the sequence are dominated by both sprites in the center and blooming from lightning near the bottom of each image. As more sprites occur, fingers extending from the blooming part appear to move upward (circled in one field). These are the embers. They appear as relatively narrow vertically extensive regions of luminosity following sprites. We will show

Smooth crawlers : insignificant vertical extent - beads

Embers : intermediate vertical extent - not wide at top
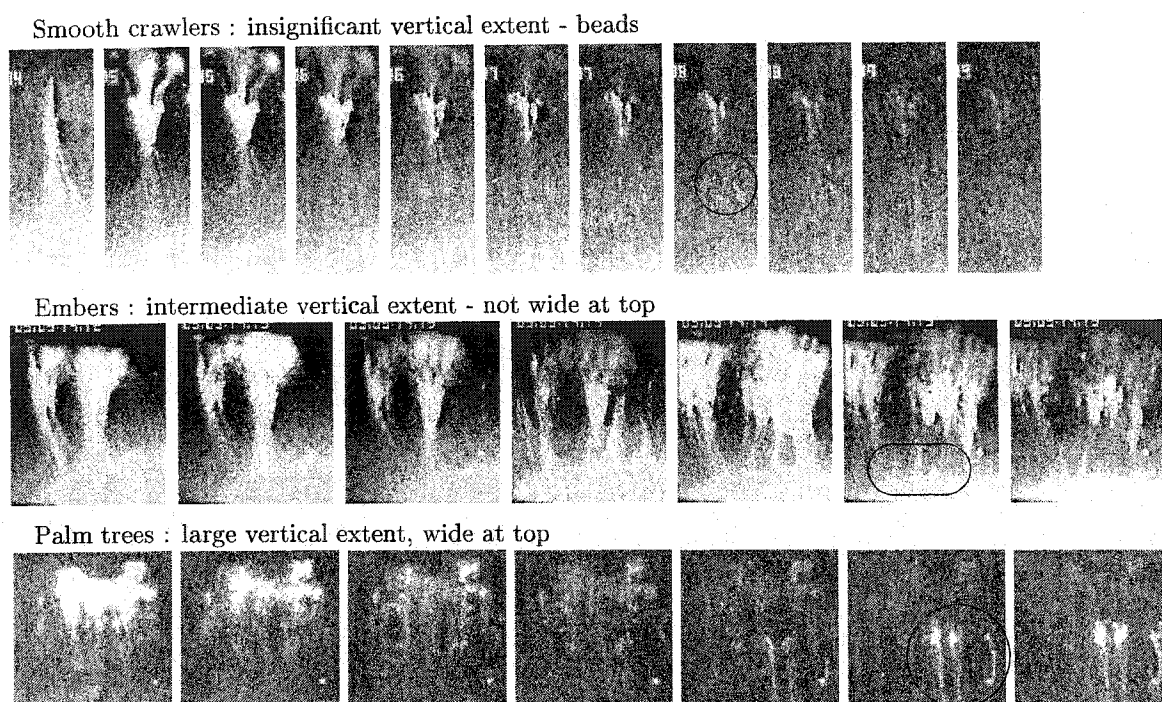

Palm trees : large vertical extent, wide at top

Figure 6.1. TV-rate examples of upward-moving bright features following some sprites. Images in each row/series are $\frac{1}{60}$ s apart. The top series shows an example of smooth-crawler (circled in one image), middle series shows an example of embers, and bottom series shows examples of palm trees. Collectively the upward moving brightnesses occurring with a short but definite time delay from sprites are known as crawlers. The first sequence shows part of event occurring at 05:03:14 UT on July 15 1998; the second sequence is part of event at 04:25:50 UT on July 29 1998; and the third sequence shows part of an event at 05:10:05 UT on August 18, 1999.

that at 1 ms time resolution, embers appear as randomly brightening beads, from which a luminosity patches moves downward. The irregular dynamics is lost in TV images due to the 17 ms time averaging.

Similar to embers, but with a wider crown on top, are palm trees, shown in the bottom series of Figure 6.1 (circled in one field). As with other crawlers, palm trees usually follow sprites. They are formed of vertically extended regions, widening near the top. Unfortunately we did not observe palm trees with the 1 ms imager.

The dynamics of the three types of crawlers from Figure 6.1 are shown in Figure 6.2 as seen at television-rate time resolution. Sequential images are ~17 ms apart, as before. The
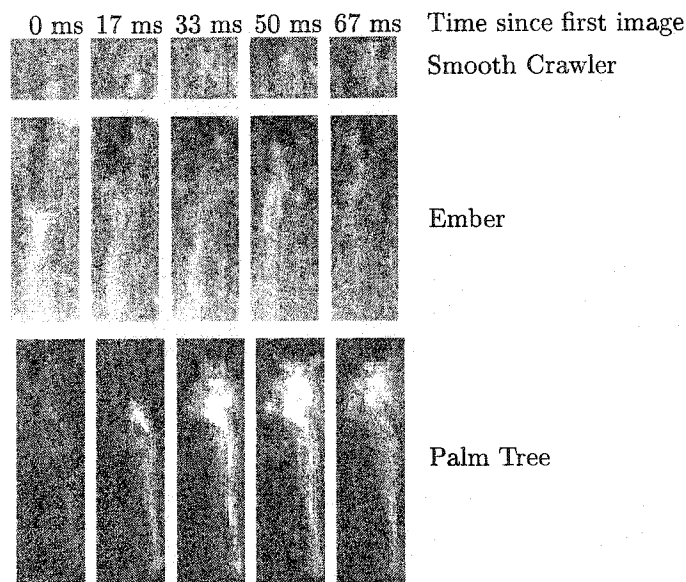
Figure 6.2. TV-rate dynamics of smooth crawlers, embers, and palm trees. Smooth crawlers are in top row, embers in the center, and palm trees in the bottom row. All are shown at television-rate time resolution. All three types of crawlers appear to "crawl" upward in these 17 ms time resolution images. The images are not shown at the same scale.

apparent upward speed based on these images is $10^4 - 10^5$ m/s. We show next with 1 ms images that the dynamics of embers as seen on TV-rate images give the wrong impression of simple upward motion. On the other hand, TV-rate images are sufficient to resolve the simple motion of smooth crawlers.

6.2 Smooth Crawlers at 1 ms Time Resolution

On August 18, 1999 we observed a sprite at 04:23:27 UT which was followed by both a smooth crawler and an ember. We use this example in upcoming sections to show the dynamics at 1 ms time resolution of the two phenomena. In Figure 6.3 we show the parent (causative) sprite at left, and at the right an image showing both the smooth crawler and ember with upper and lower arrows, respectively. The time difference from the sprite image to the ember and smooth crawler image is 110 ms. We examine 100 ms time sequences of both types of crawlers at the same spatial resolution and for the same time period.
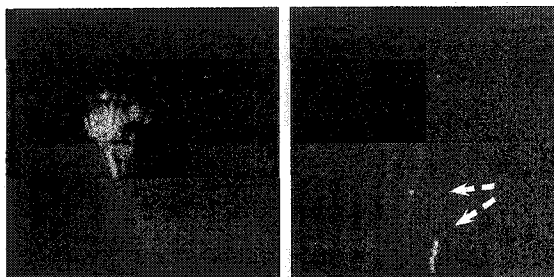
Figure 6.3. Parent sprite together with the ember and smooth crawler which followed it. Top row shows the parent sprite (left) and the ember and smooth crawler (right), 110 ms later. The tops of the images are at 110 km altitude, bottoms at 40 km altitude. The ember is vertically extended, the smooth crawler is the single bead above and to the left of the ember. In addition, multiple stars are visible. The event occurred at 04:23:27 UT on August 18, 1999.

A smooth crawler at 1 ms time resolution is shown in Figure 6.4. The Figure shows 100 ms of data, starting 123 ms after the initiation of the parent sprite. In Figure 6.4, rows and columns are indicated at side and top, respectively. The smooth crawler is visible as slightly structured emissions moving slowly upward at speeds on the order of 10^4 m/s. At 1 ms time rates, smooth crawlers appear to have "smooth" dynamics - slowly moving upward without the irregular and sporadic motions that embers undergo, introduced next.

6.3   Embers at 1 ms Time Resolution: Units, Events, Groups

At 1 ms time resolution, embers are formed of multiple sequences of a simple bead which undergo downward motion. These "units" are described next, followed by a description of the sequences.

6.3.1   Ember "Units"

Approximately 30-100 ms following the onset of a sprite, a small bead may suddenly appear and brighten at some altitude/location within the decayed tendrils of a sprite. In Figure 6.5 is a 6-ms sample sequence of this effect, showing the simplest discrete element of an ember, which we shall designate as an ember "unit," and its temporal development and decay. Following the appearance of the bead, an extrusion appears to the right and below the

bead, which then propagates downward with speed on the order of 10^6 m/s. Due to the similarity of its downward propagation to that of a sprite tendril, we call this dynamical feature of embers an "ember tendril," without any further implications. Most often the ember tendril is dimmer than the bead. The bead source of the ember tendril remains in place during the event and decays in brightness over 1-10 ms, in this case $\sim$3 ms. The region traced out by the ember tendril during its downward movement will be referred to as an "ember channel."

The region brightened by the passing ember tendril may appear to touch, but not extensively overlap, ember tendrils from the previous 1 ms frame. This behavior is suggestive of a front that propagates downward while brightening the region it passes. However, it does not have long duration at any particular altitude or vertically long spatial extent. Thus, an ember unit starts as a bead within the decayed sprite tendril, from which ember tendrils extend downward. Occasionally we see only a bead, or only tendrils, examples of which will be shown in a later section, but the above description covers most cases studied. In cases where we do not see the bead or the tendril in embers we propose that this is due to their luminosity being below the instrument sensitivity.

6.3.2 Ember "Events"

Multiple ember-units that propagate through the same channel form what we shall define as an "ember event." When an ember develops following occurrence of a previous ember unit, the bead of the subsequent ember unit may occur at the same location, below, above, or to the side of the bead of the first ember unit. In all cases, if a tendril is visible, it joins the channel of the previous unit ember on its downward propagation. Multiple beads sometimes appear at the same time. The term ember-event and ember will be used interchangeably in this paper to denote the sequence of all ember-units using the same channel. Likewise ember-unit and ember/bead-brightening will be used interchangeably to denote the blocks within that sequence.

Figure 6.6 shows an example of an ember composed of multiple units. It shows the same 100 ms temporal period shown in Figure 6.4, here shown for the region that includes the
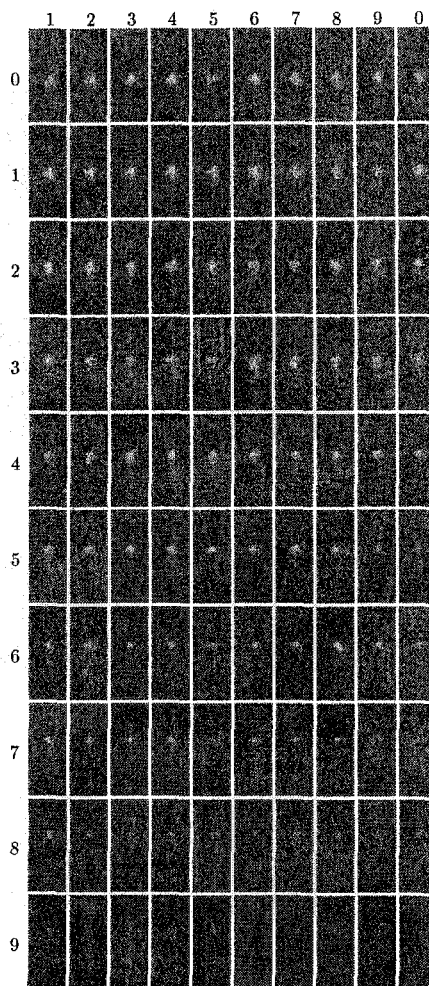
Figure 6.4. An example of a typical smooth crawler event. A total of 100 ms is shown in ten rows of 10 ms each. The time at the beginning of this sequence (field 01) occurs 123 ms after the initiation of the sprite. The region shown is approximately 5.6 by 14 km, with lower edge near 55 km altitude.
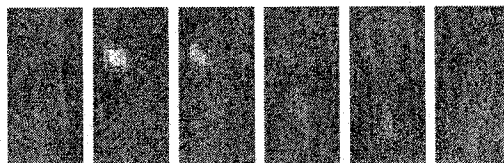
Figure 6.5. An example showing 6 ms of data of a typical ember "draining" down. A single ember "unit" includes a bead which brightens at some altitude and tendrils propagating downward from this bead. The region shown is approximately 4 × 8 km with the lower edge at 40 km altitude.
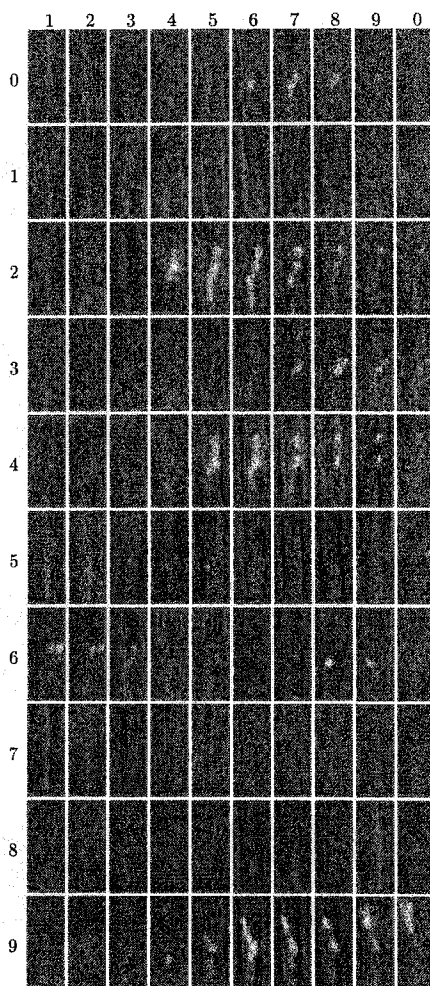
Figure 6.6. An example of a typical ember event. A total of 100 ms is shown in ten rows of 10 ms each. The time at the beginning of this sequence (field 01) occurs 123 ms after the initiation of the sprite. This event includes the ember unit shown in Fig. 6.5. The event occurred at 04:23:27 UT on Aug. 18, 1999, after a sprite. The region shown is approximately 5.6 × 14 km with the lower edge at 40 km altitude.

ember. The region is approximately 5.6 km wide by 14 km tall, with the lower edge at 40 km altitude. At the end of row 6 and continuing into row 7 is the ember unit shown in Figure 6.5.

The beads or ember units shown in Figure 6.6 brighten in a temporally irregular fashion. The first bead is visible in field 06 (row 0 column 6). The next bright ember-unit occurs starting in field 24, next around field 37, then 45, small ones on 54, 60, 68, 94, 95, and lastly in 98. There is no discernible periodicity in these intervals, ranging from 1 ms to >10 ms. The downward propagating tendrils are well visible in the ember unit on fields 24-27, and 45-48, in addition to dimmer ones elsewhere. Both of these ember units also show multiple beads brightening along the same channel. Ember units on fields 37-40 and 60-65 both have several beads to the side of one another, "draining" through the same channel; the tendrils are dimmer than elsewhere but still visible. Both of these examples also show that later ember units do not necessarily occur above earlier ones, but can be in lower altitudes than earlier beads (e.g. the bead in fields 37-40 is lower than the previous unit starting at field 24). A jump brightening, where brightness appears to jump upward from one bead to one above it, is visible in fields 95-96 and 99-100, as a diffuse emission above a bright bead, leading to the formation of a bead above. We cannot calculate absolute speed since the jump is visible only in one field, but a lower bound for the speed is on the order of 10^6 m/s. Note also that the channel can be slightly luminous in between the downward propagating ember-tendrils.

In order to see the ember tendril dynamics of this event more clearly, a thin crop 3 pixels wide was cut from the 100 successive images shown in Figure 6.6, and these crops were laid side by side, resulting effectively in a time series. This time series is shown in Figure 6.7 with shorter and longer marks below the time series indicating every 10 and 20 ms, repectively. The Figure shows mainly the time series of the channel of this ember event, since the beads sometimes occur to the side of the channel and would not be included in this relatively narrow crop. The diagonal streaks sloping downward in Figure 6.7 show the downward-propagating ember-tendrils.

The speeds of most of these ember-tendrils is $1 - 2 \times 10^6$ m/s. The slope (equivalent to the velocity) is nearly constant throughout the 100 ms. Since the time series was constructed from crops 3 pixels wide (equivalent to less than 1 km), this series also shows that subsequent
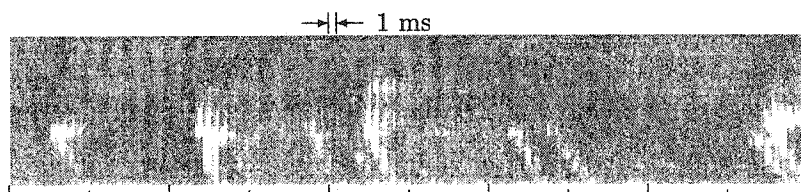
Figure 6.7. Time series of the ember shown in Figure 6.6. The downward propagating ember-tendrils are very nicely visible as diagonally downward streaks. The time series is 100 ms long, with smaller and larger marks below the series indicating every 10 and 20 ms, respectively. The lower edge of the time series corresponds to 40 km altitude, the upper one is at 55.5 km. Each slice corresponds to 1 ms.

ember units use the same channel, as proposed above. Sometimes multiple ember tendrils propagate downward within the same channel with the same velocity. It is clear that the interval between units (bead-brightenings) is variable.

6.3.3 Ember Groups

In the decayed wakes of sprite tendrils, multiple, spatially distinct ember events may simultaneously develop together, forming a group. Such a case was shown in Figure 6.1, and will be shown more extensively in the section on Ember Dynamics. Here, we comment only that a sprite can produce more than one ember.

This concludes the basic description of embers. Summarizing, embers occur in the decaying phase of sprites, within less than 1 s of sprite initiation. Each ember, or ember event, consists of one or more ember units/brightenings. Each unit consists of a bead and an ember tendril that propagates downward at a speed on the order of 10^6 m/s. The ember-units brighten in an irregular manner. If one unit brightens above a previous one, the TV-averaged motion can make it appear as if the ember is moving upwards. This upward motion is only apparent. The only real motion is that of the downward-moving ember-tendrils. More than one ember can brighten in the wake of a sprite.

6.4 Other Temporal and Spatial Characteristics

We now investigate the location of smooth crawlers and embers with respect to the parent sprite tendrils, and the dynamics of brightening of embers within an ember group.

6.4.1 Temporal and Spatial Relation of Smooth Crawlers to Parent Sprite

Smooth crawlers appear at locations of decayed sprite tendrils. At present, it appears that smooth crawlers do not correspond to any particular structure within parent sprite tendril. In some cases, smooth crawlers appear in regions where sprite tendrils did not have structure as in the top sequence of Figure 6.1. In other cases, the parent sprite tendrils saturated the imager, making it impossible to see any internal structure.

6.4.2 Temporal and Spatial Relation of Embers to Parent Sprite

As with smooth crawlers, it is often impossible to match the location of embers to structures within the parent sprite tendrils because the latter often saturates the images. Nevertheless, a few cases can be pointed out. We have one example in the high speed imager record where the sprite tendrils were not extremely bright, and included a tendril off to one side. In this case an association was possible. The sprite is shown in Figure 6.8 with the tendril magnified to the right. Approximately 60 ms following the passage of the tendril, an ember occurred within the decayed sprite tendrils. One image of the ember is shown on the extreme-right of Figure 6.8. For comparison, black lines indicate the same location in each image.

We have another case to serve as a different illustration. In the case presented in Figures 6.3 and 6.6, the ember became active in locations that were below the sprite tendrils, but not visibly penetrated by the sprite tendrils themselves. Even with extreme contrast enhancement in the images, there was no evidence that sprite tendrils penetrated the region in which the ember event occurred.

Summarizing, in many cases we cannot compare sprite tendrils to either smooth crawlers or embers due to imaging difficulties. In cases where we can, crawlers form either in sprite tendril region which initially appeared homogeneous, or which had some structure, or in region below sprite tendrils (possibly passed by sprite tendrils when they were at suboptical intensities).
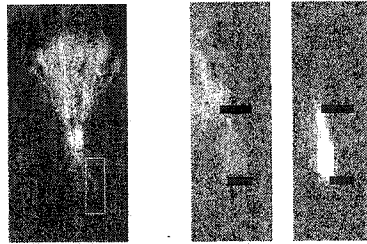
Figure 6.8. Location of sprite tendrils and ember: An image of a sprite at 04:58:14 UT is shown at left. The white rectangle shows a region magnified at right - the same image showing sprite tendrils, and an image 60 ms later of an ember. The ember closely follows the earlier sprite tendril channels. The bottom of the magnified images is at 42 km, top at 58 km, and the images are 5.4 km wide. Black lines indicate the same region on each field.

6.4.3 Ember Group Dynamics

Figure 6.9 shows five images from a complicated sprites/embers series, featuring three sprite groups and six separate ember events. The time since the initiation of the first sprite is noted above the images. The first three images show the first, second (group) and the third sprite in the series, respectively. The next two images show some of the ember events, with the image grey scale adjusted to enhance the details. Arrows indicate where the channels for the six different ember events intersect the bottom of the image, and labels (a-f) indicate the six ember events. The three ember events on the right (a-c) occurred after the first sprite, the three on the left (d-f) only after the second sprite group.

A comparison of fields 141 and 149 of Figure 6.9 shows that not all embers within a group occurred at the same time. In order to examine the relative timing of brightening of each ember with respect to the other embers, a time series 100 ms long was constructed for each. These are shown in Figure 6.10. The time series are from 65 to 164 ms after the first sprite occurred. The timing of the second sprite group and the third sprite is indicated above the top time series. In addition to sprite tendrils being visible in all the time series at the time of the second sprite group, the second sprite group was bright and resulted in a high background noise in the images due to Rayleigh-scattered light in fields 105/106, visible in all (a-f) time series at the indicated time. The third sprite at 131 ms is mainly visible only in time series (f).

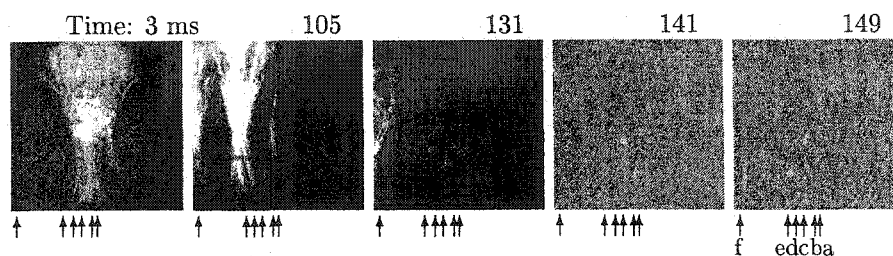Unlike the time series in Figure 6.7, it is mainly the ember beads that are visible at this

Figure 6.9. Five representative images of the three sprite groups and multiple embers at 05:24:22 UT on Aug. 18, 1999. Top edge of the images is at 99 km, bottom at 32 km (based on lightning data). The first sprite is shown 3 ms after initiation, the second group of sprites occurs 105 ms after the first sprite, and a third sprite, nearly out of the field of view, occurs at 131 ms. Two greyscale-adjusted fields show some but not all of the associated embers at 141 and 149 ms after the first sprite, respectively. Arrows indicate the location of six embers for which time series is shown in Fig. 6.10. Right-to-left in this figure corresponds to top-to-bottom in Fig. 6.10, respectively.

grey scale level, and not the ember-tendrils. The embers brighten at different times. Ember (a) is active at approximately 66 ms, 80 ms, and also generally in the interval 100-130 ms. After t=140 ms, ember (a) is inactive while embers (d-f) turn on. Ember (c) is actove during most of the timeseries. A possible interpretation of these dynamics will be presented in the Discussion section.

Before leaving this section, we wish to show part of time series (c) in Figure 6.10 to clearly show the dynamics that TV-rate cameras are missing. The magnified and expanded time series is shown in Figure 6.11. Note the discrete steps, indicated by arrows, in which the upward motion occurs, as well as extensive structure within the ember.

6.5 Discussion

The discussion section begins with a comparison of the three varieties of crawlers presented in this chapter, continues with discussing the sprite tendrils and their role in the formation of the crawlers, focusing in the following section particularly on embers and the dynamics of embers within a group. We explore the possible correspondence of embers to lightning-related phenomena, and end with a discussion of optical emissions which may be responsible for the phenomena.
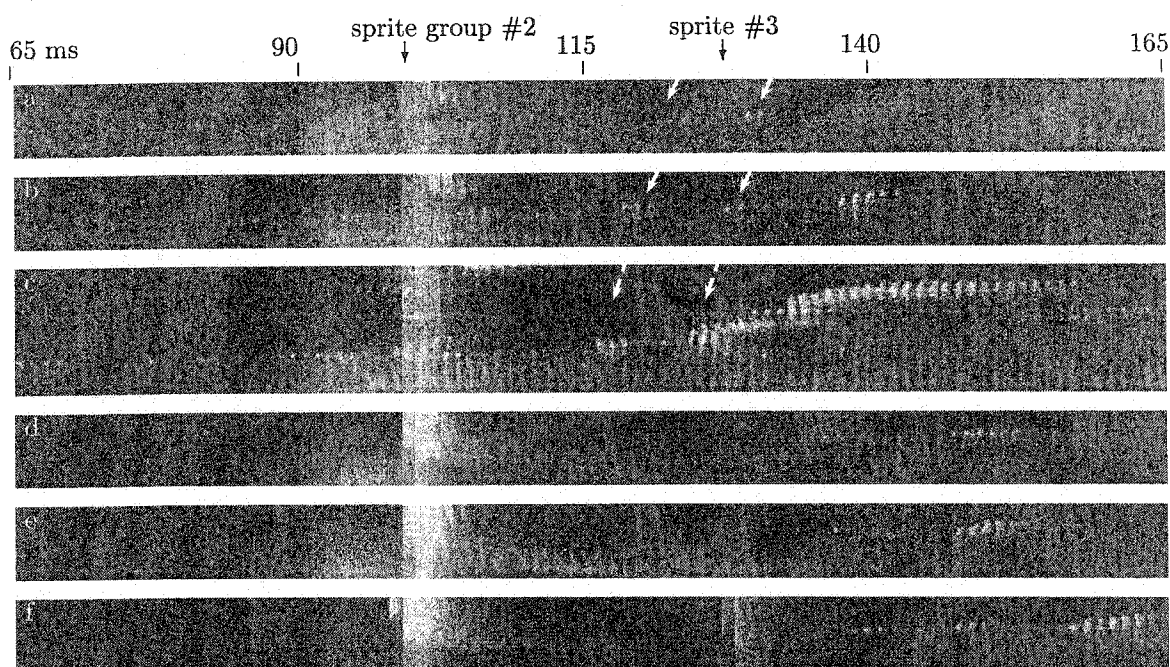
Figure 6.10. Sequences showing six embers following sprites at 05:24:22 UT on Aug. 18, 1999. Each sequence is 100 ms, or fields, long, starting at 65 ms after the first sprite occurred. The time since the beginning of the first sprite is indicated above the top sequence, same as in Figure 6.9. All timeseries have lower edge at 34 km altitude and top edge near 52 km except for sequence (c) which has the top edge near 64 km. Arrows indicate features mentioned in the Discussion.

6.5.1 Comparison of the Three Varieties of Crawlers

We have presented a smooth crawler and an ember from the same parent sprite event in Figures 6.4 and 6.6. At 100 ms, the smooth crawler moves slowly (compared to the tendrils of the ember) but steadily upward. Its brightness likewise varies slowly. In contrast, the ember moves irregularly, and its brightness is similarly irregular. Since both Figures show exactly the same time period following the parent sprite, there is no doubt that embers and smooth crawlers are two very different phenomena in terms of their dynamics.

The phenomenon that is possibly related to embers is the so-called palm tree [*Desroschers* et al., 1995; *Heavner*, 2000], presented in Figure 6.1. There are several similarities between palm trees and embers when viewed at television-rate time resolution: both have a single channel extending vertically between the apparent cloudtop and the top of the phe-
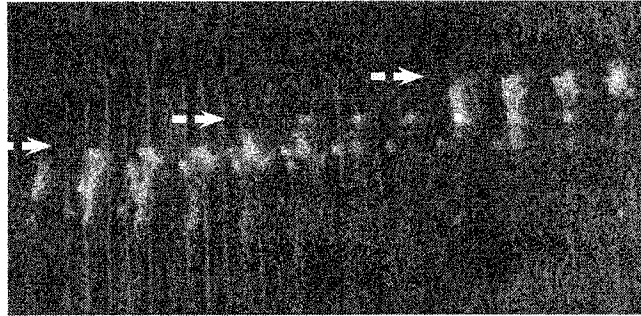
Figure 6.11. Part of record in Fig. 6.10 (c) near time 125 ms, magnified and expanded, showing 12 ms of data. Note the discrete steps of the apparent upward propagation. As before, the images span altitude range of approximately 32 to 64 km.

nomenon. Both appear to move upward. In addition, the smallest event in Fig. 6.1 bears spatial resemblance to the embers in the same Figure. Based on these characteristics, we suggest that embers and palm trees are possibly the same phenomenon. This suggestion should be easily verified or disproved when palm trees are observed at 1 ms time resolution. It is also possible that the "blue jet" of Stanley and Pasko [*Pasko* et al., 2002] is related to either/or palm trees or embers. The main difference is that their "blue jet" was not preceded by a sprite. Since our data set is limited, as is theirs, we cannot draw any conclusions as to their relation at this time.

The three crawlers presented in this paper are rare. From the 1998 and 1999 field campaigns, we have only a few examples of each after observing a few hundred groups of sprites. It appears that they may be more common over very active thunderstorms. The thunderstorm occurring on August 18, 1999 was very active (*M. Stanley, W. Lyons*, private communication), and provided us with at least two examples of each phenomenon.

6.5.2 Modification of Mesosphere and Upper Stratosphere by Sprites

The occurrence of crawlers that retrace the channels of decayed tendrils suggest the tendrils modify the properties of the medium, leaving a residue of chemically stored energy susceptible to subsequent instability. This "preconditioning" of the local medium by sprites [*Stenbaek-Nielsen* et al., 2000] was previously described based on rebrightening and new tendril formation within the body region of sprites as opposed to the tendril region dis-

cussed here. Sprite tendrils are nominally associated with streamers [*Raizer* et al., 1998; *Pasko* et al., 1998]. Streamers consist of a highly-charged head enhancing the electric field in front of it [*Raizer*, 1997, p.334], which absorbs photon-triggered electron avalanches that form in the enhanced upstream electric field. In the wake of the head, within the downstream body of the streamer, a region of weakly ionized plasma is left. The electrons in this plasma attach very quickly to ambient molecules, primarily O_2, so the plasma consists mainly of positive and negative ions, which slowly recombine or undergo chemical reactions. Compared to the electron attachment rate, the ion recombination time is long. Thus the region passed by the tip of sprite tendrils, presumably the streamer head, leaves in its wake many ions as well as vibrationally excited or metastable molecules, all effectively acting as an energy storage mechanism, which may play a role in the subsequent ember formation. Final relaxation to thermodynamic and chemical equilibrium occurs by way of a variety of pathways that may include ion neutralization and the creation or destruction of intermediate chemical products. After the region is modified by sprite tendrils, crawlers appear only in some cases.

One suggestion from this chapter is that sprite tendrils can modify the atmosphere through excitation of vibrational and electronic states at of ambient molecular species, including states that are not energetic enough to emit light detectable by our instruments. Observations of embers appearing in cases when sprite tendrils do not reach down into the region where embers appear, mentioned in Sec. 6.4.2, indicate such processes could be occurring in these cases. The region modified by sprite tendrils is itself inhomogeneous since any modification occurs on top of structured background atmosphere.

6.5.3 Ember Tendrils

As we have shown in Figure 6.7, ember units brighten at irregular temporal intervals following some sprites. The simplest explanation for this behavior is that an external forcing needs to trigger this modified region one or more times to form ember-unit(s). Upon triggering, the stored energy discussed above is released, for example by electron collisions leading to an increased electron detachment rate from negative ions. A streamer, similar to that of sprite tendrils, could form again and move down the previously modified region, resulting in the emissions of ember-tendrils. As the first ember-tendril descends through the ember-channel,

the channel is re-excited, renewing the weak plasma densities inside it and extending the lifetime of the channel. In our observations, the regions brightened by the ember-tendrils moving down a channel do not overlap extensively on successive frames, indicating that the volume emitting the light is relatively narrow in altitude compared to the altitude range it traverses in 1 ms. This is consistent with the streamer picture, as are the velocities. From the present data, we cannot estimate the diameters of the beads or the channels of the embers. The nearly constant speed of the multiple ember-tendrils moving within a channel, even those with relatively short time delays of 1-2 ms, are consistent with the model of *Pancheshnyi* et al. [2001], who simulate streamers and show near independence of streamer velocity on pre-ionization as long as photo-ionization is taken into account. At the same time, it is in contrast with *Winn* [1965] and *Suzuki* [1977], who find that streamer velocity increases with increasing background ionization, in particular, for streamers following one another with short (< 100 μs) decay [*Winn*, 1965]. One way to account for this apparent discrepancy is to assume that within the time delay between the successive ember-tendrils we observe in our data (2 ms or more), the channel decays enough to be equivalent to nearly no pre-ionization, though still providing a preferred path for the streamer.

In laboratory conditions, streamers can form in the middle of a gap and propagate towards both the anode and the cathode. A conducting material can act as the initiation source of such streamers. In the case of embers, it is possible that a region of increased conductivity formed in the wake of sprite tendrils could act as the streamer initiation point, possibly initiating both positive and negative streamers. The jump-brightening sometimes observed in our embers (Sect. 6.3.2 §3) could be due to a streamer of opposite polarity to that of the ember-tendril.

6.5.4   Dynamics Within an Ember Group

When does a region trigger to form an ember? An interesting picture emerges from Figure 6.10. Spatially nearby ember events occasionally appear partially offset in time from one another, and at other times appear with no relation to their neighbors. In particular, note the arrows indicating the brightenings of embers (a-c) between approximately 115 ms and 130 ms. Of the three embers, ember (c) brightens first, followed a small delay (2-5 ms) later by ember (b), followed by ember (a). While highly speculative, the described dy-

namics is possibly indicative of a forcing mechanism from the underlying thundercloud, as opposed to spontaneous formation from internal processes. This forcing would appear to have a delay of ~3 ms from ember (c) to (b), and from (b) to (a), and could be a response to a lightning fields from the underlying thundercloud. Horizontal lightning could trigger successive embers.

This similarity of activity within the dynamics of ember events (a-c) breaks down after 130 ms, when ember (c) is very active while embers (a) and (b) are rather inactive. If the above assumption regarding charge travelling through horizontal lightning channels within the thundercloud is a correct interpretation, the increased activity within only one ember event would indicate that the thundercloud channel was re-established to a different charge region and charge no longer flowed below ember events (a) and (b).

The interpretation we propose above for triggering of embers, of a thundercloud channel through which current pulses travel, is further supported by the following observation: ember (c) starts its greatest activity only around time 130 ms, at the time of the third sprite. The occurrence of both increased ember (c) activity and the third sprite may be explained if a large current pulse, from a newly tapped charge region, propagates through the thundercloud before finally draining down to the ground and resulting in the third sprite.

The embers (d-f) following the second sprite group are not very spectacular, compared to embers (a-c). The time series in Fig. 6.10 indicates ember events (d-f) started occurring near time 140 ms, or some 35 ms after the second sprite group.

6.5.5 Possible Correspondence of Embers to K-Changes and M-Components of Lightning

Embers possess the following characteristics: period between the units of an ember event of 1 to > 10 ms, and speeds of downward propagation near 10^6 m/s. They are thus similar to lightning K-changes and M-processes. *Thottappillil* et al. [1990] describe them as follows:

> Steplike electric field changes occurring on a millisecond time scale between strokes (during the so-called J change) and after the final stroke (during the so-called F change) of a ground flash are called K changes and are considered

to be caused by a unique in-cloud discharge termed a K process. Similar K field changes are observed in the latter portion of cloud flashes. M components are temporary increases in the luminosity of the faintly luminous channel observed after some ground strokes and are accompanied by electric field changes termed M changes.

... The geometric-mean time durations were similar: 0.7 ms for 135 K changes and 0.9 ms for 80 M changes. The geometric-mean time intervals were dissimilar: 12.5 ms for 93 K chance intervals and 2.1 ms for 48 M change intervals.

Uman [1987] states that various researchers have found velocities of K-changes to be 10^6 to 10^7 m/s, and that one researcher found that K changes were coincident to luminous pulses. *Fisher* et al. [1993] found that current pulses in the channel are associated with the channel brightening (or M-components), and *Jordan* et al. [1995] estimated that M components move downward, with speeds on the order of 10^8 m/s.

Embers thus appear similar to K-changes in terms of speed, and similar to M-components in terms of intervals, though at present it is difficult to define this term for embers, since it is dependent on the instrument sensitivity. In both K and M events the channel brightens as it does in embers. In Sec. 6.4.3 we have argued that embers might be due to current pulses travelling through existing channels in the thundercloud below (presumably M-components). The similarity indicates that embers may be either due to, or equivalent to, either K changes or M components. A near-field measurements of electric field of K and M changes together with a high speed imager observations of embers should settle this question.

6.5.6 Do Embers and Palm Trees Electrically Connect to Cloudtops?

Another interesting question is whether embers or palm trees electrically connect to cloudtops. As with sprites, at present we do not know for sure. In all the images presented here and in our data base, the sprites, embers or palm trees were either too far away so that it is not possible to see the tops of clouds due to earth's curvature, or the observations were made near the thunderstorm but the instruments included only TV-rate cameras. In this geometry TV observations typically bloom from the intense light generated by lightning

and lightning-illuminated clouds, saturating the camera in the temporal and spatial region of interest.

6.5.7 Embers and Lower Parts of Palm Trees: Stratospheric Phenomena

Parts of embers and palm trees occur below 50 km, in the stratosphere. This region is marked by increasing temperature with increasing altitude, up to approximately 270 K at the stratopause (approx. 50 km altitude). This heating is due to absorption of solar EUV by ozone. Due to the increasing temperature, the stratosphere is convectively stable.

In the upper stratosphere (above 30-35 km), ionic composition is similar to that of the mesosphere. Major positive ions in the upper stratosphere include water clusters. Negative ions in this region include mainly large clusters of sulfates, with ions up to 352 a.m.u. having been observed [*Wayne*, 1991, p302-303]. Therefore, the chemical composition for the examples presented can be thought of as similar to that of region where sprites occur, except for increasing pressure, and as a result also increasing threshold electric field necessary for breakdown and initiation of streamers. This would rather suggest that, despite the similarity of speeds for laboratory streamers and those of ember-tendril, the latter would require such high electric field that we would be more likely to observe another sprite rather than an ember.

The denser stratosphere where many embers occur, in comparison to the mesosphere where sprite spectra have been measured, also brings in the question of which emissions contribute to the ember phenomena. With lower altitudes, nitrogen and oxygen molecules or ions become increasingly quenched. For example, the main optical emission from sprites, the red (non-ionized) nitrogen first positive band emission $(N_2(B^3\Pi_g) \to (A^3\Sigma_u^+))$ has a quenching altitude of approximately 53 km [*Vallance Jones*, 1974, p.119]. At this altitude half of the nitrogen molecules in the $B^3\Pi_g$ electronic state deactivate collisionally with other N_2 molecules before they have a chance to emit light by spontaneous emission. One and a half scale heights lower, near 40 km, only ~10% of the $N_2(B^3\Pi_g)$ molecules emit light before collisional deactivation occurs. As with blue jets and blue starters [*Wescott* et al., 1995, 1998a] and sprite tendrils in these altitudes [*Sentman* et al., 1995], which are all blue, the emissions from embers are likely to be blue also. Possible emiisions include either the blue (non-ionized) N_2 second positive band emission $(N_2(C^3\Pi_u) \to (B^3\Pi_g))$ with a quenching

altitude of 30 km [*Vallance Jones*, 1974, p.119] or possibly ionized emissions (e.g. the blue N_2^+ first negative band, quenched at 48 km altitude). If the emissions from embers are blue, increased Rayleigh scattering of blue wavelengths compared to red wavelengths needs to be taken into account.

It would be interesting to observe embers at lower altitudes, for example below 30 km, where the different processes become dominant. In particular, spectral observations may clarify the dominant emissions and energy budgets of embers. Our present observations do not give any indication whether the speed of ember-tendrils slows down in increasing pressures. In the future, observations of embers into lower stratosphere may prove interesting for both of these points.

6.6   Summary of Characteristics of Crawlers

We have presented characteristics of apparently upward-propagating luminosity structures following some sprites, known collectively as crawlers. Three subgroups of crawlers have been identified: smooth crawlers, embers, and palm trees, each differentiated from others by their apparent vertical extent with respect to sprite tendrils. Observations of smooth crawlers at 1 ms resolution revealed they move smoothly upward, unlike embers. Palm trees were not observed at 1 ms time resolution. These characteristics are summarized in Table 6.1.

Detailed characteristics of embers, also called fingers, trolls, or sprite-jets by various researchers, based on 1 ms time resolution observations are as follows:

Basic characteristics: An ember-unit consists of a bead brightening at some altitude and ember-tendrils moving downwards. The region passed by the ember-tendrils is a channel. An ember-event consists of multiple ember-units moving through the same channel. The beads of subsequent units within an event can occur above, below or to the side of the beads of the previous ember-unit. Multiple beads can brighten at the same time. The ember-units/beads within an event are not regularly spaced in either time or space. Multiple ember-tendrils can move through a single channel at the same time. The downward velocity of ember-tendrils is on the order of 10^6 m/s. A sprite can be followed by multiple ember-events, forming an ember-group. Within the ember-group, units sometimes do and

Table 6.1. Description of crawler types

Name	100 ms time series from 1 ms imager	
TV image	Description of Dynamics	Velocity
Smooth Crawler		
	Both TV, 1-ms images: Beads moving upward without any apparent connection to cloudtops	
	Dynamics: Regular/smooth	Velocity: 10^4 m/s upwards
Ember		
	TV images: Thin columns moving upward, apparently connecting to cloudtops. 1-ms images: beads with tendrils moving downward.	
	Dynamics: Irregular	Velocity: 10^6 m/s downward
Palm Tree		
	Not yet observed at 1 ms time resolution	
	TV images: Thin columns moving upward with a wider crown at the top, apparently connecting to cloudtops	
	Dynamics: Unknown	Velocity: Unknown

sometimes do not brighten in unison.

Averaged characteristics: It is the irregular sequence of ember-units within an ember-event that, when averaged over TV (17 ms) time resolution, creates the impression of upward propagation. In fact, this upward motion is characterized by the time difference between ember units rather than any microphysical property. The downward-moving ember-tendrils, when averaged over 17 ms, form the single "stem" visible in TV images of these phenomena, for example, Fig 6.1.

Relationship to other phenomena: Crawlers (embers, palm trees, and smooth crawlers) appear in regions passed by bright or dim sprite tendrils, or in regions "below" sprite tendrils, which were probably passed by the slow-phase tendrils that were below the detection

limit of the instruments. Crawlers are temporally separated from sprites by 30-100 ms, during which time no activity is observed. However, it is possible that we have observed crawlers only due to a limited dataset, and that the "blue jet" of *Pasko* et al. [2002] is in fact an example of a crawler not following a sprite.

Embers have dynamics distinctly different from crawlers based on 1 ms time resolution. Smooth crawlers, bright beads slowly moving upwards, do not vary on 1 ms time scale and do not appear to have any channels connecting them to clouds. Embers might be, however, similar to palm trees, which have a channel connecting them to cloudtops, based on 17 ms time resolution images. Further studies are necessary to resolve this issue.

Embers could be caused by, or be equivalent to, K- or M- changes occurring within a lightning discharge. A near-field electric field record together with high speed images of embers could prove or disprove this point. Embers may be triggered by a current pulse moving through an existing channel in the underlying thundercloud.

Another possibility is that embers are a subset of the group of optical phenomena called in the past "upward lightning" [*Vaughan and Vonnegut*, 1989; *Vonnegut*, 1980]. At present, a challenge remains for any explanation of this phenomenon. Is it due to weak plasma formation or energy deposition from the sprite tendrils, possibly triggered by electric field from a current pulse traveling through the thundercloud below? What is the nature of the stationary ember-beads? Is the traveling wavefront, visible as an ember-tendril, a streamer? Are embers simply the extensions of processes occurring in the thundercloud itself? An investigation of the embers and their relationship both to the parent sprite and underlying thundercloud processes shall prove interesting.

Chapter 7

Conclusions

7.1 Summary

Summary tables Three summary tables of most optical emissions above active thunderstorms associated with cloud-to-ground lightning discharges that have been observed to date are given in Tables 7.1, 7.2 and 7.3. Due to the lack of association with a particular lightning flash, blue jets and blue starters are not listed. Similarly missing are the case of a "giant jet" caught on tape by Mark Stanley and Victor Pasko [*Pasko* et al., 2002], or the multitude of other, not yet well documented, phenomena mentioned by *Lyons* et al. [2001].

The principal conclusions of this thesis may be summarized as follow:

Smooth structure of elves and halos In Chapter 3 it is shown that in our images, most elves do not exhibit strong spatial variation in optical emissions. Likewise most halos observed with the high speed imager are either unstructured or have large-scale structure. Very few halos have small scale structure. This in turn implies that electric fields causing elves and halos do not possess fine scale structure.

Sprite initiation - background atmosphere The unstructured electric fields implied by elve and halo observations, combined with observations of sprites initiated outside of main halos, without halos, or from beads left over from a previous sprite, suggest that sprites are initiated from local pressure/density and compositional inhomogeneities in the background atmosphere. The pressure/density connection was shown previously with data

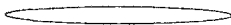Table 7.1. Summary of pre-sprite glows.

GLOWS INDEPENDENT OF SPRITES, though often preceding sprites

Name	Structure	Duration	Dimensions	Altitude Range	Summary
Elves		fraction-ms	W:100's km H:few km		Diffuse emissions, easiest to see with photometers. Explained as due to electromagnetic pulse from lightning return stroke interacting with lower ionosphere. Emissions have the shape of an expanding ring in the models, observable only at 1 ms or less time resolution.
Halos		2-10 ms	W:10's km H: 5-10 km		Diffuse emissions of longer duration than elves and thus brighter on most optical camera systems. Halos appear pancake-shaped, not much structure, if any. Explained as emissions due to quasi-electrostatic field from a lightning continuing current interacting with the mesosphere. Often appear 1-3 ms before sprites.

Table 7.2. Summary of dynamic and stationary sprite features
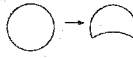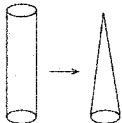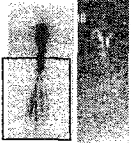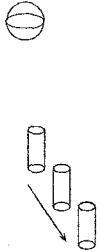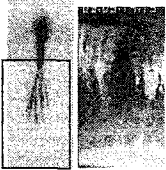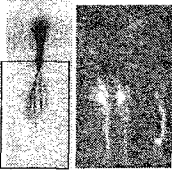
SPRITES: DYNAMIC FEATURES				(Durations are < 1 ms at any altitude)	
Name	Structure	v or T	Dimensions	Range	Summary
Tendrils		10^5-10^7 down	D:100m, L:10,000m		Common to all sprites. Basic sprite consists only of tendril(s). Sprites may have multiple temporally-separate sets of tendrils. Sprite brightness and tendril speed appear related. Modeled as streamers.
Branches		10^6-10^8 up	D:100m, L:10,000m		Two sizes, $>\sim$ 10 km and $<\sim$ 10 km. Often form puffs, beads. May 'retract' into columns. Suggested to be streamers, not yet modeled.
SPRITES: STATIONARY FEATURES				(Speeds of brightness propagation $< 10^5$ m/s)	
Puffs		2->30	D: 100-1000m		May appear at tops of both long branches (large puffs) and short branches (small puffs). Relatively long-duration. Diffuse. Not halos! Not yet explained.
Stationary bright feature		2-> 100	D:100-1000 L:10,000 m		Longer duration emissions, either in shape of a column or less elongated. May slowly transform into different shape. Not yet explained or modeled.
Beads		2->100	D:100m?		In central portion of sprites. Long duration, small extent (with respect to tendrils and branches). Appear 1-10 ms after passage of tendrils/branches. Not yet explained or modeled.

Table 7.3. Summary of sprite aftereffects.

GLOWS FOLLOWING SPRITES

Name	Structure	Speed/Dur	Size	Range	Summary
Smooth Crawlers		$10^4 - 10^5$ m/s up-ward, 10's ms	< 1 km		30-100 ms following some sprites, crawlers beads brighten and move slowly upward. Brightness does not fluctuate rapidly, and there is no apparent connection to cloudtops. Not yet explained or modeled.
Embers		Duration: 1-10 ms	< 1 km		Ember beads brighten 30-100 ms following some sprites, but unlike crawlers, an ember-tendril moves downward towards cloudtops from the bead, and the beads brighten irregularly. Not yet explained or modeled.
		10^6 m/s down	<1 km wide		
Palm trees	?	?	?		Palm trees beads brighten 30-100 ms following some sprites, but unlike embers, include a wider crown at top of the stem. Not observed at 1 ms temporal resolution.

136

from the EXL98 campaign showing alignment of sprite with gravity wave peaks and troughs in the case of very strong gravity waves, observable with unfiltered camera [EXL98 data from 7/22/98]. The suggestion is that inhomogeneities in the background atmosphere may play an important role in sprite initiation, providing sprite "seed locations." These seed locations possess a distribution of breakdown thresholds, so that while only a few seeds trigger at a relatively low electric field, increasingly more trigger at higher fields. The brightest halos would tend to develop sprites with more into tendrils than dimmer halos. Likewise, a few sprites would be triggered without any associated halo at all.

Sprite varieties - electric fields The sprite form that develops following initiation appears to be more dependent on the electric field. Observations of cases where very dim tendrils propagate down and disappear contrast strongly with cases where similarly dim tendrils suddenly brighten and form upward branches and a large sprite. Observations such as these suggest the sprite type is determined largely by electric field, its magnitude and duration.

Description of sprite dynamics The simplest sprites consist of descending tendrils, and possibly stationary beads. Slightly more complicated sprites may form a more luminous shape at the top of the tendril, either a column, bulb, or any other shape more elongated or larger than a bead. Branches may form, or start to form without reaching far, from the bottom of the bright shape, though the bright shape is not necessary for branch formation - some branches form simply from descending tendrils. The dynamical branches move up and possibly form both a stationary puff at the top and a stationary column near the bottom, the two features being separated by a gap which the dynamic branch has traversed. Effectively this appears as if the branch shoots up and then retracts into a column. Observations show the stationary column formation at the bottom of dynamic branch occurs both for some large (> 10 km) and small (< 10 km) branches. Branches may start from increasingly lower altitudes, overlapping the altitudes where a short time earlier only donwward tendrils existed. This overlap region is the body of the sprite, the brightest part, and additional processes may occur, such as additional tendrils. Most sprites with large upward branches can be called carrot sprites.

Sprite tendrils No matter how many of the processes described above occur for a particular sprite, every sprite starts out with descending tendrils. The velocities of sprite tendrils are on the order of $10^6 - 10^8$ m/s downward. In some cases, sprite tendrils slow down to 10^5 m/s, continuing at similar speed for about 10 ms in one particular example. In other examples, the dimmer brightness left behind by the passing tendrils expands horizontally outward, at speeds near 10^5 m/s. This is the first observation of the slow downward tendrils and horizontally-expanding tendrils.

Sprite aftereffects Dynamical processes are often observed in the locations of nearly-decayed sprite tendrils, and are known as crawlers. It is unknown whether these processes occur independently of sprites, and that only due to triggering on visually bright phenomena were we able to observe the phenomena independently. Three subgroups of crawlers are: (1) smooth crawlers, which at 1 ms timescales appear to smoothly move upwards at speeds around 10^5 m/s; (2) embers, which appear to have sporadic movement at 1 ms timescales with a bead brightening at some altitude and a tendril-like feature moving downward from it; and (3) palm trees, which have not yet been observed at 1 ms time resolution yet. In TV rates, all three phenomena appear to move upward. Similar to 1 ms images, at TV-rate images smooth crawlers appear as upward-moving beads without any apparent connection to cloudtop. This contrasts with embers, which at TV rates appear as thin ribbons or fingers being pulled upward from a cloudtop, and no downward motion is visible in the 17-ms averaged images. Palm trees appear as a ribbon extending upwards from cloudtops that spreads into a wide top.

7.2 Interpretation of Results

Current theories provide satisfactory models for elves and halos. However, the more complicated structure and dynamical behavior of sprites have not to date been satisfactorily modeled in detail. Sprite aftereffects, such as crawlers, have only recently been identified, and no new detailed theory exists for these. New modeling efforts focus on streamers [*Liu et al.*, 2002] as sprite tendrils and branches, but it is unknown what determines the location of streamer initiation. Here it is suggested that streamer locations are determined by spatial

inhomogeneities in the dielectric properties of the background atmosphere as opposed to electric field structure. Similarly, while streamers appear to be the process underlying dynamical sprite features, so far no suggestions have been made for what may be responsible for stationary sprite features. Images are presented that suggest stationary sprite features are responsible for a significant proportion of sprite optical emissions, based on images integrated over 17 ms. A lack of theories similar to that for stationary sprite features is noticeable in the crawler (sprite after-effects) category as well. A surprising new result presented here is that the dominant motion of embers is downward, while the time-averaged apparent motion is upward.

Overall, there is a surprising wealth of optical forms and dynamics occurring above thunderstorms.

7.3 Sprites Elsewhere in Solar System?

The question may be posed whether sprites and other mesospheric (on Earth) transient luminous events (MeTLEs) occur elsewhere in the solar or galactic system. The possibility sprites in the solar system was discussed by *Sentman* [1996]. In order to start answering this question, it is important to establish how lightning and sprites are similar and how they are different. On Earth, lightning discharges a charged region in a thundercloud, either to "ground" or to another layer in the cloud. Lightning initiates with a stepped leader, and a return stroke subsequently transfers strong current through the channel created by the stepped leader.

Sprites, elves and halos do not "dis"charge any region of the atmosphere. Sprites in particular are believed to be composed of streamers, as opposed to leaders *Stanley* [2000]; *Pasko* et al. [2000]. Streamers develop "smoothly" in time in comparison to the stepped leaders, and sprites do not possess a return stroke. All three phenomena occur as a response of the atmosphere to the electric fields from a lightning return stroke and continuing current at a distance from the lightning itself. It is this last point, which may be used to qualify what would be the requirement for identifying sprites (elves, and halos) elsewhere: the three optical phenomena would be spatially distinct from the lightning, and be produced by the electric fields from the lightning discharge. This differentiates the phenomena from,

for example, St. Elmo's fire [*Wescott* et al., 1996b], which occurs during thunderstorms at a distance from the cloud or any lightning, but is not due to a specific lightning discharge.

Having differentiated lightning and MeTLEs based on the cause-and-effect relationship at a distance, the conditions necessary for MeTLE occurrence may be considered. As mentioned in Section 1.3.6, the electric field E depends on the distance from the lightning r as well as on the value of the electric dipole moment M and its variation in time:

$$E \propto \frac{M}{r^3} + \frac{1}{cr^2}\frac{dM}{dt} + \frac{1}{c^2 r}\frac{d^2 M}{dt^2}.$$

The first term is the quasi-electrostatic term, the last is the EMP term. For the Earth, it was *Wilson* [1956] who noted the quasi-electrostatic field falls off as $\frac{1}{r^3}$ with increasing altitude r above the lightning, and can exceed the breakdown electric field, which depends on number density and is proportional to e^{-r}. For earth, this cross-over occurs near 80 km [*Stanley*, 2000, his Fig. 1.1]. This simple calculation roughly gives the correct altitude range of sprites and halos, and allows specification of the necessary conditions for sprites, elves and halos to occur. The zeroth-order conditions are:

1. Causative lightning

2. Neutral number density decreases with distance from source

Further restriction require that

- For elves, current in lightning is fast enough to launch a sufficient EMP; for halos and sprites, charge transferred creates a sufficient QE

- Crossover between breakdown field (proportional to density) and lightning field (prop. to current or charge) occurs before the waves are absorbed by the intervening medium (placing limits on the electron density)

- Atmospheric species exist that can be excited and emit light promptly, *i.e.* before collisional quenching occurs

These are necesary, but not necessarily sufficient, conditions, and can be used to check on various other locations in the solar system where such discharges could be possible.

Below are listed locations in the solar system where lightning is either known to occur or has been suggested to occur. These will be narrowed down by checking whether the number density of constituents decreases further away. Lastly, for some of the locations where lightning is known to occur, the lightning parameters will be discussed.

Of the planets in the solar system, the only ones which have not yet been suggested to have lightning are Mercury and Pluto, and excellent summaries of the others are given by *Russell* [1993] and *Desch* et al. [2002]. At present, some possible lightning signatures have been detected on Venus, but these could also be due to other sources. Lightning has been suggested to occur in Martian duststorms, so far without detection. The only lightning observed optically has been detected on Jupiter. On Saturn, Uranus and Neptune, convincing electromagnetic signatures of lightning have been detected, such as whistlers or sferics, for which lightning is the only plausible explanation.

Besides planets, moons such as Saturn's Titan have been predicted to have lightning, though so far none has been detected. Lightning has also been suggested to have occurred in the proto-solar nebula, in order to account for chondrules, small grains of glass inside meteorites [*Desch and Cuzzi*, 2000].

From this list of regions with suggested or known lightning occurrence, all satisfy the requirement that neutral density decreases with distance from the lightning source, with the exception of protosolar nebula. This requirement would also be satisfied on any extra-solar planet or other body of sufficient mass, but not in, for example, Saturn's rings.

Based on the lack of detected sferics by Galileo at Jupiter, the discharge time for lightning on Jupiter is predicted to be several ms, compared to tens to hundreds of μs for Earth [*Desch* et al., 2002, 985]. If this is the case, elves, which depend on fast discharges, may not occur on Jupiter, while sprites and halos may.

In contrast, some experimental data on Saturn, showing a flat spectrum of sferics between 10 MHz and 40 MHz, have been modeled to be possibly due to a very short, a few 10s ns, lightning discharge [*Desch* et al., 2002, p.987]. If the interpretation of the data as that due to lightning is correct, Saturnian lightning would favor elves but not halos or sprites based on its duration. Elves require fast charge transfer to create large EMP, while sprites and halos require sufficient charge transferred which generally occurs during a longer time period.

The possible occurrence of sprites, in contrast to halos, depend also specifically on the chemical composition in the region of interest. In particular, sprite tendrils are suggested to be positive streamers [*Pasko* et al., 1998; *Raizer* et al., 1998; *Stanley* et al., 1999]. In air, streamers presumably propagate via a process in which accelerated electrons collide with nitrogen molecules, ending in an excited state of N_2. The excited N_2 molecule spontaneously decays into a lower state via the emission of a photon. This photon is of sufficient energy to ionize oxygen molecules [*Raizer*, 1997, p.337], creating a new electron, and the process repeats itself. If this mechanism is correct, sprite tendrils may only occur in environments which allow an interplay between these specific or similar molecules. Thus, sprite occurrence on Jupiter, would depend specifically on whether streamers can propagate in the gas mixture present. Halos depend on atoms or molecules which can be excited into an upper state and subsequently emit light, in contrast to the presumed streamer mechanism for sprite tendrils which depends on excitation of one species and emission of a photon, with the photon subsequently absorbed by another species.

7.4 Suggestions for Future Research

The value of high speed imaging is attested to by the variety of new phenomena described in this thesis. Going to a higher temporal resolution compared to that presented here, such as the 3000 fps used by Mark Stanley [*Stanley* et al., 1999], and focusing on the central portion of sprites, which at this time appears to be the least understood, may shed some additional light on the processes occurring in sprites. Focusing only on specific altitude regions with the high speed imager would allow for a better spatial resolution than if the entire sprite needs to be imaged.

At different times, optical emissions of vastly different spatial characteristics may appear at the same altitude over time scales of 100 ms. Since presumably the background atmosphere does not significantly change on those time scales, something else must be causing the different emissions. An easy question to settle, using a high speed imager, would be whether embers and palm trees may be a smaller and larger of the same phenomena, namely, whether palm trees and embers have similar dynamical behavior. A more difficult question to settle about embers is the suggestion that they may be caused by, or be equiv-

Table 7.4. Summary of speculations and possible observations

Observation	Speculation	Possible Test
Sprites can occur away from/without halos	sprites are "seeded"	rocket seeding of sprites
Initially small tendrils can form large carrot sprites	sprite shape depends on electric field	electromagnetic measurements
Sprite aftereffects occur in stratosphere	blue emissions?	color images of sprite aftereffects
Embers and palm trees have a single stem	they are effectively the same phenomena	1 ms or better temporal resolution observation of palm trees
Ember group dynamics irregular	individual embers due to, or similar to, K and M changes in lightning	high speed optical observations of embers together with near-field electric field records from lightning

alent to, K or M-processes in lightning (see description in Chapter 6). K and M-processes are observable in near-field lightning records. Combining this measurement at a location of a large thunderstorm, together with high speed observations of embers made from several hundred km to the side of the thunderstorm may show whether K and M processes are responsible for, or equivalent to embers.

Lastly, possibility of sprite seeding should be investigated. If, as proposed here, sprites are seeded by atmospheric composition and density inhomogeneities, it should be possible to seed sprites artificially via a rocket-based program. Other rockets could be used to sample the minor atmospheric constituents at mesospheric altitudes before and after a major storm, to investigate possibility of creating of chemical species within sprites and in sprite afterglow.

In this thesis a variety of new phenomenology was presented related to sprites and sprite-like processes that occur in the high atmosphere above thunderstorms. The focus was on describing the detailed characteristics and behavior of halos, sprites, and sprite aftereffects.

Several speculations were advanced throughout the thesis. These speculations, and observations that could be made to test them, include those listed in Table 7.4.

Bibliography

Armstrong, R. A., J. A. Shorter, M. J. Taylor, D. M. Suszcynsky, W. A. Lyons, and L. S. Jeong, Photometric measurements in the SPRITES '95 & '96 campaigns of nitrogen second positive (399.8 nm) and first negative (427.8 nm) emissions, *J. Atmos. Solar-Terr. Phys.*, *60*, 787, 1998.

Barrington-Leigh, C. P., *Fast Photometric Imaging of High Altitude Optical Flashes Above Thunderstorms*, Ph.D. thesis, Stanford University, 2000, available at http://www-star.stanford.edu/~vlf/publications/theses/cpblThesis/thesis.html.

Barrington-Leigh, C. P. and U. S. Inan, Elves triggered by positive and negative lightning discharges, *Geophys. Res. Lett.*, *26*(6), 683, 1999.

Barrington-Leigh, C. P., U. S. Inan, and M. Stanley, Elves: Photometric and video signatures, *Eos Trans. Am. Geophys. Union, Fall Meeting Suppl.*, *80*(46), F224, 1999a.

Barrington-Leigh, C. P., U. S. Inan, M. Stanley, and S. A. Cummer, Sprites triggered by negative lightning discharges, *Geophys. Res. Lett.*, *26*(24), 3605, 1999b.

Barrington-Leigh, C. P., U. S. Inan, and M. Stanley, Identification of sprites and elves with intensified video and broadband array photometry, *J. Geophys. Res.*, *106*(A2), 1741, 2001.

Baumgarten, G., K. H. Fricke, and G. von Cossart, Investigation of the shape of noctilucent cloud particles by polarization lidar technique, *Geophys. Res. Lett.*, *29*(13), 1630, doi:10.1029/2001GL013877, 2002.

Bazelyan, E. M. and Y. P. Raizer, *Spark Discharge*. CRC Press, Boca Raton, Florida, 1997.

Bell, T. F., V. P. Pasko, and U. S. Inan, Runaway electrons as a source of red sprites in the mesosphere, *Geophys. Res. Lett.*, *22*, 2127, 1995.

Bering, E., D. Sentman, J. R. Benbrook, L. Bhusal, J. A. Garrett, A. M. Jackson, D. R. Moudry, E. M. Wescott, , H. C. Stenbaek-Nielsen, and W. A. Lyons, Mesospheric energy input owing to sprites and other TLE's and the possible effects thereof, *Eos Trans. Am. Geophys. Union, Fall Meeting Suppl.*, *82*(47), Abstract AE22A, 2001.

Bering III, E. A., J. R. Benbrook, A. Paredes, E. M. Wescott, D. R. Moudry, D. Sentman, H. C. Stenbaek-Nielsen, and W. A. Lyons, The electrodynamics of sprites, *Geophys. Res. Lett.*, *29*(5), 10.1029/2001GL013267, 2002.

Boccippio, D. J., E. R. Williams, S. J. Heckman, W. A. Lyons, I. T. Baker, and R. Boldi, Sprites, Extreme-Low-Frequency transients, and positive ground strokes, *Science*, *269*, 1088, 1995.

Boeck, W. L., O. H. Vaughan, Jr., R. Blakeslee, B. Vonnegut, and M. Brook, Lightning induced brightening in the airglow layer, *Geophys. Res. Lett.*, *19*, 99, 1992.

Boeck, W. L., O. H. Vaughan, Jr., R. Blakeslee, B. Vonnegut, M. Brook, and J. M. McKue, Observations of lightning in the stratosphere, *J. Geophys. Res.*, *100*, 1465, 1995.

Bucsela, E., M. J. Heavner, J. S. Morrill, S. Berg, C. Seifring, W. Benesch, E. M. Wescott, D. Sentman, D. L. Hampton, and D. R. Moudry, $N_2(B^3\Pi_g)$ and $N_2^+(A^2\Pi_u)$ vibrational distributions observed in sprites, *J. Atmos. Solar-Terr. Phys.*, 2002, in press.

Cho, M. and M. J. Rycroft, Computer simulation of the electric field structure and optical emission from cloud-top to the ionosphere, *J. Atmos. Solar-Terr. Phys.*, *60*(7), 871, 1998.

Cho, M. and M. J. Rycroft, Non-uniform ionisation of the upper atmosphere due to the electromagnetic pulse from a horizontal lightning discharge, *J. Atmos. Solar-Terr. Phys.*, *63*(6), 559, 2001.

Christian, H., R. Frost, P. Gillaspy, S. Goodman, O. Vaughn, M. Brook, B. Vonnegut, and R. E. Orville, Observations of optical lightning emissions from above thunderstorms using U-2 aircraft, *Bull. Am. Meteor. Soc.*, *64*, 120, 1983.

Clemesha, B. R., P. P. Batista, and D. M. Simonich, Long-term and solar cycle changes in the atmospheric sodium layer, *J. Atmos. Terr. Phys.*, *59*, 1673, 1997.

Cummer, S. and M. Stanley, Submillisecond resolution lightning currents and sprite development: Observations and implications, *Geophys. Res. Lett.*, *26*(20), 3205, 1999.

Cummins, K. L., M. J. Murphy, E. A. Bardo, W. L. Hiscox, R. B. Pyle, and A. E. Pifer, A combined TOA/MDF technology upgrade of the U.S. National Lightning Detection Network, *J. Geophys. Res.*, *103*(8), 9035, 1998.

Desch, S. J. and J. N. Cuzzi, The generation of lightning in the solar nebula, *Icarus*, *143*, 87, 2000.

Desch, S. J., W. J. Boricki, C. T. Russell, and A. Bar-Nun, Progress in planetary lightning, *Rep. Prog. Phys.*, *65*, 955, 2002.

Desroschers, J. T., M. J. Heavner, D. L. Hampton, D. D. Sentman, and E. M. Wescott, A preliminary morphology of optical transients above thunderstorms, *Eos Trans. Am. Geophys. Union, Fall Meeting Suppl.*, pp. A32C–04, 1995.

Ernstmeyer, J. and T. Chang, Lightning-induced electron heating in the mesosphere, *Geophys. Res. Lett.*, *25*(13), 2389, 1998.

Fernsler, R. and H. Rowland, Models of lightning-produced sprites and elves, *J. Geophys. Res.*, *101*, 29653, 1996.

Fisher, R. J., G. H. Schnetzer, R. Thottappillil, V. A. Rakov, M. A. Uman, and J. D. Goldberg, Parameters of triggered-lightning flashes in Florida and Alabama, *J. Geophys. Res.*, *98*(12), 22,887, 1993.

Franz, R. D., R. J. Nemzek, and J. R. Winckler, Television images of a large upward electrical discharge above a thunderstorm system, *Science*, *249*, 48, 1990.

Fukunishi, H., Y. Takahashi, M. Kubota, K. Sakanoi, U. S. Inan, and W. A. Lyons, Elves: Lightning-induced transient luminous events in the lower ionosphere, *Geophys. Res. Lett.*, *23*, 2157, 1996a.

Fukunishi, H., Y. Takahashi, M. Fujito, Y. Watanabe, and K. Sakanoi, Fast imaging of elves and sprites using a framing/streak camera and a multi-anode array photometer, *Eos Trans. Am. Geophys. Union, Fall Meeting Suppl.*, *77*(46), F60, 1996b.

Gerken, E. A., U. S. Inan, and C. Barrington-Leigh, Telescopic imaging of sprites, *Geophys. Res. Lett.*, *27*(17), 2637, 2000.

Green, B. D., M. E. Fraser, W. T. Rawlins, L. Jeong, W. A. Blumberg, S. B. Mende, G. R. Swenson, D. L. Hampton, E. M. Wescott, and D. D. Sentman, Molecular excitation in sprites, *Geophys. Res. Lett.*, *23*(23), 2161, 1996.

Hampton, D. L., M. J. Heavner, E. M. Wescott, and D. D. Sentman, Optical spectral characteristics of sprites, *Geophys. Res. Lett.*, *23*(1), 89, 1996.

Heavner, M. J., *Optical Spectroscopic Observations of Sprites, Blue Jets, and Elves: Inferred Microphysical Processes and Their Macrophysical Implications*, Ph.D. thesis, University of Alaska, Fairbanks, 2000.

Heavner, M. J., D. D. Sentman, D. R. Moudry, E. M. Wescott, C. L. Siefring, J. S. Morrill, and E. J. Bucsela, Sprites, blue jets, and elves: Optical evidence of energy transport across the stratopause, in D. E. Siskind, S. D. Eckerman, and M. E. Summers (eds.), *Atmospheric Science Across the Stratopause*, number 123 in Monograph Series, pp. 69–82. Am. Geophys. Union, Washington, DC, 2000.

Hu, W., S. Cummer, W. Lyons, and T. Nelson, Lightning charge moment changes for the initiation of sprites, *Geophys. Res. Lett.*, *29*(8), 120, 2002, 10.1029/2001GL014593.

Inan, U., C. Barrington-Leigh, S. Hansen, V. S. Glukhov, T. F. Bell, and R. Rairden, Rapid lateral expansion of optical luminosity in lightning-induced ionospheric flashes referred to as 'elves', *Geophys. Res. Lett.*, *24*(5), 583, 1997.

Inan, U. S., T. F. Bell, and J. V. Rodrigues, Heating and ionization of the lower ionosphere by lightning, *J. Geophys. Res.*, *18*, 705, 1991.

Inan, U. S., S. C. Reising, G. J. Fishman, and J. M. Horack, On the association of terrestrial gamma-ray bursts with lightning and implications for sprites, *Geophys. Res. Lett.*, *23*, 1017, 1996a.

Inan, U. S., W. A. Sampson, and Y. N. Taranenko, Space-time structure of optical flashes and ionization changes produced by lightning-EMP, *Geophys. Res. Lett.*, *23*(2), 133, 1996b.

Jackson, J. D., *Classical Electrodynamics*. Wiley, New York, 2nd edition, 1975.

Jordan, D. M., V. P. Idone, R. E. Orville, V. A. Rakov, and M. A. Uman, Luminosity characteristics of lightning M components, *J. Geophys. Res.*, *100*(12), 25,695, 1995.

Kirkwood, S., V. Barabash, B. U. E. Brndstrm, A. Mostrm, K. Stebel, N. Mitchell, and W. Hocking, Noctilucent clouds, pmse and 5-day planetary waves: A case study, *Geophys. Res. Lett.*, *29*(10), 1411, doi:10.1029/2001GL014022, 2002.

Kivelson, M. G., *Introduction to Space Physics*, pp. 27–57. Cambridge University Press, New York, 1995.

Kulikovsky, A. A., The role of photoionization in positive streamer dynamics , *J. Phys. D: Appl. Phys.*, *33*, 1514, 2000.

Lehtinen, N. G., T. F. Bell, V. P. Pasko, and U. S. Inan, A two-dimensional model of runaway electron beams driven by quasi-electrostatic thundercloud fields, *Geophys. Res. Lett.*, *24*(21), 2639, 1997.

Liu, N., V. P. Pasko, and T. Heffner, Dynamics of positive and negative streamers in sprites, *Eos Trans. Am. Geophys. Union, Fall Meeting Suppl.*, *83*(47), A11C, 2002.

Lyons, W. A., Characteristics of luminous structures in the stratosphere above thunderstorms as imaged by low-light video, *Geophys. Res. Lett.*, *21*, 875, 1994a.

Lyons, W. A., Low-light video observations of frequent luminous structures in the stratosphere above thunderstorms, *Monthly Weather Review*, *122*, 1940, 1994b.

Lyons, W. A., Sprite observations above the U.S. High Plains in relation to their parent thunderstorm systems, *J. Geophys. Res.*, *101*, 29641, 1996.

Lyons, W. A., T. E. Nelson, J. L. Eastman, R. A. Armstrong, E. R. Williams, D. S. Suszcynsky, M. A. Taylor, Y. Takahashi, E. A. Bering, and J. R. Benbrook, Sprites'99

campaign highlights at the Yucca Ridge Field Station, *Eos Trans. Am. Geophys. Union, Fall Meeting Suppl.*, pp. A42E–02, 1999.

Lyons, W. A., T. E. Nelson, and A. Faires, Electrical discharges into the stratosphere from the tops of intense thunderstorms, *Eos Trans. Am. Geophys. Union, Fall Meeting Suppl.*, *82*(47), abstract AE22A, 2001.

McCarthy, M. P. and G. K. Parks, On the modulation of x ray fluxes in thunderstorms, *J. Geophys. Res.*, *97*, 5857, 1992.

McHarg, M. G., R. K. Haaland, D. R. Moudry, and H. C. Stenbaek-Nielsen, Altitude-time development of sprites, *J. Geophys. Res.*, *107*(A11), 1364, 2002, doi:10.1029/2001JA000283.

Mende, S. B., R. L. Rairden, and G. R. Swenson, Sprite spectra: $N_2$1PG band identification, *Geophys. Res. Lett.*, *22*, 2633, 1995.

Morrill, J. S., E. J. Bucsela, V. P. Pasko, S. L. Berg, M. J. Heavner, D. R. Moudry, W. M. Benesch, E. M. Wescott, and D. D. Sentman, Time resolved N_2 triplet state vibrational populations and emissions associated with red sprites, *J. Atmos. Solar-Terr. Phys.*, *60*, 811, 1998.

Morrill, J. S., E. J. Bucsela, C. Siefring, M. J. Heavner, S. L. Berg, D. R. Moudry, S. Slinker, R. Fernsler, E. M. Wescott, D. D. Sentman, and D. Osborne, Electron energy and electric field estimates in sprites derived from ionized and neutral N_2 emissions, *Geophys. Res. Lett.*, *29*(10), 10.1029/2001GL014018, 2002, article 100.

Moudry, D. R., M. J. Heavner, D. D. Sentman, and E. M. Wescott, Morphology of sprites, *CEDAR (Coupling, energetics and dynamics of atmospheric regions) meeting*, 1999, Boulder, CO.

Moudry, D. R., H. C.Stenbaek-Nielsen, D. D. Sentman, and E. M. Wescott, 1 ms time development of upper atmospheric flashes, in *National Radio Science Meeting (URSI)*. 2001, G/H3-12, Boulder, CO.

Moudry, D. R., H. C. Stenbaek-Nielsen, D. D. Sentman, and E. M. Wescott, Imaging of elves, halos and sprite initiation at 1 ms time resolution, *J. Atmos. Solar-Terr. Phys.*, 2003, in press.

Muller, R. A., Red sprites triggered by meteors?, *Eos Trans. Am. Geophys. Union, Fall Meeting Suppl.*, *76*(46), F105, 1995.

Pancheshnyi, S. V., S. M. Starikovskaia, and A. Y. Starikovskii, Role of photoionization processes in propagation of cathode-directed streamer, *J. Phys. D: Appl. Phys.*, *34*, 1, 2001.

Pasko, V. P., U. S. Inan, Y. N. Taranenko, and T. F. Bell, Heating, ionization and upward discharges in the mesosphere due to intense quasi-electrostatic thundercloud fields, *Geophys. Res. Lett.*, *22*, 365, 1995.

Pasko, V. P., U. S. Inan, and T. F. Bell, Blue jets produced by quasi-electrostatic pre-discharge thundercloud fields, *Geophys. Res. Lett.*, *23*(3), 301, 1996.

Pasko, V. P., U. S. Inan, T. F. Bell, and Y. N. Taranenko, Sprites produced by quasi-electrostatic heating and ionization in the lower ionosphere, *J. Geophys. Res.*, *102*(A3), 4529, 1997.

Pasko, V. P., U. S. Inan, and T. F. Bell, Spatial structure of sprites, *Geophys. Res. Lett.*, *25*(12), 2123, 1998.

Pasko, V. P., U. S. Inan, and T. F. Bell, Mesospheric electric field transients due to tropospheric lightning discharges, *Geophys. Res. Lett.*, *26*(9), 1247, 1999.

Pasko, V. P., U. S. Inan, and T. F. Bell, Fractal structure of sprites, *Geophys. Res. Lett.*, *27*(4), 497, 2000.

Pasko, V. P., M. A. Stanley, J. D. Mathews, U. S. Inan, and T. G. Wood, Electrical discharge from a thundercloud top to the lower ionosphere, *Nature*, *416*(14 March), 152, 2002.

Raizada, S. and C. A. Tepley, Iron boltzmann lidar temperature and density observations from arecibo - an initial comparison with other techniques, *Geophys. Res. Lett.*, *29*(12), 1560, doi:10.1029/2001GL014535, 2002.

Raizer, Y. P., *Gas Discharge Physics*. Springer, Heidelberg, Germany, 1997.

Raizer, Y. P., G. M. Millikh, M. N. Shneider, and S. V. Novakovski, Long streamers in the upper atmosphere above thundercloud, *J. Phys. D: Appl. Phys.*, *31*, 3255, 1998.

Rees, M. H., *Physics and Chemistry of the Upper Atmosphere*, Cambridge Atmospheric and Space Science Series. Cambridge University Press, 1989.

Roussel-Dupré, R., E. Symbalisty, Y. Taranenko, and V. Yukhimuk, Simulations of high-altitude discharges initiated by runaway breakdown, *J. Atmos. Solar-Terr. Phys.*, *60*(7), 917, 1998.

Roussel-Dupré, R. A. and A. V. Gurevich, On runaway breakdown and upward propagating discharges, *J. Geophys. Res.*, *101*(A2), 2297, 1996.

Rowland, H., R. Fernsler, J. Huba, and P. Bernhardt, Lightning driven EMP in the upper atmosphere, *Geophys. Res. Lett.*, *22*, 361, 1995.

Rowland, H. L., Theories and simulations of elves, sprites, and blue jets, *J. Atmos. Solar-Terr. Phys.*, *60*(7), 831, 1998.

Russell, C. T., Planetary lightning, *Ann. Rev. Earth Planet. Sci.*, *21*, 43, 1993.

Sentman, D., Electrical excitation of the middle and upper atmosphere by lightning: Special issue of the Journal of Atmospheric and Solar-Terrestrial Physics, *J. Atmos. Solar-Terr. Phys.*, *60*(7-9), 667, 1998.

Sentman, D., E. M. Wescott, R. H. Picard, J. R. Winick, H. Stenbaek-Nielsen, E. Dewan, D. R. Moudry, F. S. Sabbas, and M. J. Heavner, Simultaneous observations of mesospheric gravity waves and sprites generated by a midwestern thunderstorm, *J. Atmos. Solar-Terr. Phys.*, 2003, in press.

Sentman, D. D., On the possible occurrence of sprites in other planetary atmospheres, *URSI XXVth General Assembly, Lille, France*, (Planetary Lightning and Related Phenomena I), August, 1996, E2.3.

Sentman, D. D. and E. M. Wescott, Video observations of upper atmospheric optical flashes recorded from an aircraft, *Geophys. Res. Lett.*, *20*, 2857, 1993.

Sentman, D. D. and E. M. Wescott, Red Sprites and Blue Jets, *Geophysical Institute Video Production, University of Alaska, Fairbanks*, 1994.

Sentman, D. D., E. M. Wescott, D. L. Osborne, D. L. Hampton, and M. J. Heavner, Preliminary results from the Sprites94 aircraft campaign: 1. Red Sprites, *Geophys. Res. Lett.*, *22*(10), 1205, 1995.

Sentman, D. D., E. M. Wescott, M. J. Heavner, and D. R. Moudry, Observations of sprite beads and balls, *EOS Trans. Am. Geophys. Union*, *77*(46), A71B, 1996.

Siefring, C. L., J. S. Morrill, D. Sentman, D. Moudry, E. M. Wescott, M. J. Heavner, D. L. Osborne, and E. J. Bucsela, Do sprites sometimes connect to the cloud tops?, *Eos Trans. Am. Geophys. Union, Fall Meeting Suppl.*, *80*(46), 1999, A51B-08.

Stanley, M., P. Krehbiel, W. Rison, C. Moore, and O. Vaughan, Observations of sprites and jets from Langmuir Laboratory, New Mexico, *Eos Trans. Am. Geophys. Union, Fall Meeting Suppl.*, *77*(46), F69, 1996.

Stanley, M., P. Krehbiel, M. Brook, C. Moore, W. Rison, and B. Abrahams, High speed video of initial sprite development, *Geophys. Res. Lett.*, *26*(20), 3201, 1999.

Stanley, M. A., *Sprites and Their Parent Discharges*, Ph.D. thesis, New Mexico Inst. of Mining and Technology, Socorro, NM, 2000.

Stenbaek-Nielsen, H. C., D. R. Moudry, E. M. Wescott, D. D. Sentman, and F. T. S. Sabbas, Sprites and possible mesospheric effects, *Geophys. Res. Lett.*, *27*(23), 3829, 2000.

Suszcynsky, D. M., R. Roussel-Dupré, W. A. Lyons, and R. A. Armstrong, Blue-light imagery and photometry of sprites, *J. Atmos. Solar-Terr. Phys.*, *60*(7), 801, 1998.

Suszcynsky, D. M., R. Strabley, R. Roussel-Dupré, E. M. D. Symbalisty, R. A. Armstrong, W. A. Lyons, and M. Taylor, Video and photometric observations of a sprite in coincidence with a meteor-triggered jet event, *J. Geophys. Res.*, *104*(24), 31,361, 1999.

Suzuki, T., Propagation of ionizing waves in glow discharge, *J. Appl. Phys.*, *48*(12), 5001, 1977.

Svanberg, S., *Atomic and Molecular Spectroscopy*. Springer-Verlag, Heidelberg, Germany, 1991.

Symbalisty, E. M. D., R. A. Roussel-Dupré, D. O. ReVelle, D. M. Suszcynsky, and V. Yukhimuk, Meteor trails and columniform sprites, *Icarus*, *148*(1), 65, 2000.

Takahashi, Y., H. Fukunishi, M. Fujito, Y. Watanabe, and K. Sakanoi, Temporal development of carrot-like sprites, *Eos Trans. Am. Geophys. Union, Fall Meeting Suppl.*, *77*(46), F69, 1996.

Taranenko, Y. N. and R. Roussel-Dupré, High-altitude discharges and gamma-ray flashes: A manifestation of runaway air breakdown, *Geophys. Res. Lett.*, *23*(5), 571, 1996.

Taranenko, Y. N., U. S. Inan, and T. F. Bell, Optical signatures of lightning-induced heating of the D region, *Geophys. Res. Lett.*, *19*(18), 1815, 1992.

Taranenko, Y. N., U. S. Inan, and T. F. Bell, Interaction with the lower ionosphere of electromagetnic pulses from lightning: heating attachment, and ionization, *Geophys. Res. Lett.*, *20*, 1539, 1993a.

Taranenko, Y. N., U. S. Inan, and T. F. Bell, The interaction with the lower ionosphere of electromagnetic pulses from lightning: excitation of optical emissions, *Geophys. Res. Lett.*, *20*, 2675, 1993b.

Thottappillil, R., V. A. Rakov, and M. A. Uman, K and M changes produced in close lightning flashes in Florida, *J. Geophys. Res.*, *95*(11), 18,631, 1990.

Triplett, L. A., R. A. Roussel-Dupré, D. M. Suszcynsky, and H. E. Tierney, Spectral output of sprites from both conventional and runaway breakdown, *Eos Trans. Am. Geophys. Union, Fall Meeting Suppl.*, *83*(47), A11C, 2002.

Uman, M. A., *The Lightning Discharge*, volume 39 of *International Geophysics Series*. Academic Press, Inc., Orlando, Florida, 1987.

Valdivia, J., G. Milikh, and K. Papadopoulos, Red sprites: Lightning as a fractal antenna, *Geophys. Res. Lett.*, *24*(24), 3169, 1997.

Vallance Jones, A., *Aurora*. D. Reidel Publishing Co., Boston, MA, 1974.

Vaughan, Jr., O. H. and B. Vonnegut, Lightning to the ionosphere?, *Weatherwise*, *35*(82), 70, 1982.

Vaughan, Jr., O. H. and B. Vonnegut, Recent observations of lightning discharges from the top of a thundercloud into the clear air above, *J. Geophys. Res.*, *94*, 13179, 1989.

Veronis, G., V. Pasko, and U. Inan, Characteristics of mesospheric optical emissions produced by lighting discharges, *J. Geophys. Res.*, *104*, 12645, 1999.

Vonnegut, B., Cloud-to-stratosphere lightning, *Weather*, *35*(2), 59, 1980.

Vonnegut, B., O. H. Vaughan, and M. Brook, Nighttime/daytime optical survey of lightning and convective phenomena experiment (NOSL), Technical report, 1980.

Vonnegut, B., O. H. Vaughan, Jr., and M. Brook, Photographs of lightning from the space shuttle, *Bull. Am. Meteor. Soc.*, *64*, 150, 1983.

Wayne, R. P., *Chemistry of Atmospheres*. Oxford University Press, Oxford Science Publications, New York, NY, 2nd edition, 1991.

Wescott, E. M., D. D. Sentman, D. L. Osborne, D. L. Hampton, and M. J. Heavner, Preliminary results from the Sprites94 aircraft campaign: 2. Blue Jets, *Geophys. Res. Lett.*, *22*(10), 1209, 1995.

Wescott, E. M., D. D. Sentman, M. J. Heavner, D. L. Hampton, D. L. Osborne, and O. H. Vaughan, Jr., Blue starters: Brief upward discharges from an intense Arkansas thunderstorm, *Geophys. Res. Lett.*, *23*(16), 2153, 1996a.

Wescott, E. M., D. D. Sentman, M. J. Heavner, T. J. Hallinan, D. L. Hampton, and D. L. Osborne, The optical spectrum of aircraft St. Elmo's fire, *Geophys. Res. Lett.*, *23*(25), 3687, 1996b.

Wescott, E. M., D. D. Sentman, M. J. Heavner, D. L. Hampton, and O. H. Vaughan, Jr., Blue Jets: their relationship to lightning and very large hailfall, and their physical mechanisms for their production, *J. Atmos. Solar-Terr. Phys.*, *60*, 713, 1998a.

Wescott, E. M., D. D. Sentman, M. J. Heavner, D. L. Hampton, W. A. Lyons, and T. Nelson, Observations of 'Columniform' sprites, *J. Atmos. Solar-Terr. Phys.*, *60*, 733, 1998b.

Wescott, E. M., H. C. Stenbaek-Nielsen, D. D. Sentman, M. J. Heavner, D. R. Moudry, and F. T. S. Sabbas, Triangulation of sprites, associated halos and their possible relation to causative lightning and micro-meteors, *J. Geophys. Res.*, *106*(A6), 10467, 2001.

Wescott, L. W., E. M. Wescott, H. C. Stenbaek-Nielsen, D. D. Sentman, D. R. Moudry, M. J. Heavner, and F. T. S. Sabbas, Triangulation of sprites and elves from the NASA 1999 sprites balloon campaign, *Eos Trans. Am. Geophys. Union, Fall Meeting Suppl.*, *80*(46), F217, 1999.

Wilson, C. T. R., The electric field of a thunderstorm and some of its effects, *Proc. Phys. Soc. London*, *37*, 32D, 1925.

Wilson, C. T. R., A theory of thundercloud electricity, *Proc. Royal Meteor. Soc. London*, *236*(32D), 297, 1956.

Winckler, J. R., Further observations of cloud-ionosphere electrical discharges above thunderstorms, *J. Geophys. Res.*, *100*, 14335, 1995.

Winn, W. P., A laboratory analog to the dart leader and return stroke of lightning, *J. Geophys. Res.*, *70*(14), 3265, 1965.

Yamada, Y., H. Fukunishi, T. Nakamura, and T. Tsuda, Breaking of small-scale gravity wave and transition to turbulence observed in OH airglow, *Geophys. Res. Lett.*, *28*(11), 2153, 2001.

Yukhimuk, V., R. A. Roussel-Dupré, and E. M. D. Symbalisty, On the temporal evolution of red sprites: Runaway theory versus data, *Geophys. Res. Lett.*, *26*(6), 679, 1999.

Yukhimuk, V. A., R. A. Roussel-Dupré, E. M. D. Symbalisty, and Y. Taranenko, Optical characteristics of red sprites produced by runaway air breakdown, *J. Geophys. Res.*, *103*(D10), 11473, 1998.

Zabotin, N. A. and J. W. Wright, Role of meteoric dust in sprite formation, *Geophys. Res. Lett.*, *28*(13), 2593, 2001.